# Nuclear Chiral Dynamics and Thermodynamics

Jeremy W. Holt[1], Norbert Kaiser[2], Wolfram Weise[2,3]

[1]Physics Department, University of Washington, Seattle, WA 98195-1550, USA
[2]Physik-Department, Technische Universität München, D-85747 Garching, Germany
[3]ECT*, Villa Tambosi, I-38123 Villazzano (Trento), Italy

April 24, 2013

**Abstract**

This presentation reviews an approach to nuclear many-body systems based on the spontaneously broken chiral symmetry of low-energy QCD. In the low-energy limit, for energies and momenta small compared to a characteristic symmetry breaking scale of order 1 GeV, QCD is realized as an effective field theory of Goldstone bosons (pions) coupled to heavy fermionic sources (nucleons). Nuclear forces at long and intermediate distance scales result from a systematic hierarchy of one- and two-pion exchange processes in combination with Pauli blocking effects in the nuclear medium. Short distance dynamics, not resolved at the wavelengths corresponding to typical nuclear Fermi momenta, are introduced as contact interactions between nucleons. Apart from a set of low-energy constants associated with these contact terms, the parameters of this theory are entirely determined by pion properties and low-energy pion-nucleon scattering observables. This framework (in-medium chiral perturbation theory) can provide a realistic description of both isospin-symmetric nuclear matter and neutron matter, with emphasis on the isospin-dependence determined by the underlying chiral NN interaction. The importance of three-body forces is emphasized, and the role of explicit $\Delta(1232)$-isobar degrees of freedom is investigated in detail. Nuclear chiral thermodynamics is developed and a calculation of the nuclear phase diagram is performed. This includes a successful description of the first-order phase transition from a nuclear Fermi liquid to an interacting Fermi gas and the coexistence of these phases below a critical temperature $T_c$. Density functional methods for finite nuclei based on this approach are also discussed. Effective interactions, their density dependence and connections to Landau Fermi liquid theory are outlined. Finally, the density and temperature dependence of the chiral (quark) condensate is investigated.

## 1 Introduction

Almost eight decades ago, Yukawa's pioneering article [1] introduced the framework for a systematic approach to the nucleon-nucleon interaction, based on the exchange of a boson identified later as the pion. In the footsteps of Yukawa's original work the next generation of Japanese theorists already made impressive efforts to proceed from the long-range part of the interaction to shorter distances between nucleons. A cornerstone of these developments was the visionary conceptual design by Taketani et al. [2] of an inward-bound hierarchy of scales governing the nucleon-nucleon potential, sketched in Fig. 1. The long distance region I is determined by one-pion exchange. It continues inward to the region II of intermediate distances dominated by two-pion exchange. The basic idea was to construct the NN

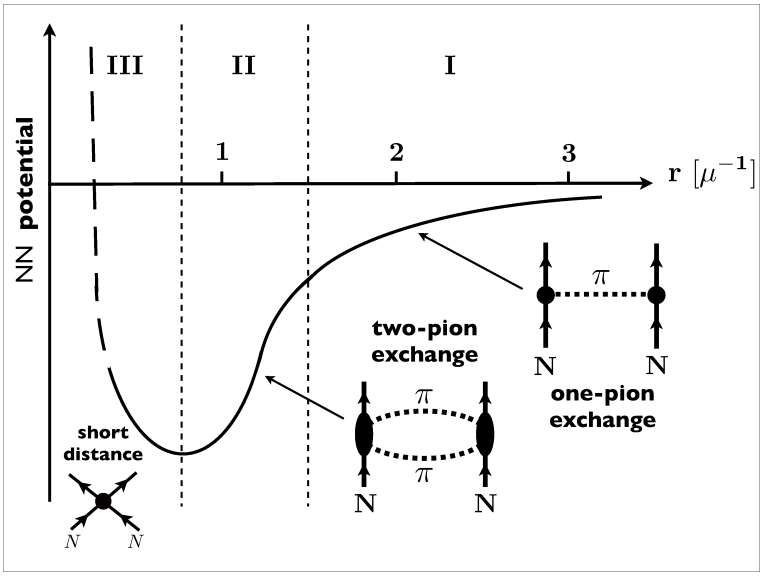


Figure 1: Schematic picture displaying the hierarchy of scales governing the nucleon-nucleon potential (adapted from Taketani [3]). The distance $r$ is given in units of the pion Compton wavelength $\mu^{-1} \simeq 1.4$ fm.

potential in regions I and II by explicit calculation of $\pi$ and $2\pi$ exchange processes, whereas the detailed behaviour of the interaction in the short distance region III remains unresolved at the low-energy scales characteristic of nuclear physics. This short distance part is then given a suitably parametrized form. The parameters are fixed by comparison with scattering data.

Taketani's picture, although at the time of its appearance not at all universally accepted by the international community of theorists, turned out to be immensely useful. Today this strategy is the one pursued by modern effective field theory approaches. It is amazing how far this program had already been developed in the late fifties of the twentieth century. One example is the pioneering calculation of the two-pion exchange potential [4, 5] (using dispersion relation techniques) and early knowledge [6] of the resonant pion-nucleon amplitude which anticipated the $\Delta$-isobar models of later decades [7].

Today's theory of the strong interaction is Quantum Chromodynamics (QCD). There exist two limiting situations in which QCD is accessible with "controlled" approximations. At momentum scales exceeding several GeV (corresponding to short distances, $r < 0.1$ fm), QCD is a theory of weakly interacting quarks and gluons. At low momentum scales considerably smaller than 1 GeV (corresponding to long distances, $r > 1$ fm), QCD is governed by color confinement and a non-trivial vacuum: the ground state of QCD hosts strong condensates of quark-antiquark pairs and gluons. Confinement is accompanied by the dynamical (spontaneous) breaking of Chiral Symmetry, a global symmetry of QCD that is exact in the limit of massless quarks. Spontaneous chiral symmetry breaking in turn implies the existence of pseudoscalar Nambu-Goldstone bosons. For two quark flavours ($N_f = 2$) with (almost) massless $u$ and $d$ quarks, these Goldstone bosons are identified with the isospin triplet of pions. Low-energy QCD is thus realized as a (chiral) effective field theory in which these Goldstone bosons are the active, light degrees of freedom. In the low-energy, long-wavelength limit, Goldstone bosons interact weakly with one another or with any massive hadrons. In this limit perturbative methods are applicable and a systematic expansion in powers of a "small" parameter can be performed (chiral perturbation theory [8, 9]).

The chiral effective field theory (ChEFT) just sketched provides the interface between QCD and nuclear physics. This theory has become the framework for a successful description of the nucleon-nucleon interaction [10, 11, 12], and it is the starting point of a systematic approach to the nuclear many-body problem and its thermodynamics at densities and temperatures well within the confined

(hadronic) phase of QCD. This review is written to serve as an introduction and state-of-the-art overview of this active area of research. It does not aim for completeness, however, and should be read in combination with complementary overviews, such as refs. [10, 11, 12].

# 2 Low-Energy QCD and Chiral Symmetry

Before turning to the more detailed presentation of the ChEFT approach to nuclear many-body systems, it is useful and instructive to briefly recall how the special role of the pion emerges in the context of chiral symmetry in QCD, through the Nambu-Goldstone mechanism of spontaneous symmetry breaking. In other words: how does Yukawa's pion figure in the framework of QCD?

## 2.1 *Chiral Symmetry and the Pion*

Historically, the foundations for understanding the pion as a Nambu-Goldstone boson [13, 14] were initiated in the 1960's, culminating in the current algebra approaches [15] (combined with the PCAC relation for the pion) of the pre-QCD era. A most inspiring work from this early period is the one by Nambu and Jona-Lasinio [14] (NJL). Just as the BCS theory provided an understanding of the basic mechanism behind superconductivity, the NJL model helped clarify the dynamics that drives spontaneous chiral symmetry breaking and the formation of pions as Goldstone bosons.

Consider as a starting point the color current of quarks, $\mathbf{J}^a_\mu = \bar{q}\gamma_\mu \mathbf{t}^a q$, where $\mathbf{t}^a$ $(a = 1, ..., 8)$ are the generators of the $SU(3)_c$ color gauge group and $q$ denotes the quark fields with $4N_cN_f$ components representing their spin, color and flavor degrees freedom ($N_c = 3$). This current couples to the gluon fields. Assume that the distance over which color propagates is restricted to a short correlation length $l_c$. Then the interaction experienced by low-momentum quarks can be schematically viewed as a local coupling between their color currents:

$$\mathcal{L}_{\rm int} = -G_c\, \mathbf{J}^a_\mu(x)\, \mathbf{J}^\mu_a(x)\ , \tag{1}$$

where $G_c \sim \bar{g}^2\, l_c^2$ is an effective coupling strength of dimension *length*$^2$ which encodes the QCD coupling, $g$, averaged over the relevant distance scales, in combination with the squared correlation length, $l_c^2$.

Now adopt the local interaction Eg.(1) and write the following model Lagrangian for the quark fields $q(x)$:

$$\mathcal{L} = \bar{q}(x)(i\gamma^\mu\partial_\mu - m_q)q(x) + \mathcal{L}_{\rm int}(\bar{q}, q)\,. \tag{2}$$

In essence, by "integrating out" gluon degrees of freedom and absorbing them in the four-fermion interaction $\mathcal{L}_{\rm int}$, the local $SU(3)_c$ gauge symmetry of QCD is now replaced by a global one only. Confinement is obviously lost, but all other symmetries of QCD are maintained. The mass matrix $m_q$ incorporates small "bare" quark masses. In the limit $m_q \to 0$, the Lagrangian (2) has a chiral symmetry of left- and right-handed quarks, $SU(N_f)_L \times SU(N_f)_R$, that it shares with the original QCD Lagrangian for $N_f$ massless quark flavors.

A Fierz transform of the color current-current interaction (1) produces a set of exchange terms acting in quark-antiquark channels. For the $N_f = 2$ case:

$$\mathcal{L}_{\rm int} \to \frac{G}{2}\left[(\bar{q}q)^2 + (\bar{q}\, i\gamma_5\, \vec{\tau}\, q)^2\right] + ...\ , \tag{3}$$

with the isospin Pauli matrices $\vec{\tau} = (\tau_1, \tau_2, \tau_3)$. For brevity we have not shown a series of terms with combinations of vector and axial vector currents, both in color singlet and color octet channels. The constant $G$ is proportional to the color coupling strength $G_c$. The ratio of these two constants is uniquely determined by the number of colors and flavors, $N_c$ and $N_f$.

The steps just outlined can be viewed as a contemporary way of introducing the time-honored NJL model [14]. This model has been further developed and applied [16, 17] to a variety of problems in hadron physics. The virtue of this schematic model is its simplicity in illustrating the basic mechanism of spontaneous chiral symmetry breaking, as follows. In the mean-field (Hartree) approximation the equation of motion derived from the Lagrangian (2) leads to a gap equation

$$M_q = m_q - G\langle 0|\bar{q}q|0\rangle \ , \tag{4}$$

which links the dynamical generation of a constituent quark mass $M_q$ to the appearance of the chiral quark condensate

$$\langle 0|\bar{q}q|0\rangle = -\mathrm{tr}\lim_{x\to 0}\langle 0|\mathcal{T}q(0)\bar{q}(x)|0\rangle = -2iN_fN_c\int\frac{d^4p}{(2\pi)^4}\frac{M_q\,\theta(\Lambda-|\vec{p}|)}{p^2-M_q^2+i\epsilon} \ . \tag{5}$$

This condensate plays the role of an order parameter of spontaneous chiral symmetry breaking. Starting from $m_q = 0$ a non-zero quark mass $M_q$ develops dynamically, together with a non-vanishing chiral condensate $\langle 0|\bar{q}q|0\rangle$, once $G$ exceeds a critical value of order $G_{\rm crit} \simeq 10$ GeV$^{-2}$. The procedure requires a momentum cutoff $\Lambda \simeq 2M_q$ beyond which the interaction is "turned off". Note that the strong non-perturbative interactions, by polarizing the vacuum and turning it into a condensate of quark-antiquark pairs, transmute an initially pointlike quark with its small bare mass $m_q$ into a massive quasi-particle with a size of order $(2M_q)^{-1}$.

## 2.2 *The Pseudoscalar Meson Spectrum*

The NJL model demonstrates lucidly the appearance of chiral Nambu-Goldstone bosons. Solving Bethe-Salpeter equations in the color singlet quark-antiquark channels generates the lightest mesons as quark-antiquark excitations of the correlated QCD ground state with its condensate structure. Several such calculations have been performed in the past with $N_f = 3$ quark flavors [16, 17, 18]. Such a model has an unwanted $U(3)_L \times U(3)_R$ symmetry to start with, but due to the axial $U(1)_A$ anomaly of QCD this symmetry[1] should be reduced to $SU(3)_L \times SU(3)_R \times U(1)_V$. In the NJL model, instanton driven interactions are incorporated in the form of a flavor determinant [19] $\det[\bar{q}_i(1\pm\gamma_5)q_j]$. This interaction involves all three flavors $u, d, s$ simultaneously in a genuine three-body (contact) term.

The symmetry breaking pattern resulting from such a calculation is apparent in the pseudoscalar meson spectrum of Fig. 2. Starting from massless $u, d$ and $s$ quarks, the pseudoscalar octet emerges as a set of massless Goldstone bosons of spontaneously broken $SU(3)_L \times SU(3)_R$, while the broken $U(1)_A$ drives the singlet $\eta_0$ away from the Goldstone boson sector. Finite quark masses shift the pseudoscalar ($J^\pi = 0^-$) nonet into its empirically observed position, including $\eta_0$-$\eta_8$ mixing.

The very special nature of the pion as a Nambu-Goldstone boson is manifest in the famous Gell-Mann-Oakes-Renner relation [20] derived from current algebra and PCAC:

$$m_\pi^2\, f_\pi^2 = -\frac{1}{2}(m_u + m_d)\langle 0|\bar{q}q|0\rangle + \mathcal{O}(m_{u,d}^2 \ln m_{u,d}). \tag{6}$$

It involves the pion decay constant, $f_\pi = 92.4\,$MeV, defined by the matrix element which connects the pion-state with the QCD vacuum via the isovector axial vector current, $A_a^\mu = \bar{q}\gamma^\mu\gamma_5\frac{\tau_a}{2}q$:

$$\langle 0|A_a^\mu(0)|\pi_b(p)\rangle = i\delta_{ab}\,p^\mu f_\pi \ . \tag{7}$$

Just like the chiral condensate $\langle 0|\bar{q}q|0\rangle$, the pion decay constant $f_\pi$ is a measure of spontaneous chiral symmetry breaking expressed in terms of a characteristic scale $\Lambda_\chi \sim 4\pi f_\pi \sim 1$ GeV. The non-zero pion

[1] The axial $U(1)$-transformations of quarks, $q \to \exp(i\alpha\gamma_5)q$, constitute only a symmetry of classical chromodynamics, but not of its quantum version.

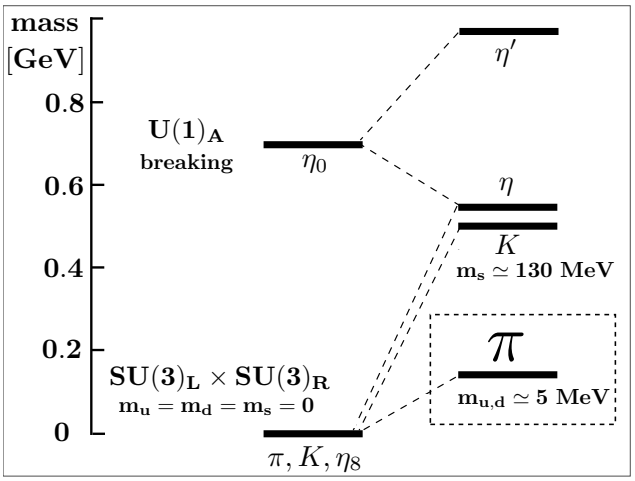


Figure 2: Symmetry breaking pattern in the pseudoscalar meson nonet calculated in the three-flavor NJL model [18] .

mass, $m_\pi \simeq 138\,\mathrm{MeV} \ll \Lambda_\chi$, reflects the explicit symmetry breaking by the small quark masses, with $m_\pi^2 \sim m_q$. One should note that the quark masses $m_{u,d}$ and the condensate $\langle 0|\bar{q}q|0\rangle$ are both scale dependent quantities. Only their product is scale independent, i.e. invariant under the renormalization group. At a renormalization scale of about 2 GeV, a typical average quark mass $\frac{1}{2}(m_u + m_d) \simeq 3.5$ MeV implies $\langle 0|\bar{q}q|0\rangle \simeq -(0.36\,\mathrm{GeV})^3$.

### 2.3 *Scales and Symmetry Breaking Patterns*

The quark masses are the only parameters that set primary scales in QCD. Their classification into sectors of "light" and "heavy" quarks determines very different physics phenomena. While the heavy quarks (i.e. the $t$, $b$ and - within limits - the $c$ quarks) offer a natural "small parameter" in terms of their reciprocal masses, such that non-relativistic approximations (expansions of observables in powers of $1/m_{t,b,c}$) tend to work increasingly well with increasing quark mass, the sector of the light quarks (i.e. the $u$, $d$ quarks and - to some extent - the $s$ quark) is governed by quite different principles and rules. Evidently, the quark masses themselves are now "small parameters", to be compared with a characteristic "large" scale of dynamical origin. This large scale is visible as a characteristic mass gap of about 1 GeV which separates the QCD vacuum from almost all of its excitations, with the exception of the pseudoscalar meson octet of pions, kaons and the eta meson. This mass gap is in turn comparable to $4\pi f_\pi$, the scale associated with spontaneous chiral symmetry breaking in QCD.

## 3 Chiral Effective Field Theory

Low-energy QCD is the physics of systems of light quarks at energy and momentum scales smaller than the 1 GeV mass gap observed in the hadron spectrum. This 1 GeV scale set by $4\pi f_\pi$ offers a natural separation between "light" and "heavy" (or, correspondingly, "fast" and "slow") degrees of freedom. The basic idea of an effective field theory is to introduce the active light particles as collective degrees of freedom, while the heavy particles are frozen and treated as (almost) static sources. The dynamics is described by an effective Lagrangian which incorporates all relevant symmetries of the underlying fundamental theory. In QCD, confinement and spontaneous chiral symmetry breaking implies that the "fast" degrees of freedom are the Nambu-Goldstone bosons. With Yukawa's pion in mind, we restrict ourselves to $N_f = 2$.

### 3.1 *The Nambu-Goldstone Boson Sector*

We first briefly summarize the steps [8, 9] required in the pure meson sector (baryon number $B = 0$) and later for the pion-nucleon sector ($B = 1$). A chiral field is introduced as

$$U(x) = \exp\left(\frac{i}{f_\pi}\,\vec{\tau}\cdot\vec{\pi}(x)\right) \in SU(2)\ , \tag{8}$$

with the Goldstone pion fields $\vec{\pi}(x)$ divided by the pion decay constant $f_\pi$ in the chiral limit ($m_\pi \to 0$). The QCD Lagrangian is replaced by an effective Lagrangian which involves the chiral field $U(x)$ and its derivatives:

$$\mathcal{L}_{QCD} \to \mathcal{L}_{eff}(U, \partial^\mu U, ...). \tag{9}$$

Goldstone bosons interact only when they carry non-zero four-momenta, so the low-energy expansion of (9) is an ordering in powers of $\partial^\mu U$. Lorentz invariance permits only even numbers of derivatives. One writes a series

$$\mathcal{L}_{\rm eff} = \mathcal{L}^{(2)}_{\pi\pi} + \mathcal{L}^{(4)}_{\pi\pi} + \dots\,, \tag{10}$$

where the leading term (the non-linear sigma model) involves just two derivatives:

$$\mathcal{L}^{(2)}_{\pi\pi} = \frac{f_\pi^2}{4}{\rm tr}(\partial^\mu U \partial_\mu U^\dagger)\,. \tag{11}$$

At fourth order, the terms permitted by symmetries are (apart from further contributions involving the light quark mass $m_q$ and external fields, not shown here):

$$\mathcal{L}^{(4)}_{\pi\pi} = \frac{\ell_1}{4}\Big[{\rm tr}(\partial^\mu U \partial_\mu U^\dagger)\Big]^2 + \frac{\ell_2}{4}{\rm tr}(\partial_\mu U \partial_\nu U^\dagger)\,{\rm tr}(\partial^\mu U \partial^\nu U^\dagger) + \dots\,, \tag{12}$$

The constants $\ell_1, \ell_2$ (following canonical notations [9]) absorb divergences of loops, and their finite scale-dependent parts must be determined from experiment.

The symmetry breaking mass term is small, so that it can be handled perturbatively, together with the power series in small momenta. The leading contribution introduces a term linear in the quark mass matrix $m_q = {\rm diag}(m_u, m_d)$:

$$\mathcal{L}^{(2)}_{\pi\pi} = \frac{f_\pi^2}{4}{\rm tr}(\partial_\mu U \partial^\mu U^\dagger) + \frac{f_\pi^2}{4}m_\pi^2\,{\rm tr}(U + U^\dagger)\,, \tag{13}$$

with $m_\pi^2 \sim (m_u + m_d)$. The fourth order term $\mathcal{L}^{(4)}_{\pi\pi}$ also receives explicit chiral symmetry breaking contributions (proportional to $m_q$ and $m_q^2$) with additional low-energy constants $\ell_{3,4}$.

To the extent that the effective Lagrangian includes all terms allowed by symmetries of QCD, the chiral effective field theory is the low-energy equivalent [21, 22] of the original QCD Lagrangian. Given the effective Lagrangian, the framework for systematic perturbative calculations of (on-shell) $S$-matrix elements involving Goldstone bosons, Chiral Perturbation Theory (ChPT), is then defined by the following rules:
Collect all Feynman diagrams generated by $\mathcal{L}_{eff}$. Classify all terms according to powers of a small quantity $p$ which stands generically for three-momenta or energies of Goldstone bosons, or for the pion mass $m_\pi$. The small expansion parameter is $q/(4\pi f_\pi)$. Loops are evaluated in dimensional regularization and get renormalized by appropriate chiral counter terms.

## 3.2 *The Chiral Pion-Nucleon Effective Lagrangian*

The prominent role played by the pion as a Goldstone boson of spontaneously broken chiral symmetry has its impact on the low-energy structure and dynamics of nucleons as well [23]. When probing the nucleon with long-wavelength electroweak fields, a substantial part of the response comes from the pion cloud, the "soft" surface of the nucleon. The calculational framework for this, baryon chiral perturbation theory [24, 25] has been applied quite successfully to a variety of low-energy processes (such as low-energy pion-nucleon scattering, threshold pion photo- and electroproduction and Compton scattering on the nucleon).

Consider now the sector with baryon number $B = 1$ and the physics of the pion-nucleon system. The nucleon is represented by an isospin-1/2 doublet, Dirac spinor $\Psi = \binom{p}{n}$ of proton and neutron. The free Lagrangian

$$\mathcal{L}_N^{\rm free} = \bar\Psi(i\gamma_\mu\partial^\mu - M_0)\Psi \tag{14}$$

includes the nucleon mass in the chiral limit, $M_0$. One should note that the nucleon, unlike the pion, has a large mass of the same order as the chiral symmetry breaking scale $4\pi f_\pi$, which survives in the limit of vanishing quark masses, $m_{u,d} \to 0$.

The previous pure meson Lagrangian $\mathcal{L}_{eff}$ is now replaced by $\mathcal{L}_{eff}(U, \partial^\mu U, \Psi, ...)$ which also includes the nucleon field. The additional term involving the nucleon, denoted by $\mathcal{L}_{\pi N}$, is expanded again in powers of derivatives (external momenta) of the Goldstone boson field and of the quark masses:

$$\mathcal{L}_{\pi N} = \mathcal{L}_{\pi N}^{(1)} + \mathcal{L}_{\pi N}^{(2)} + \dots \tag{15}$$

In the leading term, $\mathcal{L}_{\pi N}^{(1)}$ there is a replacement of $\partial^\mu$ by a chiral covariant derivative which introduces a vector current coupling between the pions and the nucleon. Secondly, there is an axial vector coupling. This structure of the $\pi N$ effective Lagrangian is again dictated by chiral symmetry. We have

$$\mathcal{L}_{\pi N}^{(1)} = \bar\Psi\Big[i\gamma_\mu(\partial^\mu + \Gamma^\mu) - M_0 + g_A\gamma_\mu\gamma_5\, u^\mu\Big]\Psi\,, \tag{16}$$

with vector and axial vector quantities involving the Goldstone boson (pion) fields via $\xi = \sqrt{U}$ in the form:

$$\Gamma^\mu = \frac{1}{2}[\xi^\dagger, \partial^\mu\xi] = \frac{i}{4f_\pi^2}\,\vec\tau\cdot(\vec\pi\times\partial^\mu\vec\pi) + ...\ \ , \tag{17}$$

$$u^\mu = \frac{i}{2}\{\xi^\dagger, \partial^\mu\xi\} = -\frac{1}{2f_\pi}\,\vec\tau\cdot\partial^\mu\vec\pi + ...\ \ , \tag{18}$$

where the last steps result when expanding $\Gamma^\mu$ and $u^\mu$ to leading order in the pion fields. So far, the only parameters that enter are the nucleon mass $M_0$, the pion decay constant $f_\pi$, and the nucleon axial vector coupling constant $g_A$, all three taken in the chiral limit.

At next-to-leading order, $\mathcal{L}_{\pi N}^{(2)}$, the chiral symmetry breaking quark mass term enters. It has the effect of shifting the nucleon mass from its value in the chiral limit to the physical one. The nucleon sigma term

$$\sigma_N = m_q\frac{\partial M_N}{\partial m_q} = \langle N|m_q(\bar uu + \bar dd)|N\rangle \tag{19}$$

measures the contribution of the non-vanishing quark mass, $m_q = \frac{1}{2}(m_u + m_d)$, to the nucleon mass $M_N$. Its empirical value is in the range $\sigma_N \simeq (45 \pm 8)$ MeV and has been deduced [26] by a sophisticated extrapolation of low-energy pion-nucleon data using dispersion relation techniques. Up to this point, the $\pi N$ effective Lagrangian, expanded to second order in the pion field, has the form

$$\begin{aligned}\mathcal{L}_{eff}^N &= \bar\Psi(i\gamma_\mu\partial^\mu - M_N)\Psi - \frac{g_A}{2f_\pi}\bar\Psi\gamma_\mu\gamma_5\vec\tau\,\Psi\cdot\partial^\mu\vec\pi \\ &\quad -\frac{1}{4f_\pi^2}\bar\Psi\gamma_\mu\vec\tau\,\Psi\cdot(\vec\pi\times\partial^\mu\vec\pi\,) + \frac{\sigma_N}{2f_\pi^2}\,\bar\Psi\Psi\,\vec\pi^{\,2} + ...\ \ ,\end{aligned} \tag{20}$$

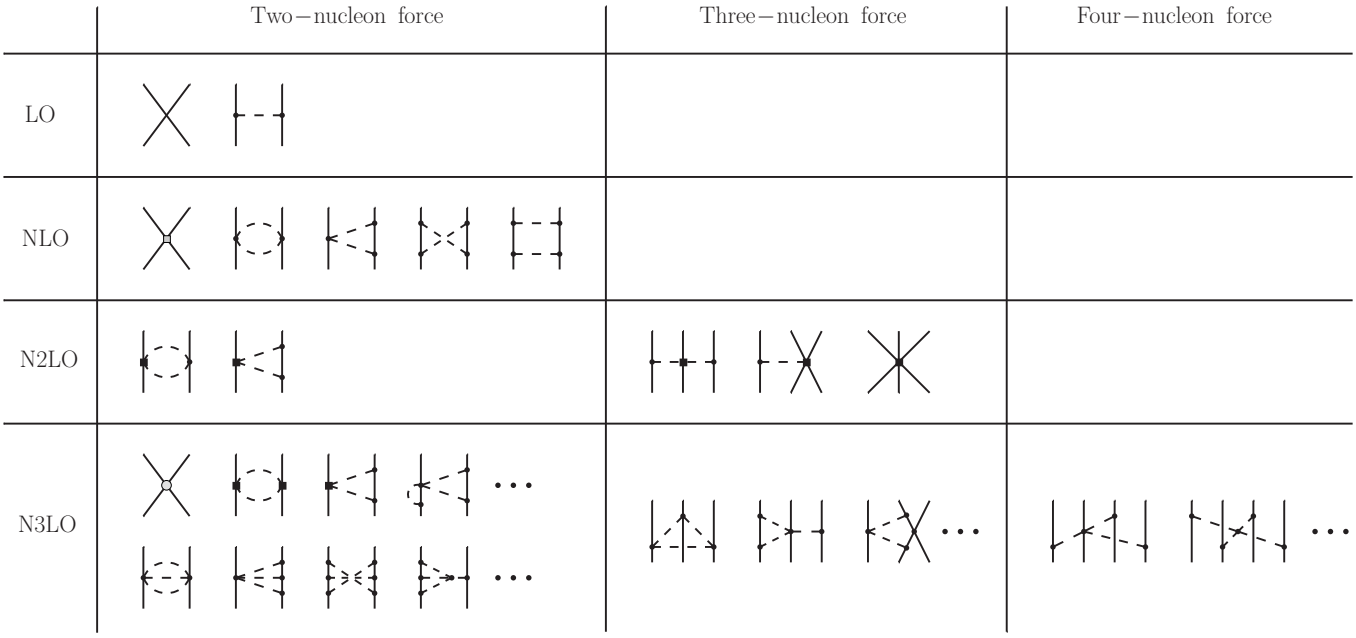


Figure 3: Hierarchical organization of nuclear forces in chiral effective field theory.

where we have not shown a series of additional terms involving $(\partial^\mu \vec{\pi})^2$ arising from the complete Lagrangian $\mathcal{L}^{(2)}_{\pi N}$. These terms come with further low-energy constants $c_{3,4}$ encoding physics at smaller distances or higher energies. These constants need to be fitted to experimental data, e.g. from pion-nucleon scattering.

The "effectiveness" of such an effective field theory relies on the proper identification of the active low-energy degrees of freedom. Pion-nucleon scattering is known to be dominated by the $p$-wave $\Delta(1232)$ resonance with spin and isospin 3/2. The excitation energy of this resonance, given by the mass difference $\Delta = M_\Delta - M_N \simeq 293\,\mathrm{MeV}$, is not large, although it does not vanish in the chiral limit. If the physics of the $\Delta(1232)$ is absorbed in low-energy constants of an effective theory that works with pions and nucleons only (as done in heavy-baryon ChPT), the limits of applicability of such a theory is clearly narrowed down to an energy-momentum range small compared to $\Delta$. The $B = 1$ chiral effective Lagrangian is therefore often extended [27] by incorporating the $\Delta(1232)$ isobar as an explicit degree of freedom.

# 4 Chiral Nuclear Interactions

## 4.1 *Two-nucleon interaction*

In this section, we briefly review the structure of the chiral nucleon-nucleon potential in momentum-space [10, 11, 12]. It amounts to a series of contributions from explicit multi-pion exchanges and short-distance contact-terms (shown in Fig. 3) controlled by chiral symmetry and an expansion in small external momenta. The leading-order contribution consists of the well-known one-pion exchange piece and two contact-terms operating in the spin-singlet and spin-triplet $S$-waves:

$$V^{(\mathrm{LO})}_{NN} = -\frac{g_A^2}{4f_\pi^2}\,\frac{\vec{\sigma}_1\cdot\vec{q}\;\vec{\sigma}_2\cdot\vec{q}}{m_\pi^2+q^2}\,\vec{\tau}_1\cdot\vec{\tau}_2 + C_S + C_T\,\vec{\sigma}_1\cdot\vec{\sigma}_2\,. \tag{21}$$

Here, $\vec{\sigma}_{1,2}$ and $\vec{\tau}_{1,2}$ denote usual spin- and isospin operators of the two nucleons and $\vec{q}$ is the momentum transfer between both nucleons. At next-to-leading order the two-pion exchange diagrams generated by

the vertices of the chiral $\pi N$-Lagrangian $\mathcal{L}^{(1)}_{\pi N}$ come into play. The corresponding potential reads [28]:

$$V_{NN}^{(2\pi-\mathrm{NLO})} = \frac{1}{384\pi^2 f_\pi^4}\Big\{4m_\pi^2(1+4g_A^2-5g_A^4)+q^2(1+10g_A^2-23g_A^4)-\frac{48g_A^4m_\pi^4}{4m_\pi^2+q^2}\Big\}L(q)\;\vec\tau_1\cdot\vec\tau_2 + \frac{3g_A^4}{64\pi^2 f_\pi^4}L(q)\,(\vec\sigma_1\cdot\vec\sigma_2\,\vec q^{\,2}-\vec\sigma_1\cdot\vec q\,\vec\sigma_2\cdot\vec q)\,, \tag{22}$$

with the logarithmic loop function

$$L(q)=\frac{\sqrt{4m_\pi^2+q^2}}{q}\ln\frac{q+\sqrt{4m_\pi^2+q^2}}{2m_\pi}\,. \tag{23}$$

Notably, there are only contributions to the isovector central channel and the isoscalar spin-spin and tensor channel of the NN-interaction. Additional polynomial pieces generated by the pion-loops have been left out in the above expression. Without loss of information, these can be absorbed into the most general contact-term at NLO:

$$V_{NN}^{(\mathrm{ct}-\mathrm{NLO})} = C_1\,\vec q^{\,2}+C_2\,\vec k^{\,2}+(C_3\,\vec q^{\,2}+C_4\,\vec k^{\,2})\,\vec\sigma_1\cdot\vec\sigma_2+\frac{i}{2}C_5\,(\vec\sigma_1+\vec\sigma_2)\cdot(\vec q\times\vec k\,) + C_6\,\vec\sigma_1\cdot\vec q\,\vec\sigma_2\cdot\vec q+C_7\,\vec\sigma_1\cdot\vec k\,\vec\sigma_2\cdot\vec k\,, \tag{24}$$

with $\vec k=(\vec p+\vec p\,')/2$ the half-sum of initial and final nucleon momenta. The low-energy contants $C_1,\ldots,C_7$ are adjustable parameters to be determined in fits to empirical NN-phase shifts. Note that $C_5$ parametrizes the strength of the short-distance spin-orbit NN-interaction. In fact it dominates over the finite-range contributions to the spin-orbit interaction which arise at higher orders. The low-energy constant $C_5$ will reappear in the discussion of the nuclear energy density functional, where the same coupling determines the (self-consistent) single-particle spin-orbit potential in finite nuclei proportional to the density gradient.

The most important pieces from chiral two-pion exchange which generate attraction in the isoscalar central channel and reduce the too strong $1\pi$-exchange isovector tensor force are still absent at this level. These arise first from subleading $2\pi$-exchange through the chiral $\pi\pi NN$ contact couplings $c_{1,3,4}$ in $\mathcal{L}^{(2)}_{\pi N}$ or from the inclusion of the $\Delta(1232)$-isobar as an explicit degree of freedom. In the first approach one gets [28]:

$$V_{NN}^{(2\pi-\mathrm{N^2LO})} = \frac{3g_A^2}{16\pi f_\pi^4}\Big[c_3\,q^2+2m_\pi^2(c_3-2c_1)\Big](2m_\pi^2+q^2)A(q) + \frac{g_A^2c_4}{32\pi f_\pi^4}(4m_\pi^2+q^2)A(q)\,(\vec\sigma_1\cdot\vec\sigma_2\,\vec q^{\,2}-\vec\sigma_1\cdot\vec q\,\vec\sigma_2\cdot\vec q)\,\vec\tau_1\cdot\vec\tau_2\,, \tag{25}$$

with the loop function

$$A(q)=\frac{1}{2q}\arctan\frac{q}{2m_\pi}\,. \tag{26}$$

At the same order there are additional relativistic $1/M_N$-corrections to $2\pi$-exchange. Their explicit form depends on the precise definition of the nucleon-nucleon potential $V_{NN}$, which by itself is not an observable. Covariant perturbation theory [28] and the method of unitary transformations [10] thus lead to slightly different expressions for these small $1/M_N$-corrections. As the state of the art, the chiral NN-potential has been constructed up to order $\mathrm{N^3LO}$ and it includes two-loop $2\pi$-exchange, $3\pi$-exchange and contact-terms quartic in the momenta parametrized by 15 additional low-energy constants $D_1,\ldots,D_{15}$. When inserted into the Lippmann-Schwinger equation (in order to solve for the unitary $S$-matrix or the $T$-matrix) the chiral NN-potential is multiplied by an exponential regulator function with

a cutoff scale $\Lambda = 500 - 700\,\mathrm{MeV}$ in order to restrict the potential to the low-momentum region where chiral perturbation theory is applicable. Furthermore, methods of spectral function regularization [10] have been employed in order to eliminate the high-momentum region in the pion-loop integrals directly. In this case the loop functions $L(q)$ and $A(q)$ receive an additional dependence on a regulator scale $\tilde{\Lambda}$.

At order N$^3$LO the chiral NN-potential reaches the quality of a "high-precision" potential in reproducing empirical NN-phase shifts and deuteron properties. At the same time it provides the appropriate two-body interaction constrained by chiral symmetry of QCD for nuclear few- and many-body calculations.

## 4.2 *Nuclear Many-Body Forces*

Within the chiral effective field theory framework employing nucleons and pions as the explicit degrees of freedom, the leading-order contribution to the nuclear three-body force arises at order N$^2$LO and consists of three terms. The two-pion exchange three-nucleon force contains terms proportional to the low-energy constants $c_1$, $c_3$, and $c_4$ and has the form

$$V_{3N}^{(2\pi)} = \sum_{i\neq j\neq k} \frac{g_A^2}{8f_\pi^4} \frac{\vec{\sigma}_i\cdot\vec{q}_i\,\vec{\sigma}_j\cdot\vec{q}_j}{(\vec{q}_i^{\,2}+m_\pi^2)(\vec{q}_j^{\,2}+m_\pi^2)} F_{ijk}^{\alpha\beta}\tau_i^\alpha\tau_j^\beta\,, \tag{27}$$

where $\vec{q}_i$ denotes the difference between the final and initial momenta of nucleon $i$, and the isospin tensor $F_{ijk}^{\alpha\beta}$ is explicitly written

$$F_{ijk}^{\alpha\beta} = \delta^{\alpha\beta}\left(-4c_1m_\pi^2 + 2c_3\,\vec{q}_i\cdot\vec{q}_j\right) + c_4\,\epsilon^{\alpha\beta\gamma}\tau_k^\gamma\,\vec{\sigma}_k\cdot(\vec{q}_i\times\vec{q}_j)\,, \tag{28}$$

resulting in $c_1$ and $c_3$ terms proportional to $\vec{\tau}_i\cdot\vec{\tau}_j$ and the $c_4$ term proportional to $\vec{\tau}_k\cdot(\vec{\tau}_i\times\vec{\tau}_j)$. The low-energy constants $c_1$, $c_3$, and $c_4$ can be fit to pion-nucleon [29] or nucleon-nucleon scattering data [30, 31].

The one-pion exchange term in the N$^2$LO chiral three-nucleon interaction is proportional to the low-energy constant $c_D$ and has the form

$$V_{3N}^{(1\pi)} = -\sum_{i\neq j\neq k} \frac{g_A c_D}{8f_\pi^4\,\Lambda} \frac{\vec{\sigma}_j\cdot\vec{q}_j}{\vec{q}_j^{\,2}+m_\pi^2}\,\vec{\sigma}_i\cdot\vec{q}_j\,\vec{\tau}_i\cdot\vec{\tau}_j\,, \tag{29}$$

while the three-nucleon contact interaction introduces the low-energy constant $c_E$:

$$V_{3N}^{(\mathrm{ct})} = \sum_{i\neq j\neq k} \frac{c_E}{2f_\pi^4\,\Lambda}\,\vec{\tau}_i\cdot\vec{\tau}_j\,, \tag{30}$$

where $\Lambda = 700$ MeV sets a natural scale. The low-energy constants $c_D$ and $c_E$, associated with the one-pion exchange and contact three-nucleon forces respectively, ideally are fit to properties of three-body systems only. The binding energies of $A = 3$ nuclei and the $\beta$-decay lifetime of $^3$H provide largely uncorrelated nuclear observables with which to fit these two low-energy constants [32].

At order N$^3$LO in the chiral power counting, corresponding to $\mathcal{O}(q^4)$ in powers of momentum, additional three- and four-nucleon force contributions arise without any additional undetermined low-energy constants. The N$^3$LO three-body force can be written schematically as

$$V_{3N}^{(4)} = V_{2\pi}^{(4)} + V_{2\pi-1\pi}^{(4)} + V_{\mathrm{ring}}^{(4)} + V_{1\pi-\mathrm{cont.}}^{(4)} + V_{2\pi-\mathrm{cont.}}^{(4)} + V_{1/m}^{(4)}, \tag{31}$$

where the individual terms denote specific topologies. The $2\pi$ and $1\pi-$cont. topologies are present already in the N$^2$LO chiral three-nucleon force, whereas the $2\pi-1\pi$, ring, and $2\pi-$cont. topologies enter first at order N$^3$LO. All contributions have been worked out and presented in refs. [33, 34, 35]. The N$^3$LO four-nucleon force requires the evaluation of much fewer diagrams than the N$^3$LO three-body force, and the resulting analytic expressions (presented in ref. [36]) are also considerably simpler.

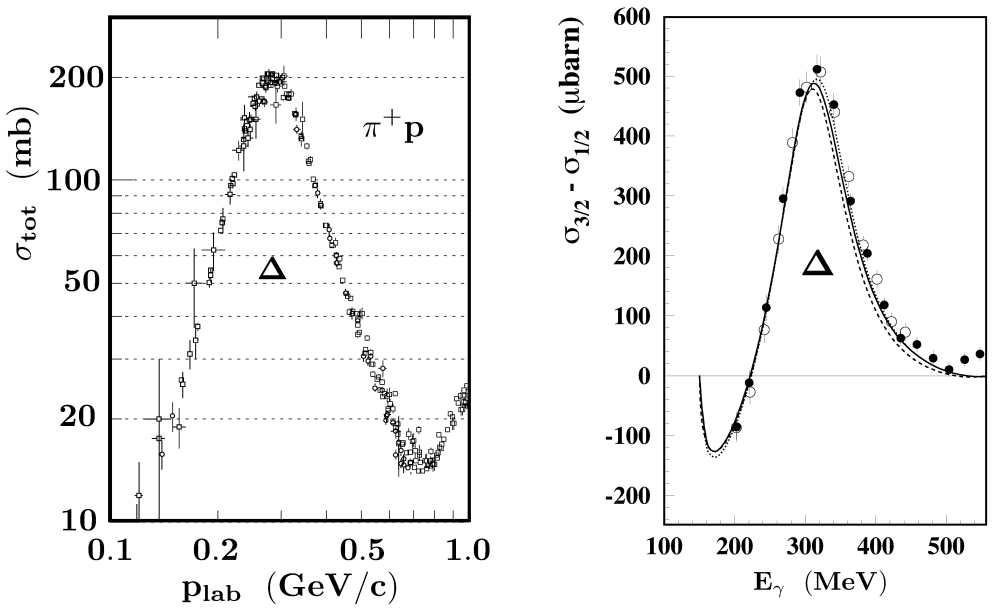


Figure 4: Left: Total $\pi^+ p$ cross section in the region of the $\Delta(1232)$ resonance (adapted from [37]). Right: Difference of polarized Compton scattering cross sections of the proton, $\sigma_{3/2}$ and $\sigma_{1/2}$, referring to channels with total angular momentum $\frac{3}{2}$ and $\frac{1}{2}$, respectively. Data taken from [38]. Curves represent dispersion relation and multipole analysis cited in [38].

### 4.3 *Role of Explicit $\Delta(1232)$ Degrees of Freedom*

The standard version of chiral meson-baryon effective field theory works with pions and nucleons only, both of which are stable particles with respect to the strong interaction. Effects of the $\Delta(1232)$ are encoded in low-energy constants such as $c_3$ and $c_4$ that are determined either by pion-nucleon scattering data or by fits to nucleon-nucleon phase shifts.

On the other hand, the mass difference between the $\Delta(1232)$ isobar and the nucleon is only about $0.3\,\mathrm{GeV} \simeq 2m_\pi$, yet another "small" scale compared to the chiral symmetry breaking scale, $4\pi f_\pi \sim 1\,\mathrm{GeV}$. This suggests incorporating the $\Delta(1232)$ as an additional *explicit* degree of freedom in the effective field theory. In fact the $\Delta$ isobar is by far the dominant feature in the excitation spectrum of the nucleon observed in pion and photon scattering measurements. An example is the strong spin-isospin excitation observed in pion-nucleon scattering (see Fig. 4, left). The $\Delta(1232)$ is also seen prominently in polarized Compton scattering on the proton (Fig. 4, right).

In the low-energy expansion of the spin-independent $\pi N$ scattering amplitude, the strong spin-isospin response of the nucleon manifests itself in a large "axial" polarizabilty:

$$\alpha_A^{(\Delta)} = \frac{g_A^2}{f_\pi^2 (M_\Delta - M_N)} \simeq 5\,\mathrm{fm}^3 \quad . \tag{32}$$

Here the factor $g_A^2/f_\pi^2$ comes from the axial vector coupling of the pion that drives the $\pi N \to \Delta$ transition. The mere magnitude of this polarizability, several times the volume of the nucleon itself, already illustrates the importance of this effect.

When implemented in the nucleon-nucleon interaction, the $\Delta$ isobar plays an important role in two-pion exchange processes such as the one shown in Fig. 5 (left). This mechanism contributes a large

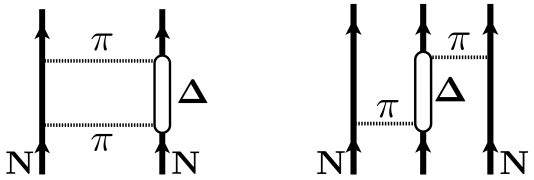


Figure 5: Left panel: two-pion exchange involving a virtual $N \to \Delta \to N$ transition. Right panel: three-nucleon interaction generated by the same mechanism.

part of the attractive isoscalar central part of the NN interaction [39], the one often parametrized in terms of an ad-hoc "sigma" boson in phenomenological one-boson exchange potentials. A parameter-free calculation of this isoscalar central potential with single and double $\Delta$ excitation [40] agrees almost perfectly with phenomenological "$\sigma$" exchange at distances r $> 2$ fm, but not at shorter distances. The detailed behavior of the $2\pi$-exchange isoscalar central potential with virtual excitation of a single $\Delta$ is instead more reminiscent of a van der Waals potential:

$$V_C^{N\Delta}(r) = -\frac{3g_A^2\,\alpha_A^{(\Delta)}}{(8\pi f_\pi)^2}\,\frac{e^{-2m_\pi r}}{r^6}P(m_\pi r) \quad , \tag{33}$$

where $P(x) = 6 + 12x + 10x^2 + 4x^3 + x^4$ is a fourth-order polynomial in $x = m_\pi r$. The familiar $r^{-6}$ dependence of the non-relativistic van der Waals interaction emerges in the chiral limit, $m_\pi \to 0$.

When "integrating out" the $\Delta$ degrees of freedom, the van der Waals – like two-pion exchange mechanism just described – gives rise to an important effective three-nucleon interaction, Fig. ref2piDelta (right), that was actually suggested already more than half a century ago by Fujita and Miyazawa [41]. In a many-body framework with explicit $\Delta$ degrees of freedom, such a mechanism automatically occurs as an iterated one-pion exchange process involving the $N \to \Delta \to N$ transition. In this case the low-energy constants $c_3$ and $c_4$ in eq. (28), the ones related to $p$-wave pion-nucleon scattering, are readjusted and considerably reduced in magnitude since they have to account only for the remaining non-resonant background, once the $\Delta(1232)$ is treated explicitly. Then important physics of the $\Delta$ such as the terms illustrated in Fig. 5 (left) are actually promoted from N$^2$LO to NLO in the chiral hierarchy of NN interaction terms [10], leading to improved convergence.

These considerations about the role of the $\Delta(1232)$ in the low-energy description of nuclear forces should already suffice to answer one of the principal questions at the starting point of the chiral effective field theory approach: how much information about the intrinsic structure of the nucleon is actually needed in order for this theory to work efficiently? The $\Delta(1232)$ is indeed by far the dominant feature of nucleon structure in the relevant low-energy range. Other, less prominent properties such as baryon resonances appearing at higher energies are conveniently absorbed in the set of low-energy constants.

# 5 Nuclear Chiral Dynamics

## 5.1 *In-medium Chiral Perturbation Theory: Nuclear Matter*

The tool to investigate the implications of spontaneous and explicit chiral symmetry breaking in QCD is chiral perturbation theory [9]. Observables are calculated within the framework of an effective field theory of interacting pions (Goldstone bosons) and nucleons [25]. The diagrammatic expansion in the number of loops has a one-to-one correspondence to an expansion in small external momenta and the pion (or light quark) mass. In nuclear matter, the relevant momentum scale is the Fermi momentum $k_f$, related to the nucleon density by $\rho = 2k_f^3/3\pi^2$. At the empirical saturation density $\rho_0 \simeq 0.16\,\mathrm{fm}^{-3}$ the Fermi momentum and the pion mass are of comparable magnitude, $k_{f0} \simeq 2m_\pi$. This immediately

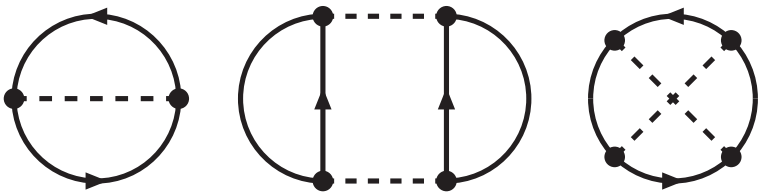

Figure 6: One-pion exchange Fock diagram and iterated one-pion exchange Hartree and Fock diagrams contributing to the energy density $\rho\bar{E}(k_f)$ of isospin-symmetric nuclear matter.

implies that pions must be included as explicit degrees of freedom: their propagation in nuclear matter is resolvable and thus relevant at the densities of interest. With two small scales, $k_f$ and $m_\pi$, at hand the nuclear matter equation of state as obtained from in-medium chiral perturbation theory will be given by an expansion in powers of the Fermi momentum. The expansion coefficients are non-trivial functions of $k_f/m_\pi$, the dimensionless ratio of the two relevant small scales inherent to the problem.

The only new feature in performing calculations in a nuclear many-body system (as compared to scattering processes in the vacuum) is the in-medium nucleon propagator. For a non-relativistic nucleon with four-momentum $p^\mu = (p_0, \vec{p})$ it reads:

$$G(p_0, \vec{p}) = \frac{i}{p_0 - \vec{p}^{\,2}/2M_N + i\epsilon} - 2\pi\delta(p_0 - \vec{p}^{\,2}/2M_N)\,\theta(k_f - |\vec{p}|)\,, \tag{34}$$

where the second term, the so-called "medium insertion", accounts for the presence of a filled Fermi sea of nucleons. The expression for $G(p_0, \vec{p})$ is identical to the conventional decomposition of the in-medium propagator into particle and hole components used in non-relativistic many-body perturbation theory. With the decomposition into vacuum propagator and medium insertion, closed multi-loop diagrams representing the energy density can then be organized systematically in the number of medium insertions. The non-relativistic approximation is also compatible with the $k_f$-expansion at leading order.

We outline the leading contributions to the energy per particle $\bar{E}(k_f)$ of isospin-symmetric spin-saturated nuclear matter [42]. The relativistically improved kinetic energy is of course well-known:

$$\bar{E}(k_f)^{(\mathrm{kin})} = \frac{3k_f^2}{10M_N} - \frac{3k_f^4}{56M_N^3}\,. \tag{35}$$

Nuclear chiral dynamics up to three loop-order introduces the closed one- and two-ring diagrams shown in Fig. 6. The contribution of the one-pion exchange Fock term (represented by the left diagram) to the energy per particle reads:

$$\bar{E}(k_f)^{(1\pi)} = \frac{3g_A^2 m_\pi^3}{(4\pi f_\pi)^2}\Big\{\frac{u^3}{3} + \frac{1}{8u} - \frac{3u}{4} + \arctan 2u - \Big(\frac{3}{8u} + \frac{1}{32u^3}\Big)\ln(1+4u^2)\Big\}\,, \tag{36}$$

with the dimensionless variable $u = k_f/m_\pi$. Next in the $k_f$-expansion come the contributions from iterated (second-order) $1\pi$-exchange. The latter refers to the (two-particle) reducible part of the planar $2\pi$-exchange box diagram which gets enhanced by a small energy denominator proportional to differences of nucleon kinetic energies. The corresponding Hartree term (see middle diagram in Fig. 6) with two medium insertions reads:

$$\bar{E}(k_f)^{(H2)} = \frac{3g_A^4 M_N m_\pi^4}{5(8\pi)^3 f_\pi^4}\Big\{\frac{9}{2u} - 59u + (60+32u^2)\arctan 2u - \Big(\frac{9}{8u^3} + \frac{35}{2u}\Big)\ln(1+4u^2)\Big\}\,. \tag{37}$$

The analytical evaluation of this contribution is based on the iterated $1\pi$-exchange amplitude in the forward direction. For the Fock diagram (see right diagram in Fig. 6) with two medium insertions

one encounters, in the same way, the iterated $1\pi$-exchange amplitude in the backward direction. The corresponding contribution to the energy per particle reads:

$$\bar{E}(k_f)^{(F2)} = \frac{g_A^4 M_N m_\pi^4}{(4\pi)^3 f_\pi^4}\Big\{\frac{u^3}{2} + \int_0^u dx \frac{3x(u-x)^2(2u+x)}{2u^3(1+2x^2)}\Big[(1+8x^2+8x^4)\arctan x - (1+4x^2)\arctan 2x\Big]\Big\}\,. \tag{38}$$

Note that the expressions for these two-body terms do not include the contribution of a linear divergence $\int_0^\infty dl\,1$ of the momentum-space loop integral. Such a linear divergence is set to zero in dimensional regularization, but employing a cutoff regularization gives a contribution proportional to the momentum cutoff $\Lambda$. There is an interpretational problem with results of dimensional regularization. Contributions which are expected to be attractive according to second-order perturbation theory arguments show only their finite repulsive parts. We restore the attractive component via a term linear in the cutoff and the density

$$\bar{E}(k_f)^{(\Lambda)} = -\frac{10 g_A^4 M_N}{(4\pi f_\pi)^4}\,\Lambda\, k_f^3\,, \tag{39}$$

to which the Hartree and Fock diagrams have contributed in the ratio $4:1$.

The Pauli blocking corrections due to the nuclear medium are included through diagrams with three medium insertions. The corresponding Hartree term has the form:

$$\bar{E}(k_f)^{(H3)} = \frac{9 g_A^4 M_N m_\pi^4}{(4\pi f_\pi)^4 u^3}\int_0^u dx\, x^2 \int_{-1}^1 dy \Big[2uxy + (u^2 - x^2y^2)\ln\frac{u+xy}{u-xy}\Big]\Big\{\frac{2s^2+s^4}{1+s^2} - 2\ln(1+s^2)\Big\}\,, \tag{40}$$

with the abbreviation $s = xy + \sqrt{u^2 - x^2 + x^2y^2}$. Similarly, the Fock-diagram in Fig. 6 containing three medium insertions has the form:

$$\bar{E}(k_f)^{(F3)} = \frac{9 g_A^4 M_N m_\pi^4}{(4\pi f_\pi)^4 u^3}\int_0^u dx\Big\{\frac{G^2}{8} + \frac{x^2}{4}\int_{-1}^1 dy \int_{-1}^1 dz \frac{yz\,\theta(y^2+z^2-1)}{|yz|\sqrt{y^2+z^2-1}}\Big[s^2 - \ln(1+s^2)\Big]\Big[\ln(1+t^2) - t^2\Big]\Big\}\,, \tag{41}$$

with the auxiliary function,

$$G = u(1+u^2+x^2) - \frac{1}{4x}[1+(u+x)^2][1+(u-x)^2]\ln\frac{1+(u+x)^2}{1+(u-x)^2}\,, \tag{42}$$

and $t = xz + \sqrt{u^2 - x^2 + x^2z^2}$. Let us emphasize that Pauli blocking has been treated here exactly, without employing any simplification due to angular averaging.

Summing the contributions to the energy per particle $\bar{E}(k_f)$ listed above and treating the cutoff scale $\Lambda$ as an adjustable parameter to incorporate (in a global fashion) unresolved short-distance dynamics, one obtains the equation of state of nuclear matter as shown in Fig. 7. With a fine-tuned cutoff scale of $\Lambda = 611\,\mathrm{MeV}$, the saturation minimum lies at $\rho_0 = 0.173\,\mathrm{fm}^{-3}$ and $\bar{E}(k_{f0}) = -15.3\,\mathrm{MeV}$. The nuclear matter compressibility, related to the curvature of the saturation line at its minimum, comes out as $K = k_{f0}^2 \bar{E}''(k_{f0}) = 252\,\mathrm{MeV}$, in good agreement with the presently accepted empirical value of $K = (250 \pm 50)\,\mathrm{MeV}$ [43, 44, 45]. Although this looks at first sight to be a very successful reproduction of nuclear matter bulk properties, one should not hide the fact that strong cancellations between individually large terms of opposite sign are involved here. For example, the adjusted term linear in density amounts to $-177.4\,\mathrm{MeV}$ at saturation density. The feature that strong cancellations are involved, which is also common to other approaches to nuclear matter, does not allow to make definite statements about the convergence of the $k_f$-expansion or to give reliable theoretical error bars. The appropriate framework to address such questions is a many-body calculation based on chiral low-momentum interactions whose long- and short-distance parts are determined together by empirical NN phase shifts and not separated any further.

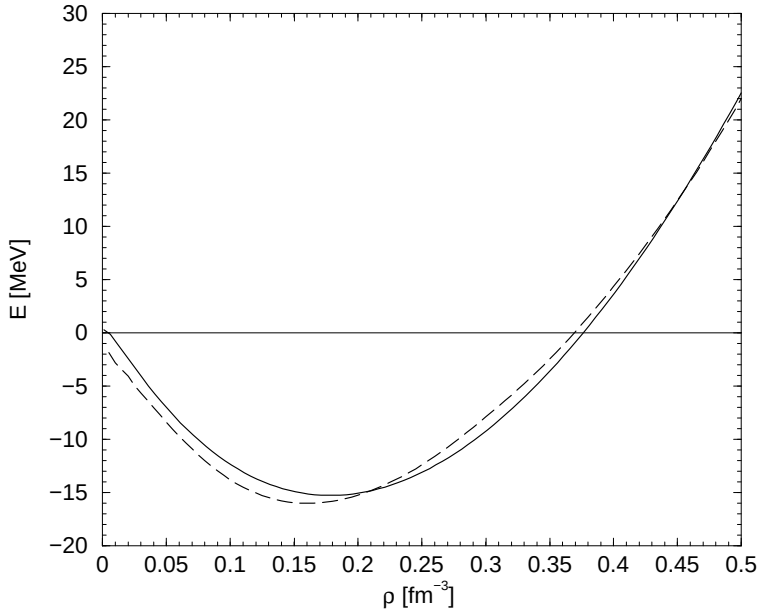


Figure 7: Saturation curve of nuclear matter obtained from $1\pi$-exchange and iterated $1\pi$-exchange together with a fine-tuned short-distance term linear in density. The dashed line stems from the many-body calculation of ref. [46].

Let us now give an explanation for how saturation of nuclear matter is achieved in the framework of in-medium chiral perturbation theory. For that purpose it is instructive to consider the following simple parametrization of the energy per particle [42]:

$$\bar{E}(k_f) = \frac{3k_f^2}{10M_N} - \alpha\frac{k_f^3}{M_N^2} + \beta\frac{k_f^4}{M_N^3}\,, \tag{43}$$

which includes an attractive $k_f^3$-term and a repulsive $k_f^4$-term. This two-parameter form has generically a saturation minimum if $\alpha, \beta > 0$. Its striking feature is than once $\alpha = 5.27$ and $\beta = 12.22$ are adjusted to the empirical saturation point $\rho_0 = 0.16\,\mathrm{fm}^{-3}$, $\bar{E}_0 = -16$ MeV the compressibility $K \simeq 240\,\mathrm{MeV}$ comes out correctly. Moreover, such a parametrized curve for $\bar{E}(k_f)$ follows the results of sophisticated many-body calculations [46] up to quite high densities $\rho \simeq 1\,\mathrm{fm}^{-3}$.

In the chiral limit $m_\pi = 0$ the leading interaction contributions calculated from $1\pi$- and iterated $1\pi$-exchange turn into exactly such a two-parameter form with the coefficient $\beta$ of the $k_f^4$-term given by [42]:

$$\beta = \frac{3}{70}\left(\frac{g_{\pi N}}{4\pi}\right)^4(4\pi^2 + 237 - 24\ln 2) = 13.6\,, \tag{44}$$

where $g_{\pi N} = g_A M_N/f_\pi = 13.2$ is the strong pion-nucleon coupling constant. This number is quite close to $\beta = 12.22$ as extracted from a realistic nuclear matter equation of state. The mechanism for nuclear matter to saturate can be summarized roughly as follows: while pion-exchange at second order generates the necessary attraction, the Pauli-blocking effects due to the nuclear medium counteract this attraction in the form of a repulsive contribution with a stronger density dependence (a $k_f^4$-term).

Calculations of nuclear matter in this framework have been extended further by including the (irreducible) two-pion exchange contributions in the medium [39]. A compact form of the corresponding Fock term is given in terms of a (subtracted) spectral function representation:

$$\bar{E}(k_f)^{(2\pi F)} \;=\; \frac{1}{8\pi^3}\int_{2m_\pi}^{\infty} d\mu\,\mathrm{Im}(V_C + 3W_C + 2\mu^2 V_T + 6\mu^2 W_T)\Big\{3\mu k_f - \frac{4k_f^3}{3\mu}$$

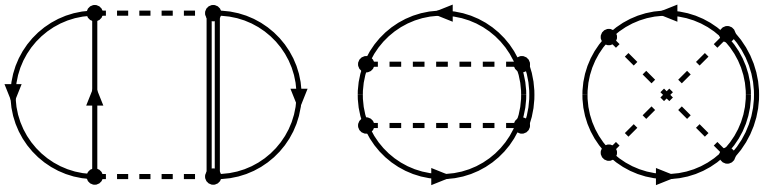

Figure 8: Hartree and Fock three-body diagrams related to $2\pi$-exchange with virtual $\Delta(1232)$-isobar excitation. They represent long-range interactions between three nucleons in the Fermi sea.

$$+\frac{8k_f^5}{5\mu^3}-\frac{\mu^3}{2k_f}-4\mu^2\arctan\frac{2k_f}{\mu}+\frac{\mu^3}{8k_f^3}(12k_f^2+\mu^2)\ln\left(1+\frac{4k_f^2}{\mu^2}\right)\Big\}\,, \tag{45}$$

where $\mathrm{Im}V_C$, $\mathrm{Im}W_C$, $\mathrm{Im}V_T$ and $\mathrm{Im}W_T$ are the imaginary parts (or spectral functions) of the isoscalar and isovector central and tensor NN-amplitudes, respectively. At this level also the $2\pi$-exchange with excitation of virtual $\Delta(1232)$-isobars comes into play. It is known to provide a dominant mechanism for intermediate range attraction in the isoscalar central channel [40]. Furthermore, the Pauli-blocking effects to these $\Delta(1232)$-induced $2\pi$-exchange mechanisms, as represented by diagrams with three medium insertions, are equivalent to contributions from genuine long-range three-body forces. The two-ring Hartree diagram in Fig. 8 leads to the following contribution to the energy per particle [39]:

$$\bar{E}(k_f)^{(\Delta H3)}=\frac{g_A^4m_\pi^6}{\Delta(2\pi f_\pi)^4}\Big[\frac{2}{3}u^6+u^2-3u^4+5u^3\arctan 2u-\frac{1}{4}(1+9u^2)\ln(1+4u^2)\Big]\,, \tag{46}$$

with $\Delta=293\,\mathrm{MeV}$ the delta-nucleon mass splitting. On the other hand, the total contribution of the one-ring Fock diagrams in Fig. 8 reads:

$$\bar{E}(k_f)^{(\Delta F3)}=-\frac{3g_A^4m_\pi^6u^{-3}}{4\Delta(4\pi f_\pi)^4}\int_0^u dx\Big[2G_S^2(x,u)+G_T^2(x,u)\Big]\,, \tag{47}$$

where we have introduced the two auxiliary functions:

$$\begin{aligned}G_S(x,u) &= \frac{4ux}{3}(2u^2-3)+4x\Big[\arctan(u+x)+\arctan(u-x)\Big]\\ &\quad+(x^2-u^2-1)\ln\frac{1+(u+x)^2}{1+(u-x)^2}\,,\end{aligned} \tag{48}$$

$$\begin{aligned}G_T(x,u) &= \frac{ux}{6}(8u^2+3x^2)-\frac{u}{2x}(1+u^2)^2\\ &\quad+\frac{1}{8}\Big[\frac{(1+u^2)^3}{x^2}-x^4+(1-3u^2)(1+u^2-x^2)\Big]\ln\frac{1+(u+x)^2}{1+(u-x)^2}\,.\end{aligned} \tag{49}$$

Evidently, the three-body Hartree term is repulsive while the corresponding Fock term is weakly attractive.

The subtraction constants asscociated with the spectral function representation eq. (45) give rise to short-distance contributions of the form

$$\bar{E}(k_f)^{(sd)}=B_3\frac{k_f^3}{M_N^2}+B_5\frac{k_f^5}{M_N^4}+B_6\frac{k_f^6}{M_N^5}\,, \tag{50}$$

where the last term stems from a three-body contact term. The parameters $B_3, B_5, B_6$ are assumed to represent all unresolved short-distance NN-dynamics relevant for isospin-symmetric nuclear matter at

low and moderate densities. They are adjusted to few empirical bulk properties of nuclear matter, and thereafter the approach is able to make predictions for more detailed quantities like the single-particle potential or the thermodynamic properties of nuclear matter at finite temperatures. Another benefit of this approach is that the pion-mass dependence of all interaction terms is explicitly known. By differentiating the nuclear matter equation of state with respect to the light quark mass or pion mass one gets access to the density and temperature dependent chiral condensate $\langle \bar{q}q \rangle(\rho, T)$.

## 5.2 *Resummation Strategies for Neutron Matter at Low Densities*

Dilute degenerate many-fermion systems with large scattering lengths have attracted much interest in recent years [47]. Experimental advances have allowed the possibility to tune (magnetically) atomic interactions in ultracold fermionic gases through so-called Feshbach resonances, enabling the exploration of weakly and strongly interacting many-body systems together with transitions from the superconducting BCS phase to the Bose-Einstein condensed state. Of special interest is the so-called unitary limit in which the two-body interaction is capable of supporting a single bound state at zero energy and the $S$-wave scattering length diverges, $a \to \infty$. Under these conditions the strongly-interacting many-fermion system is scale invariant. The ground-state energy per particle is then determined by a universal number, the so-called Bertsch parameter $\xi$, which is equal to the ratio of the energy per particle of the strongly interacting system at unitary, $\bar{E}(k_f)^{(\infty)}$, to that of a free Fermi gas, $\bar{E}(k_f)^{(0)} = 3k_f^2/10M$.

Low-density ($\rho_n = k_f^3/3\pi^2 < 0.05\,\mathrm{fm}^3$) neutron matter is expected to behave as a unitary Fermi gas due to the very large neutron-neutron $S$-wave scattering length, $a_{nn} \simeq 19\,\mathrm{fm}$ [48]. The results of a variety of sophisticated many-body calculations [49, 50] indicate that at low densities the interactions behind the large neutron-neutron $S$-wave scattering length lead to a reduction of the free Fermi gas energy by approximately a factor $\xi_{nn} \simeq 1/2$.

Here, we outline the basic steps of a novel resummation technique [51] which allows to sum up the complete series of fermionic in-medium ladder diagrams generated by a contact interaction proportional to the scattering length $a$. The solution of this (restricted) problem is enabled through a different organization of the many-body calculation. Instead of treating particles and holes separately, one keeps them together and takes into account effects of the filled Fermi sea by a "medium-insertion". This approach is realized by the following identical rewriting of the (non-relativistic) in-medium single-particle propagator:

$$\begin{aligned} G(p_0, \vec{p}) &= i\Big(\frac{\theta(|\vec{p}| - k_f)}{p_0 - \vec{p}^{\,2}/2M + i\epsilon} + \frac{\theta(k_f - |\vec{p}|)}{p_0 - \vec{p}^{\,2}/2M - i\epsilon}\Big) \\ &= \frac{i}{p_0 - \vec{p}^{\,2}/2M + i\epsilon} - 2\pi\,\delta(p_0 - \vec{p}^{\,2}/2M)\,\theta(k_f - |\vec{p}|)\,, \end{aligned} \tag{51}$$

for an internal fermion line with energy $p_0$ and momentum $\vec{p}$. In the above equation, $M$ denotes the large fermion mass.

Many-body contributions to the energy per particle come from diagrams with at least two medium-insertions. For the closed ladder diagram, shown to the left in Fig. 9, this minimal pair of medium-insertions must be placed on opposing positions of the double-ring. By opening them one obtains a planar ladder diagram containing energy denominators that are all given as differences of fermion kinetic energies. It is only for this planar topology that the factors of $M$ from the energy denominators balance the $1/M$ factors coming from the interaction vertices in such a way that in the non-relativistic limit a finite result remains (to any order $a^n$). The open ladder diagram, shown to the right in Fig. 9, comes in with additional medium-insertions on internal lines in all possible ways. Due to the special nature of the momentum-independent contact interaction, all multi-loop diagrams factorize (successive loops are independent), which allows their sum to be written in the form of a power of the in-medium loop.

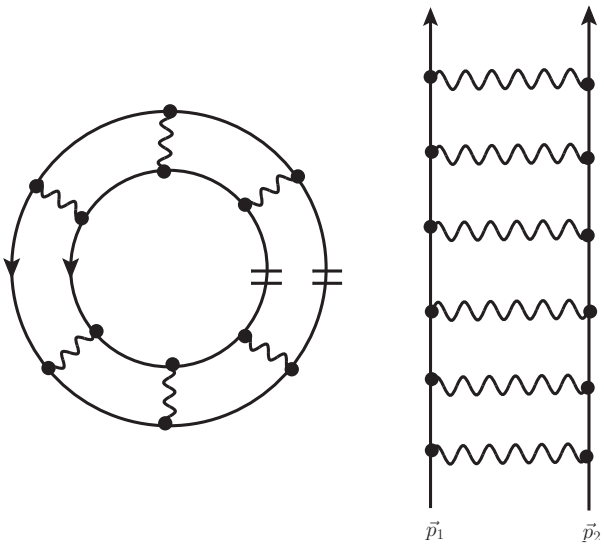


Figure 9: Left: Closed multi-loop diagram representing a contribution to the energy density. Right: Planar ladder diagram obtained by opening at a minimal pair of adjacent medium-insertions. Wavy lines symbolize the contact interaction proportional to the scattering length $a$.

The in-medium loop is decomposed into contributions from zero, one and two medium insertions: $B_0 + B_1 + B_2$ (see Fig. 10). The first term $B_0$ is the well-known rescattering in vacuum:

$$B_0 = 4\pi a \int \frac{d^3l}{(2\pi)^3} \frac{1}{\vec{l}^2 - \vec{q}^2 - i\epsilon} = \frac{2a}{\pi} \int_0^\infty dl \left(1 + \frac{\vec{q}^2}{l^2 - \vec{q}^2 - i\epsilon}\right) = 0 + i\, a|\vec{q}\,|\,, \tag{52}$$

where the rule $\int_0^\infty dl\, 1 = 0$ of dimensional regularization has been exploited. In a regularization scheme employing a momentum-space cutoff, the emerging scale-dependent constant $-2\Lambda/\pi$ can be absorbed into $a^{-1}$, from which one defines the renormalized (or physical) scattering length. The expression for the contribution $B_1$ to the in-medium loop with one medium insertion reads:

$$B_1 = -4\pi a \int \frac{d^3l}{(2\pi)^3} \frac{1}{\vec{l}^2 - \vec{q}^2 - i\epsilon} \Big\{\theta(k_f - |\vec{P} - \vec{l}\,|) + \theta(k_f - |\vec{P} + \vec{l}\,|)\Big\}\,. \tag{53}$$

Solving this integral, one obtains the following result for the real part:

$$\mathrm{Re}\, B_1 = -\frac{ak_f}{\pi}\, R(s,\kappa)\,, \tag{54}$$

where

$$R(s,\kappa) = 2 + \frac{1}{2s}[1 - (s+\kappa)^2] \ln\frac{1+s+\kappa}{|1-s-\kappa|} + \frac{1}{2s}[1 - (s-\kappa)^2] \ln\frac{1+s-\kappa}{1-s+\kappa}\,, \tag{55}$$

is a logarithmic function written in terms of two dimensionless variables $s = |\vec{p}_1 + \vec{p}_2|/2k_f$ and $\kappa = |\vec{p}_1 - \vec{p}_2|/2k_f$. An additional constraint, $s^2 + \kappa^2 < 1$, arises from the fact that both external momenta $\vec{p}_1$ and $\vec{p}_2$ lie inside the Fermi sphere.

Finally, there is the contribution $B_2$ with two medium insertions which in fact is purely imaginary. Summing up all contributions gives for the total imaginary part of the in-medium loop:

$$\begin{aligned} \mathrm{Im}(B_0 + B_1 + B_2) \;=\; & 4\pi a \int \frac{d^3l}{(2\pi)^3}\, \pi\, \delta(\vec{l}^2 - \vec{q}^2) \\ & \times \Big\{ \Big[1 - \theta(k_f - |\vec{P} - \vec{l}\,|)\Big]\Big[1 - \theta(k_f - |\vec{P} + \vec{l}\,|)\Big] \\ & + \theta(k_f - |\vec{P} - \vec{l}\,|)\, \theta(k_f - |\vec{P} + \vec{l}\,|) \Big\}\,, \end{aligned} \tag{56}$$

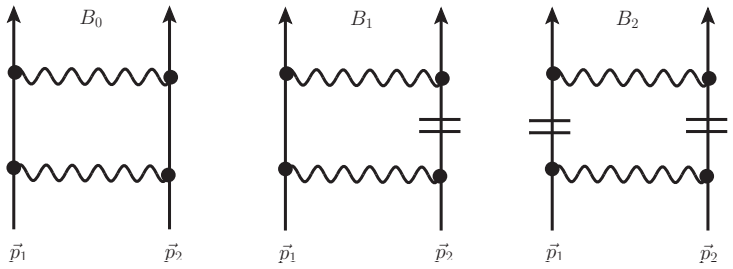


Figure 10: In-medium loop with different numbers of medium insertions. The middle diagram has a reflected partner. The external momenta $|\vec{p}_{1,2}| < k_f$ are inside the Fermi sphere.

where terms with zero, one, and two step-functions have suitably arranged. The first term has the form $[1-\theta(...)][1-\theta(...)]$ and gives no contribution to the imaginary part since energy conservation prohibits the on-shell scattering of two particles within the Fermi sea into the region outside the Fermi sea. Consequently, the result for the imaginary part of the in-medium loop takes the form:

$$\mathrm{Im}(B_0+B_1+B_2)=\frac{B_2}{2i}=ak_f\,I(s,\kappa)\,, \tag{57}$$

where $I(s,\kappa)$ is the non-smooth function

$$I(s,\kappa)=\kappa\,\theta(1-s-\kappa)+\frac{1}{2s}(1-s^2-\kappa^2)\,\theta(\kappa+s-1)\,. \tag{58}$$

In this expression $\kappa$ is restricted to lie in the interval $0<\kappa<\sqrt{1-s^2}$. Putting together the real and imaginary parts, the complex-valued in-medium loop is written

$$B_0+B_1+B_2=-\frac{ak_f}{\pi}\Big\{R(s,\kappa)-i\pi\,I(s,\kappa)\Big\}\,. \tag{59}$$

We observe that if the contribution from the diagram with two medium-insertions is separated off, then the imaginary part of the expression in eq. (59) changes sign:

$$B_0+B_1=-\frac{ak_f}{\pi}\Big\{R(s,\kappa)+i\pi\,I(s,\kappa)\Big\}\,. \tag{60}$$

Indeed, this particular property of the in-medium loop will play a critical role in the derivation of the correct expression for the energy per particle.

In ref. [51] it was shown how the contributions to the energy per particle $\bar{E}(k_f)$ at a given order in $a^n$ can be constructed from the in-medium loop and how the resulting series in $ak_f$ can even be summed to all orders. A naive iteration method would suggest $(R-i\pi I)^{n-1}$ as the integrand for the energy density at order $a^n$, but it is complex-valued. The deficit of the naive iteration method lies in the fact that a closed diagram with a repeated double medium-insertion has a symmetry factor which is not included in the binomial series expansion of $[(R+i\pi I)+(-2i\pi I)]^{n-1}$. A detailed combinatorial analysis [51] shows that the $j$-th power of $-2i\pi I$ coming from the diagrams with repeated double medium-insertions has to be re-weighted by a factor $1/(j+1)$. This crucial observation leads to the following formula

$$\sum_{j=0}^{n-1}(R+i\pi I)^{n-1-j}(-2i\pi I)^j\binom{n-1}{j}\frac{1}{j+1}=\frac{1}{2i\pi In}\Big\{(R+i\pi I)^n-(R-i\pi I)^n\Big\}\,, \tag{61}$$

where the right hand side is now manifestly real for all $n$. In this form the whole subset of ladder diagrams can be summed to all orders, since the series $\sum_{n=1}^{\infty}[-ak_f(R\pm i\pi I)/\pi]^n/n$ is solved easily

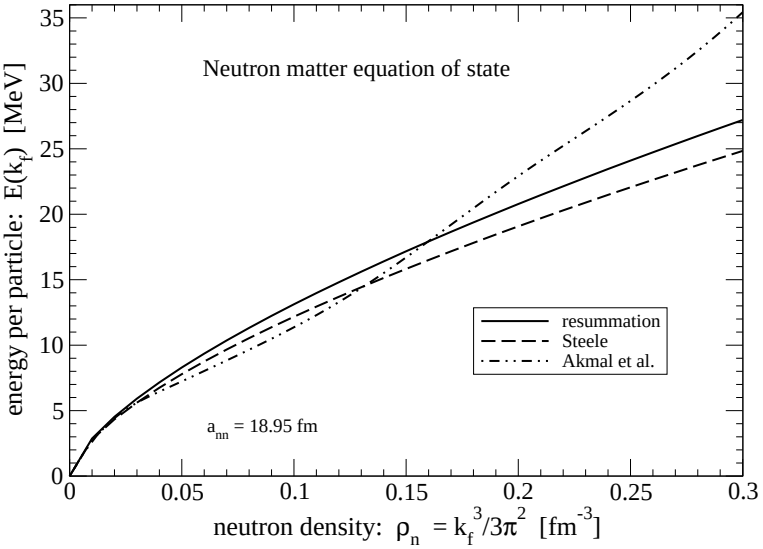


Figure 11: The energy per particle of neutron matter as a function of the neutron density $\rho_n$. The dash-dotted line is a reproduction of the results from the variational many-body calculation of ref. [54].

in terms of a (complex) logarithm. Putting all pieces together the final expression for the resummed energy per particle reads [51]:

$$\bar{E}(k_f)^{(\mathrm{lad})} = -\frac{24k_f^2}{\pi M}\int_0^1 ds\, s^2 \int_0^{\sqrt{1-s^2}} d\kappa\, \kappa\, \arctan\frac{ak_f\, I(s,\kappa)}{1+\pi^{-1}ak_f\, R(s,\kappa)}\,, \tag{62}$$

where the arctangent function refers to the usual branch with odd parity taking on values in the interval $[-\pi/2, \pi/2]$.

The expansion of the resummed energy per particle $\bar{E}(k_f)^{(\mathrm{lad})}$ in powers of $ak_f$ has been checked against known results from many-body perturbation theory based on the traditional particle-hole counting scheme [52, 53]. Up to the order $a^4$ where such results are presently available the agreement is perfect. Moreover, since only double integrals are involved, the pertinent coefficients can be calculated with very high numerical precision [51].

As an application of eq. (62) for the exact resummation of in-medium ladder diagrams, one can consider the equation of state of pure neutron matter. The very large neutron-neutron scattering length $a_{nn} = (18.95 \pm 0.40)\,\mathrm{fm}$ [48] necessitates a non-perturbative treatment of neutron matter at low densities. In Fig. 11 we reproduce the energy per particle of neutron matter as a function of the density in the approximation $\bar{E}(k_f)^{(\mathrm{lad})} + 3k_f^2/10M$ [51]. The solid line is obtained from eq. (62) by substituting $a = a_{nn} = 18.95\,\mathrm{fm}$ for the scattering length and $M = M_n = 939.57\,\mathrm{MeV}$ for the large fermion mass. The dash-dotted line comes from a sophisticated variational many-body calculation [54] representative of realistic neutron matter calculations. In Fig. 11 the dashed line corresponds to Steele's suggestion [53] of a simple geometrical series, $\bar{E}(k_f)^{(St)} = -ak_f^3[3M(\pi + 2ak_f)]^{-1}$. Up to rather high neutron densities, $\rho_n \simeq 0.2\,\mathrm{fm}^{-3}$, where the dimensionless parameter $a_{nn}k_f \simeq 34$, there is rather good agreement among the different calculations. For neutron densities beyond that of saturated nuclear matter, repulsive effects from three-body forces (present in the variational calculation of ref. [54]) begin to play a more important role. Including the neutron-neutron $S$-wave effective range $r_{nn} = (2.75 \pm 0.11)\,\mathrm{fm}$ can also modify the equation of state, as shown in ref. [55].

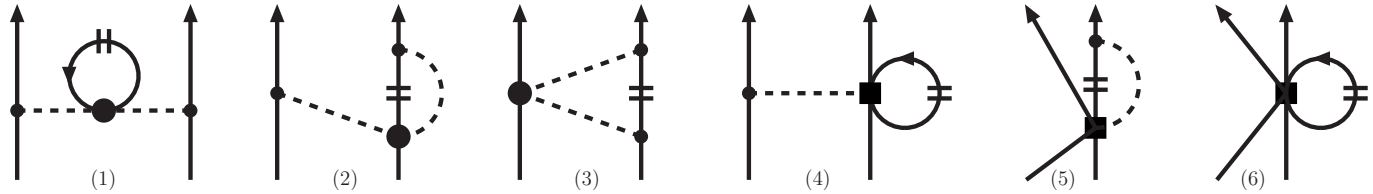


Figure 12: Diagrammatic contributions to the quasiparticle interaction in neutron matter generated from the two-pion exchange, one-pion exchange, and contact three-nucleon forces. The short double-line denotes the summation over the filled Fermi sea of nucleons. Reflected diagrams of (2), (3), (4), and (5) are not shown.

### 5.3 *In-Medium Effective Nucleon-Nucleon Interaction*

In applications of chiral effective field theory to light nuclei, the N$^2$LO chiral three-nucleon force is routinely implemented exactly [10, 56]. For heavier systems, however, the inclusion of three-nucleon forces is computationally demanding and requires resources approximately an order of magnitude larger than that for two-nucleon forces alone. An alternative strategy has therefore been explored in a number of recent calculations [57, 58, 59, 60, 61, 62] of finite nuclei as well as infinite nuclear and neutron matter in which three-nucleon forces are replaced by medium-dependent effective two-body interactions. The three-body force in second-quantized notation

$$V_{3N} = \frac{1}{36} \sum_{123456} \langle 123|\bar{V}|456\rangle \hat{a}_1^\dagger \hat{a}_2^\dagger \hat{a}_3^\dagger \hat{a}_6 \hat{a}_5 \hat{a}_4 \tag{63}$$

with antisymmetrized matrix elements $\langle 123|\bar{V}|456\rangle$, is normal ordered with respect to a convenient reference state $|\Omega\rangle$ which yields

$$\begin{aligned} V_{3N} &= \frac{1}{6}\sum_{ijk}\langle ijk|\bar{V}_{3N}|ijk\rangle + \frac{1}{2}\sum_{ij14}\langle ij1|\bar{V}_{3N}|ij4\rangle :\hat{a}_1^\dagger\hat{a}_4: + \frac{1}{4}\sum_{i1245}\langle i12|\bar{V}_{3N}|i45\rangle :\hat{a}_1^\dagger\hat{a}_2^\dagger\hat{a}_5\hat{a}_4: \\ &\quad + \frac{1}{36}\sum_{123456}\langle 123|\bar{V}_{3N}|456\rangle :\hat{a}_1^\dagger\hat{a}_2^\dagger\hat{a}_3^\dagger\hat{a}_6\hat{a}_5\hat{a}_4:, \end{aligned} \tag{64}$$

where the (alphabetic) indices $i, j, k$ represent filled orbitals in the reference state, and : : denotes the normal-ordered product of operators satisfying

$$:\hat{a}_1^\dagger \ldots \hat{a}_n: |\Omega\rangle = 0. \tag{65}$$

In refs. [58, 59] the reference state was chosen to be a filled Fermi sea of noninteracting nucleons characterized by the density as well as the isospin asymmetry parameter $\delta_{np} = (\rho_n - \rho_p)/(\rho_n + \rho_p)$. With the additional kinematical restriction that the scattering takes place in the rest frame of the medium, the on-shell scattering amplitude (equivalent to the normal-ordered two-body part of the full three-nucleon force) has the same form as the free-space nucleon-nucleon interaction:

$$\begin{aligned} V_{NN}^{\rm med} &= V_C + W_C\,\vec{\tau}_1\cdot\vec{\tau}_2 + [V_S + W_S\,\vec{\tau}_1\cdot\vec{\tau}_2]\,\vec{\sigma}_1\cdot\vec{\sigma}_2 + [V_T + W_T\,\vec{\tau}_1\cdot\vec{\tau}_2]\,\vec{\sigma}_1\cdot\vec{q}\,\vec{\sigma}_2\cdot\vec{q} \\ &+ [V_{LS} + W_{LS}\,\vec{\tau}_1\cdot\vec{\tau}_2]\,i(\vec{\sigma}_1+\vec{\sigma}_2)\cdot(\vec{q}\times\vec{p}) + [V_Q + W_Q\,\vec{\tau}_1\cdot\vec{\tau}_2]\,\vec{\sigma}_1\cdot(\vec{q}\times\vec{p})\vec{\sigma}_2\cdot(\vec{q}\times\vec{p}), \end{aligned} \tag{66}$$

where the different scalar functions $V$ and $W$ depend on $p$ and $q$, the initial relative momentum and the momentum transfer, respectively. The resulting in-medium two-nucleon interaction can then be implemented in the many-body method of choice, provided that one takes care of the different symmetry factors in the zero- and one-body normal-ordered components of a three-nucleon force compared to those from two-body interactions [60].

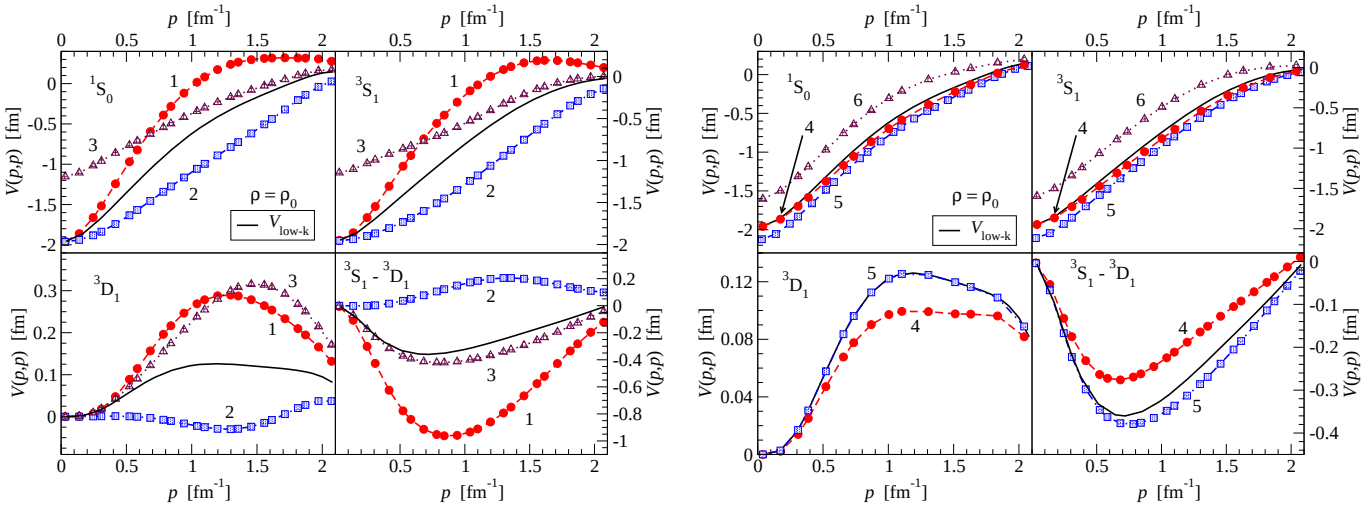


Figure 13: Contributions to the on-shell $S$- and $D$-wave matrix elements from the density-dependent nucleon-nucleon interaction derived in ref. [58, 59]. The solid curve denotes the matrix elements of a renormalization-group evolved NN potential and the numbered lines show the modification due to the six classes of diagrams shown in Fig. 12.

For the N$^2$LO chiral three-nucleon force, there are six topologically distinct diagrams contributing to the in-medium nucleon-nucleon interaction shown in Fig. 12. The contributions labeled (1), (2), and (4) give corrections to one-pion exchange, while contributions (5) and (6) adjust the strength of the nucleon-nucleon contact interaction. On the other hand, the Pauli-blocked two-pion exchange diagram, labeled (3) in Fig. 12, gives rise to central, spin-spin, tensor, spin-orbit, and quadratic spin-orbit contributions. In Fig. 13 we reproduce the on-shell momentum-space matrix elements of the renormalization-group evolved Idaho N$^3$LO chiral two-nucleon force together with the modifications arising from the six different components of the density-dependent nucleon-nucleon interaction in selected relative $S$ and $D$ waves. The values of the relevant low-energy constants are $c_1 = -0.76\,\mathrm{GeV}^{-1}$, $c_3 = -4.78\,\mathrm{GeV}^{-1}$, $c_4 = -3.96\,\mathrm{GeV}^{-1}$, $c_D = -2.06$, and $c_E = -0.625$. The dominant effects arise from two-pion exchange dynamics, but in all partial waves the pion self-energy correction $V_{NN}^{\mathrm{med},1}$ and the pion-exchange vertex correction $V_{NN}^{\mathrm{med},2}$ approximately cancel. This leaves Pauli-blocking effects in two-pion exchange, represented by $V_{NN}^{\mathrm{med},3}$, together with additional repulsion from the chiral three-body contact interaction, encoded in $V_{NN}^{\mathrm{med},6}$, as the dominant effects from three-body forces.

The normal-ordering approximation, in which the residual three-nucleon force in eq. (64) is neglected, has proven to be a useful approximation for calculations in medium-mass nuclei where exact *ab-initio* many-body methods incorporating three-body forces are computationally challenging. Within this approximation three-nucleon forces were shown to provide the microscopic origin of the anomalously-long beta-decay lifetime of $^{14}$C [58], which subsequent no-core shell model calculations [63] have confirmed and clarified. In Fig. 14, we show the Gamow-Teller strengths from low-lying states in $^{14}$C to the ground state of $^{14}$N computed with density-dependent low-momentum chiral nucleon-nucleon interactions. In fact, only the ground state to ground state transition receives significant medium modifications that result in a strong enhancement of the $^{14}$C lifetime. Further work has employed normal-ordered two-body interactions to study three-nucleon force effects on the neutron drip-line in oxygen isotopes [61, 64] as well as on the shell structure of calcium isotopes [65, 66]. Benchmark calculations of the normal ordering approximation in closed shell nuclei have been carried out in the importance-truncated no-core shell model, and it was found that beyond the lightest nuclei, normal-ordered Hamiltonians provide an accurate substitute for full three-nucleon forces [67]. In Fig. 15 we reproduce from ref. [67] the expectation values of the leading-order chiral three-nucleon force at different levels of the normal-ordering

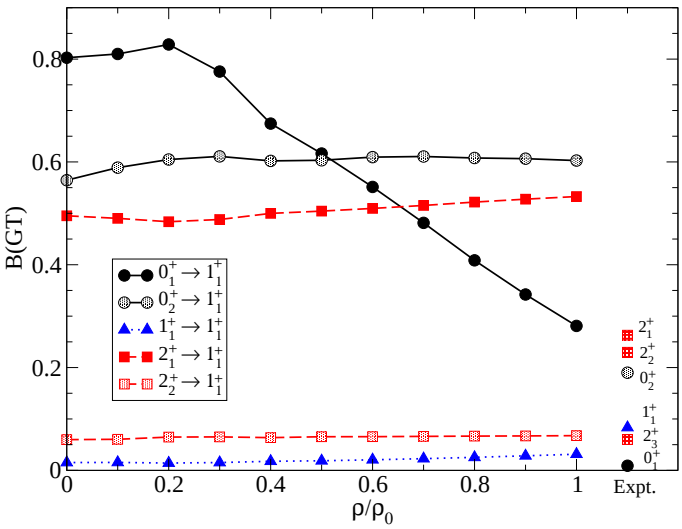


Figure 14: Gamow-Teller strengths for transitions from the low-energy even-parity states of $^{14}$C to the ground state of $^{14}$N as a function of the nuclear density.

approximation. For both $^{16}$O and $^{40}$Ca, the difference between the expectation of the normal-ordered 2B approximation, consisting of the first three terms in eq. (64), and the expectation value of the exact three-body interaction is negligible.

Density-dependent nucleon-nucleon interactions have also been used extensively in calculations of the equation of state of isospin-symmetric nuclear matter and neutron matter [60, 68, 69, 70]. This has allowed the study of three-nucleon forces beyond the Hartree-Fock approximation, but certain topologies are necessarily omitted in such an approximation. The inclusion of the full second-order contribution to the energy per particle from a three-nucleon force has been carried out only in the case of a three-body contact interaction [71]. There it was found that the complete set of second-order three-body diagrams gives a contribution to the energy per particle that is roughly half that from the density-dependent nucleon-nucleon interaction.

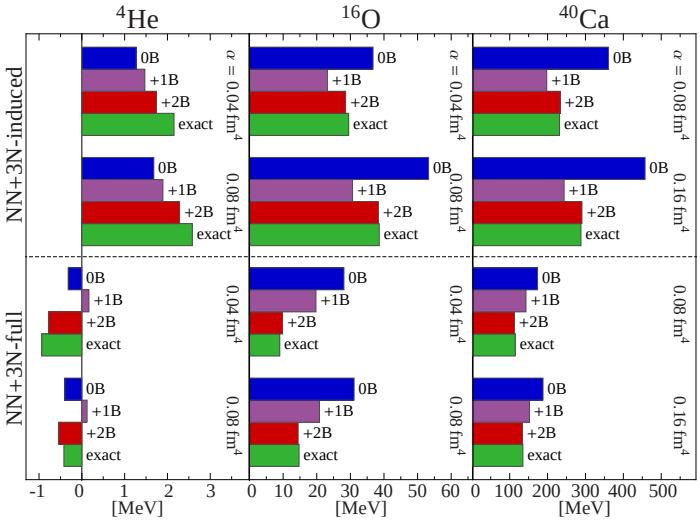


Figure 15: Ground-state expectation values of the N$^2$LO chiral three-nucleon force at different normal-ordering approximations. The bars are labeled according to the highest $n$-body ($n$B) contribution included in the calculation. Similarity renormalization group evolved interactions were employed for two different values of the flow parameter $\alpha$. Figure reproduced from ref. [67].

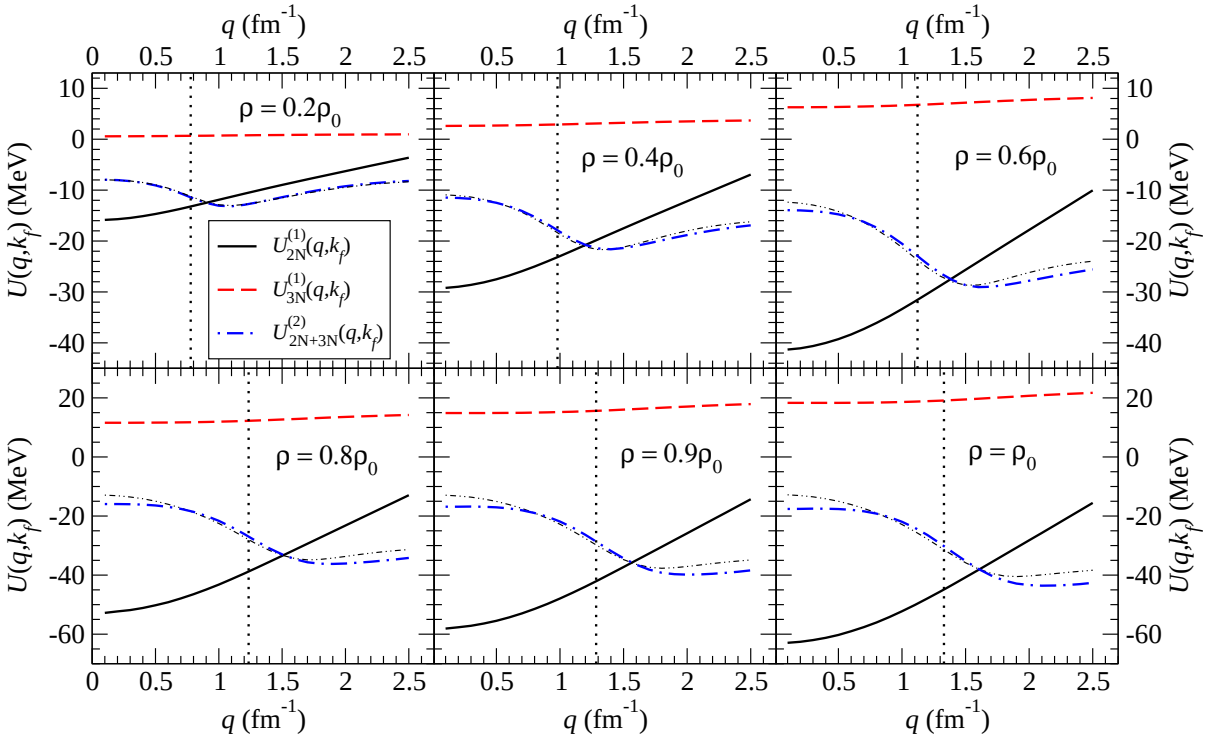


Figure 16: Contributions to the real part of the on-shell ($\omega = q^2/(2M_N)$) momentum- and density-dependent optical potential from chiral two- and three-nucleon forces. The solid and dashed-dotted lines are the first- and second-order contributions from the two-body potential, while the dashed line is the first-order contribution from the chiral three-nucleon force. The vertical dotted line indicates the Fermi momentum, and the dashed-double-dotted line is the second-order contribution without three-body forces.

## 5.4 *Nuclear Mean Field*

The average single-particle potential acting on a nucleon in a finite nucleus is a central concept in nuclear structure and reaction theory. For negative energy bound states, the nuclear mean field is associated with the shell model potential, while for positive energy scattering states it is identified with the optical model potential. The latter is complex and strongly absorptive, in contrast to the shell model potential which is a real-valued quantity. While phenomenological optical potentials have been used extensively to describe reactions on target nuclei close to the valley of stability, microscopic optical potentials have no adjustable parameters and therefore provide a reliable basis for extending to reactions on exotic, neutron-rich nuclei that will be studied at the next generation of radioactive beam facilities. Numerous microscopic many-body methods have been used to compute the single-particle potential (self-energy), including the Brueckner-Hartree-Fock [72, 73, 74], Dirac-Brueckner-Hartree-Fock [75, 76], and Green's function [77, 78] methods. Here we review only the recent calculations [79, 39, 80] that have been carried out in the framework of in-medium chiral perturbation theory for infinite isospin-symmetric nuclear matter.

The starting point is the high-precision Idaho chiral two-nucleon potential with a cutoff of $\Lambda = 500\,\mathrm{MeV}$ supplemented with the leading-order chiral three-nucleon force whose low-energy constants ($c_1 = -0.81\,\mathrm{GeV}^{-1}$, $c_3 = -3.2\,\mathrm{GeV}^{-1}$, $c_4 = 5.4\,\mathrm{GeV}^{-1}$, $c_D = -0.2$, and $c_E = -0.205$) have been fit to nucleon-nucleon scattering phase shifts [31] and the binding energy and lifetime of the triton [32]. Within microscopic many-body theory, the nuclear mean field is identified with the nucleon self-energy, $\Sigma(\vec{r},\vec{r}\,',E) = U(\vec{r},\vec{r}\,',E) + iW(\vec{r},\vec{r}\,',E)$. For a homogeneous medium the self-energy can be written

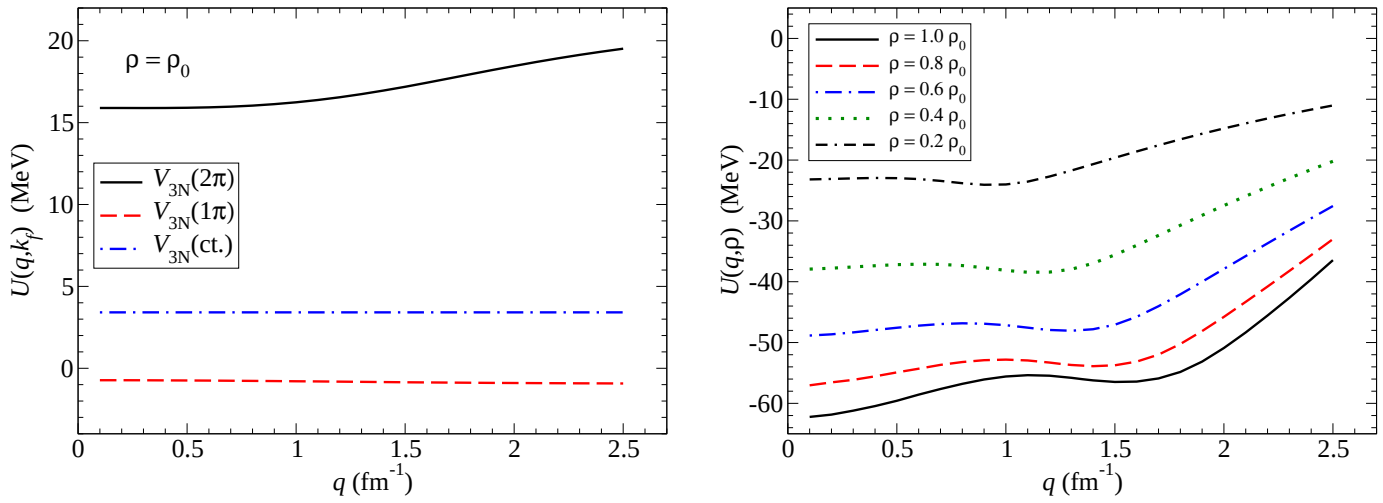


Figure 17: Left panel: Three-body Hartree-Fock contributions to the real part of the nuclear optical potential. The individual single-particle potentials from the three components of the N$^2$LO chiral three-nucleon force are shown separately and plotted as a function of the momentum at nuclear matter saturation density. Right panel: Density dependence of the real part of the momentum-dependent optical potential at second order in perturbation theory from chiral two- and three-body forces.

as a function of the momentum, energy, and density (or Fermi momentum) $\Sigma(q,\omega;k_f)$. The first two perturbative contributions from two-nucleon forces are given by

$$\begin{aligned}
\Sigma^{(1)}_{2N}(q,\omega;k_f) &= \sum_1 \langle \vec{q}\,\vec{h}_1 s s_1 t t_1 | \bar{V}_{2N} | \vec{q}\,\vec{h}_1 s s_1 t t_1 \rangle n_1, \\
\Sigma^{(2)}_{2N}(q,\omega;k_f) &= \frac{1}{2}\sum_{123} \frac{|\langle \vec{p}_1\vec{p}_3 s_1 s_3 t_1 t_3 | \bar{V}_{2N} | \vec{q}\,\vec{h}_2 s s_2 t t_2 \rangle|^2}{\omega + \epsilon_2 - \epsilon_1 - \epsilon_3 + i\eta} \bar{n}_1 n_2 \bar{n}_3 (2\pi)^3 \delta(\vec{p}_1 + \vec{p}_3 - \vec{q} - \vec{h}_2), \\
&+ \frac{1}{2}\sum_{123} \frac{|\langle \vec{h}_1\vec{h}_3 s_1 s_3 t_1 t_3 | \bar{V}_{2N} | \vec{q}\,\vec{p}_2 s s_2 t t_2 \rangle|^2}{\omega + \epsilon_2 - \epsilon_1 - \epsilon_3 - i\eta} n_1 \bar{n}_2 n_3 (2\pi)^3 \delta(\vec{h}_1 + \vec{h}_3 - \vec{q} - \vec{p}_2),
\end{aligned} \tag{67}$$

where $\bar{V}_{2N}$ is the antisymmetrized two-body potential, $n_i = \theta(k_f - |\vec{k}_i|)$ is the zero-temperature Fermi distribution, $\bar{n}_i = 1 - n_i$, and the sum is over the momentum, spin, and isospin of the intermediate states. The first-order contribution from three-body forces has the form

$$\Sigma^{(1)}_{3N}(q,\omega;k_f) = \sum_{12} \langle \vec{q}\,\vec{h}_1\vec{h}_2; s s_1 s_2; t t_1 t_2 | \bar{V}_{3N} | \vec{q}\,\vec{h}_1\vec{h}_2; s s_1 s_2; t t_1 t_2 \rangle n_1 n_2, \tag{68}$$

where $\bar{V}_{3N}$ is the antisymmetrized three-body interaction. As discussed in the previous section, the density-dependent two-nucleon interaction [58, 59] can be used in the last equation of (67) to study the effects of three-nucleon forces beyond the Hartree-Fock approximation.

In Fig. 16 we reproduce results from ref. [80] for the real part of the on-shell self-energy ($\omega = q^2/(2M_N)$) as a function of the density and momentum. The leading-order Hartree-Fock contribution from two- and three-body forces are given by the solid lines and dashed lines, respectively. Both contributions are real and explicitly energy independent, but they have qualitatively different properties. The Hartree-Fock contribution from two-body forces is attractive up to the maximum momentum plotted in Fig. 16 and decreases in magnitude as the momentum increases. The N$^2$LO chiral three-nucleon force, on the other hand, gives a repulsive contribution to the single-particle potential that increases nearly linearly with the background density but which varies only mildly with the momentum of the propagating nucleon. As shown in the left panel of Fig. 17, the two-pion exchange component

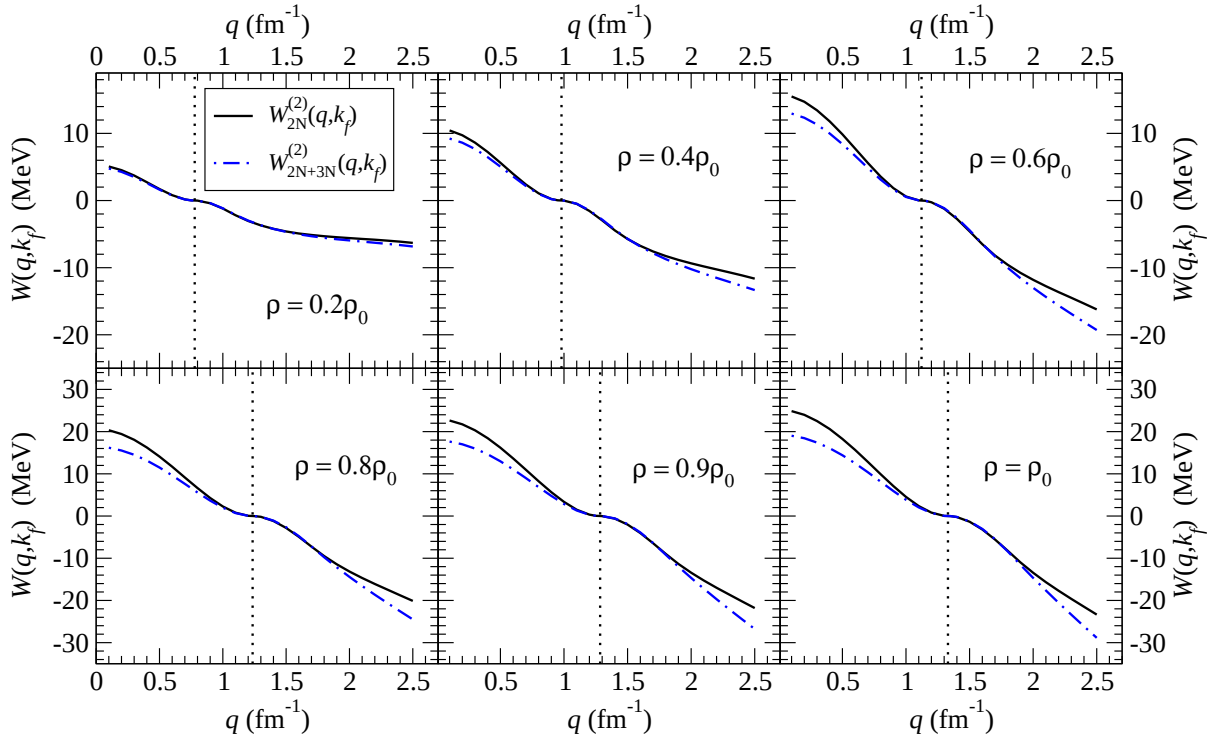


Figure 18: The imaginary part of the nuclear optical potential from chiral two- and three-body forces at second order in many-body perturbation theory. The vertical dotted line indicates the Fermi momentum $k_f$.

of the N$^2$LO chiral three-nucleon force provides about 80% of the total repulsion and is responsible for nearly all of the momentum dependence of the three-body Hartree-Fock mean field.

A notable feature of the contact and $1\pi$-exchange three-body forces is that they generate a momentum-independent and a nearly momentum-independent single-particle potential, respectively. This implies a strong correlation in the low-energy constants $c_D$ and $c_E$, where variations along the line

$$c_E = \alpha \cdot c_D + \text{const} \tag{69}$$

give nearly equivalent descriptions of the mean field. The constant of proportionality has the value $\alpha \simeq 0.21 \pm 0.02$ and is weakly dependent on the momentum and density. As noted in ref. [80], in the chiral limit the single-particle potential associated with the one-pion exchange three-body force has a particularly simple form which then yields the correlation coefficient $\alpha = g_A/4 \simeq 0.3$.

Second-order contributions to the single-particle potential from two- and three-body forces are shown as the dashed-dotted lines in Fig. 16. The momentum dependence of the second-order terms peaks close to the Fermi surface, and when combined with the Hartree-Fock mean field from two- and three-body forces the resulting momentum dependence is quite small below $k_f$. The result is a nucleon effective mass at the Fermi surface that is close to the free-space mass. In Fig. 16 we show with the dashed-double-dotted line also the second-order contribution without three-nucleon forces. Second-order effects from three-body forces appear to be rather small and result in additional attraction at both low and high momenta. In the right panel of Fig. 17 we show the total real part of the nucleon self-energy as a function of density and momentum. For low to moderate densities the single-particle potential is nearly momentum independent below $k_f$. The overall well depth for scattering at zero incident energy ($q = k_f$) is approximately $-57\,\text{MeV}$ at nuclear matter saturation density, which is within about 10% of the depth, $-52\,\text{MeV}$, of phenomenological optical potentials [81].

In Fig. 18 we show the imaginary part of the single-particle potential as a function of the density and momentum. At positive energies (measured with respect to the Fermi energy) the imaginary part of the potential is negative and strongly absorptive for particles propagating with large momenta. We see that the imaginary part vanishes quadratically close to the Fermi surface for both two- and three-nucleon force contributions, in agreement with Luttinger's theorem [82]. With two-body forces alone the imaginary part is approximately inversion-symmetric about the Fermi momentum, $W(q, k_f) \simeq -W(2k_f - q, k_f)$, but three-nucleon forces lower the imaginary part at momenta well below and above $k_f$. For intermediate-energy scattering, $E \sim 100\,\mathrm{MeV}$, the phenomenological strength of the imaginary part of the optical potential is approximately $|W| \simeq 10\,\mathrm{MeV}$ [81], which is much less than the value $\sim 30\,\mathrm{MeV}$ obtained in the second-order calculation with two- and three-body forces. Effective mass corrections [83, 84], self-consistent single-particle energies in the denominators of eq. (67), and an inclusion of an energy gap at the Fermi surface are all expected to reduce significantly the magnitude of the imaginary part of the calculated optical potential. Future comparisons to rare-isotope reactions will require also the inclusion of isospin asymmetry and the extension to finite nuclear systems.

# 6 Density Functional Methods and Finite Nuclei

In this section we review how chiral low-momentum interactions can be employed for the description of properties of finite nuclei [85, 86, 87, 88, 89, 90]. We leave aside the highly sophisticated ab-initio methods which have been developed over the past decades in order to solve (numerically) the nuclear $A$-body problem with a given two- and three-nucleon interaction. Here we concentrate on the nuclear energy density functional approach, which remains the many-body method of choice to compute the properties of medium-mass and heavy nuclei [91, 92]. Non-relativistic Skyrme functionals [93, 94] with a small number of adjustable parameters as well as relativistic mean-field models [95, 96] have been employed in such self-consistent mean-field calculations to describe a wide range of nuclear properties. An alternative and complementary scheme [97, 98, 88] focuses less on fitting to experimental data and attempts instead to constrain the analytical form of the functional as well as the values of its couplings from a microscopic approach based on many-body perturbation theory with realistic two- and three-nucleon forces. The use of low-momentum nucleon-nucleon potentials [99, 100], rather than conventional hard-core interactions, is essential in this regard, because the former exhibit much improved convergence properties compared to the latter in perturbative solutions to the nuclear many-body problem. Indeed, when evolved low-momentum interactions are employed at second-order in perturbation theory, including also three-body forces, a good description of the bulk correlations in infinite nuclear matter [101, 68] and in doubly-magic nuclei [102] can be achieved.

Within the framework of many-body perturbation theory, contributions to the energy are given in terms of density-matrices convoluted with finite-range interaction kernels. The resulting expression for the energy is then highly non-local in both space and time. In order for mean-field calculations with such functionals to be numerically feasible in heavy open-shell nuclei, it is essential to develop approximations for these functionals in which only local densities and currents enter. For this purpose the density-matrix expansion is highly useful as it provides a means to remove the non-local character of the exchange contribution to the energy by expanding it in the form a generalized Skyrme functional with couplings that depend on the density. For many years such an approach has been based on the density-matrix expansion of Negele and Vautherin [103], but recently Gebremariam, Duguet and Bogner [85] have suggested an improved version that specifically addresses the challenges that arise for spin-unsaturated nuclei. In fact, the phase-space averaging techniques they employed were shown to allow for a consistent expansion of both the spin-independent part as well as the spin-dependent part of the nuclear density-matrix. The improved features of the phase-space averaged density-matrix expansion have been studied [85] via the Fock energy densities of schematic finite-range central, spin-orbit, and

tensor interactions for a large group of semi-magic nuclei.

Making use of these new developments a microscopically constrained nuclear energy density functional derived from the chiral NN potential at order N$^2$LO has been presented in ref. [86]. There it has been suggested that the density-dependent couplings associated with pion-exchange should be added to a standard Skyrme functional with re-adjusted parameters. In a subsequent study [45], it has been shown that this new energy density functional yields numerically stable results and that it exhibits a small yet systematic reduction of the $\chi^2$ deviation in comparison to traditional Skyrme functionals without any explicit pion-exchange dynamics.

In this section we report on a derivation of the nuclear energy density functional with improved (chiral) two- and three-nucleon interactions [89, 90]. For the two-body interaction the N$^3$LO chiral NN-potential is used, which reaches at this order in the chiral expansion the quality of a high-precision nucleon-nucleon potential in reproducing empirical NN scattering phase shifts and properties of the deuteron. The N$^3$LO chiral potential contains long-range one- and two-pion exchange interactions as well as a short-distance part that is parameterized in terms of 24 low-energy constants. The latter contact potential is written in momentum space and provides the most general contribution up to fourth power in nucleon momenta. This high-precision nucleon-nucleon potential is supplemented with the N$^2$LO chiral three-nucleon force. In addition to the equation of state of infinite homogeneous nuclear matter, the energy density functional includes strength functions associated with the $(\vec{\nabla}\rho)^2$ surface term and the spin-orbit coupling term. In phenomenological Skyrme parametrizations these strength functions are treated as constants, whereas in a microscopic approach based on realistic nuclear interactions the finite-range character of the pion-exchange terms gives rise to specific density dependences for these strength functions.

## 6.1 *Density-Matrix Expansion and Energy Density Functional*

The construction of an explicit nuclear energy density functional starts from the density-matrix given as a sum over the energy eigenfunctions $\Psi_\alpha(\vec{r})$ associated with occupied orbitals of the non-relativistic many-body Fermi system. Gebremariam, Duguet and Bogner [85] have shown that it can be expanded in center-of-mass and relative coordinates, $\vec{r}$ and $\vec{a}$, in the following way

$$\begin{aligned}\sum_\alpha \Psi_\alpha(\vec{r}-\vec{a}/2)\Psi^\dagger_\alpha(\vec{r}+\vec{a}/2) &= \frac{3\rho}{ak_f}\,j_1(ak_f) - \frac{a}{2k_f}\,j_1(ak_f)\Big[\tau - \frac{3}{5}\rho k_f^2 - \frac{1}{4}\vec{\nabla}^2\rho\Big] \\ &\quad + \frac{3i}{2ak_f}\,j_1(ak_f)\,\vec{\sigma}\cdot(\vec{a}\times\vec{J}) + \ldots\,, \end{aligned} \tag{70}$$

where $j_1(x) = (\sin x - x\cos x)/x^2$ is a spherical Bessel function. The right-hand side of eq. (70) is written in terms of the nucleon density $\rho(\vec{r}) = 2k_f^3(\vec{r})/3\pi^2 = \sum_\alpha \Psi^\dagger_\alpha(\vec{r})\Psi_\alpha(\vec{r})$, the kinetic energy density $\tau(\vec{r}) = \sum_\alpha \vec{\nabla}\Psi^\dagger_\alpha(\vec{r})\cdot\vec{\nabla}\Psi_\alpha(\vec{r})$, and the spin-orbit density $\vec{J}(\vec{r}) = i\sum_\alpha \vec{\Psi}^\dagger_\alpha(\vec{r})\vec{\sigma}\times\vec{\nabla}\Psi_\alpha(\vec{r})$.

Nuclear interactions derived within the framework of chiral effective field theory are generally given in momentum space. Therefore the Fourier transform of the expanded density-matrix eq. (70) with respect to the coordinates $\vec{a}$ and $\vec{r}$ provides the appropriate tool for an efficient calculation of the nuclear energy density functional. This Fourier transform:

$$\begin{aligned}\Gamma(\vec{p},\vec{q}) &= \int d^3r\, e^{-i\vec{q}\cdot\vec{r}}\Big\{\theta(k_f-|\vec{p}|) + \frac{\pi^2}{4k_f^4}\Big[k_f\,\delta'(k_f-|\vec{p}|) - 2\delta(k_f-|\vec{p}|)\Big] \\ &\quad\times\Big(\tau - \frac{3}{5}\rho k_f^2 - \frac{1}{4}\vec{\nabla}^2\rho\Big) - \frac{3\pi^2}{4k_f^4}\,\delta(k_f-|\vec{p}|)\,\vec{\sigma}\cdot(\vec{p}\times\vec{J})\Big\}\,, \end{aligned} \tag{71}$$

generalizes the concept of "medium-insertion" to inhomogeneous many-nucleon systems characterized by the time-reversal-even fields $\rho(\vec{r})$, $\tau(\vec{r})$ and $\vec{J}(\vec{r})$. At a practical level $\Gamma(\vec{p},\vec{q})$ extends the step-

function-like momentum distribution $\theta(k_f - |\vec{p}|)$ for infinite nuclear matter to inhomogeneous many-nucleon systems. Note that the delta-function $\delta(k_f - |\vec{p}|)$ in eq. (71) gives weight to the nucleon-nucleon interactions in the vicinity of the local Fermi momentum $|\vec{p}| = k_f(\vec{r})$ only.

Up to second order in spatial gradients, characterizing deviations from homogeneity, the energy density functional appropriate for $N = Z$ even-even nuclei has the form

$$\begin{aligned}\mathcal{E}[\rho,\tau,\vec{J}] &= \rho\,\bar{E}(\rho) + \Big[\tau - \frac{3}{5}\rho k_f^2\Big]\Big[\frac{1}{2M_N} - \frac{k_f^2}{4M_N^3} + F_\tau(\rho)\Big] \\ &\quad + (\vec{\nabla}\rho)^2\,F_\nabla(\rho) + \vec{\nabla}\rho\cdot\vec{J}\,F_{so}(\rho) + \vec{J}^{\,2}\,F_J(\rho)\,. \end{aligned} \tag{72}$$

In this equation, $\bar{E}(\rho)$ represents the energy per particle of symmetric nuclear matter evaluated at the local nucleon density. The strength function $F_\tau(\rho)$ is associated with an effective density-dependent nucleon mass $M^*(\rho)$, and it is related to the nuclear single-particle potential $U(p,k_f)$:

$$F_\tau(\rho) = \frac{1}{2k_f}\frac{\partial U(p,k_f)}{\partial p}\Big|_{p=k_f} = -\frac{k_f}{3\pi^2}f_1(k_f)\,, \tag{73}$$

where $\rho = 2k_f^3/3\pi^2$. The second equality gives the relation to the "spin and isospin independent" p-wave Fermi-liquid parameter $f_1(k_f)$. A new feature of the improved density-matrix expansion is that it leads to the same concept of effective mass as established in Fermi-liquid theory for quasi-particles on the Fermi surface. For the original density-matrix expansion of Negele and Vautherin [103] this close relationship does not hold in general, e.g. when $U(p,k_f)$ deviates from a simple quadratic $p$-dependence.

The strength function $F_\nabla(\rho)$ associated with the $(\vec{\nabla}\rho)^2$ surface term can be decomposed into two terms:

$$F_\nabla(\rho) = \frac{1}{4}\,\frac{\partial F_\tau(\rho)}{\partial\rho} + F_d(\rho)\,, \tag{74}$$

where $F_d(\rho)$ is composed of all contributions for which the $(\vec{\nabla}\rho)^2$-factor originates directly from the momentum dependence of the interactions (expanded up to order $\vec{q}^{\,2}$ and combined with a Fourier transformation). It is worth noting that only the nuclear matter component $\theta(k_f - |\vec{p}|)$ of the density-matrix expansion enters into the derivation of the strength function $F_d(\rho)$. The next-to-last term in eq. (72), namely $\vec{\nabla}\rho\cdot\vec{J}\,F_{so}(\rho)$ with its associated strength function $F_{so}(\rho)$, gives the spin-orbit interaction in nuclei. The last term, $\vec{J}^{\,2}\,F_J(\rho)$, in the expression for energy density is the quadratic spin-orbit term. It gives rise to an additional spin-orbit single-particle potential proportional to $\vec{J}$, whereas the ordinary spin-orbit potential is provided by the density-gradient $\vec{\nabla}\rho$.

## 6.2 *Two- and Three-Body Contributions*

Here, the two- and three-body contributions to the various density-dependent strength functions entering the nuclear energy density functional $\mathcal{E}[\rho,\tau,\vec{J}]$ are presented. One would prefer to calculate the two-body contributions with perturbative nucleon-nucleon potentials, of which the low-momentum NN interaction $V_{\rm low-k}$ [100] is the prototypical example. Low-momentum two-body potentials are however non-local and given in terms of partial-wave matrix elements, which makes their implementation in the density-matrix expansion rather difficult. An explicit representation of the momentum-space nucleon-nucleon potential (without non-localities) in terms of spin- and isospin-operators is much more suitable for this purpose. As a convenient substitute for $V_{\rm low-k}$ one can use the chiral NN-potential N$^3$LOW developed in refs. [12, 104] by imposing a sharp cutoff at the scale $\Lambda = 414\,$MeV. This value of the cutoff coincides with the resolution scale below which evolved low-momentum NN potentials become nearly model-independent and exhibit desirable convergence properties in many-body perturbation theory calculations. The finite-range part of the N$^3$LOW chiral NN-potential arises from one- and two-pion

exchange processes that have the general form:

$$\begin{aligned} V_{NN}^{(\pi)} &= V_C(q) + \vec{\tau}_1\cdot\vec{\tau}_2\, W_C(q) + [V_S(q) + \vec{\tau}_1\cdot\vec{\tau}_2\, W_S(q)]\,\vec{\sigma}_1\cdot\vec{\sigma}_2 \\ &\quad + [V_T(q) + \vec{\tau}_1\cdot\vec{\tau}_2\, W_T(q)]\,\vec{\sigma}_1\cdot\vec{q}\,\vec{\sigma}_2\cdot\vec{q} \\ &\quad + [V_{SO}(q) + \vec{\tau}_1\cdot\vec{\tau}_2\, W_{SO}(q)]\, i(\vec{\sigma}_1+\vec{\sigma}_2)\cdot(\vec{q}\times\vec{p})\,, \end{aligned} \tag{75}$$

where $\vec{q}$ is the momentum transfer and $\vec{p}$ a single nucleon momentum. A special and convenient feature of $V_{NN}^{(\pi)}$ is that it is a local potential: all occurring functions $V_C(q),\ldots,W_{SO}(q)$ depend only on the momentum transfer $q$, and quadratic spin-orbit components $\sim \vec{\sigma}_1\cdot(\vec{q}\times\vec{p})\,\vec{\sigma}_2\cdot(\vec{q}\times\vec{p})$ are absent.

In the Hartree-Fock approximation the finite-range part of the nucleon-nucleon potential arising from explicit pion exchange leads to the following two-body contributions to the energy density functional:

$$\begin{aligned} \bar{E}(\rho) &= \frac{\rho}{2}V_C(0) - \frac{3\rho}{2}\int_0^1 dx\, x^2(1-x)^2(2+x)\Big[V_C(q) + 3W_C(q) \\ &\qquad + 3V_S(q) + 9W_S(q) + q^2V_T(q) + 3q^2W_T(q)\Big]\,, \end{aligned} \tag{76}$$

$$F_\tau(\rho) = \frac{k_f}{2\pi^2}\int_0^1 dx(x-2x^3)\Big[V_C(q) + 3W_C(q) + 3V_S(q) + 9W_S(q) + q^2V_T(q) + 3q^2W_T(q)\Big]\,, \tag{77}$$

$$F_d(\rho) = \frac{1}{4}V_C''(0)\,, \tag{78}$$

$$F_{so}(\rho) = \frac{1}{2}V_{SO}(0) + \int_0^1 dx\, x^3\Big[V_{SO}(q) + 3W_{SO}(q)\Big]\,, \tag{79}$$

$$F_J(\rho) = \frac{3}{8k_f^2}\int_0^1 dx\Big\{(2x^3-x)\Big[V_C(q) + 3W_C(q) - V_S(q) - 3W_S(q)\Big] - x^3q^2\Big[V_T(q) + 3W_T(q)\Big]\Big\}\,, \tag{80}$$

where $q = 2xk_f$. The above expressions are obtained from the density matrix-expansion employing the product of two medium-insertions $\Gamma(\vec{p}_1,\vec{q})\,\Gamma(\vec{p}_2,-\vec{q})$). In eq. (78) the double-prime denotes the second derivative, and it is worth noting that $F_J(\rho)$ stays finite in the low-density limit $k_f\to 0$.

In addition to the finite-range parts of the NN potential there are two-body contributions from the zero-range contact forces. At order N$^3$LO the corresponding expressions in momentum-space include constant, quadratic, and quartic terms in momenta [105]. The density-dependent strength functions arising from the contact NN potential read:

$$\bar{E}(\rho) = \frac{3\rho}{8}(C_S - C_T) + \frac{3\rho k_f^2}{20}(C_2 - C_1 - 3C_3 - C_6) + \frac{9\rho k_f^4}{140}(D_2 - 4D_1 - 12D_5 - 4D_{11})\,, \tag{81}$$

$$F_\tau(\rho) = \frac{\rho}{4}(C_2 - C_1 - 3C_3 - C_6) + \frac{\rho k_f^2}{4}(D_2 - 4D_1 - 12D_5 - 4D_{11})\,, \tag{82}$$

$$F_d(\rho) = \frac{1}{32}(16C_1 - C_2 - 3C_4 - C_7) + \frac{k_f^2}{48}(9D_3 + 6D_4 - 9D_7 - 6D_8 - 3D_{12} - 3D_{13} - 2D_{15})\,, \tag{83}$$

$$F_{so}(\rho) = \frac{3}{8}C_5 + \frac{k_f^2}{6}(2D_9 + D_{10})\,, \tag{84}$$

$$F_J(\rho) = \frac{1}{16}(2C_1 - 2C_3 - 2C_4 - 4C_6 + C_7) + \frac{k_f^2}{32}(16D_1 - 16D_5 - 4D_6 - 24D_{11} + D_{14})\,. \tag{85}$$

The 24 low-energy constants $C_{S,T}$, $C_j$ and $D_j$ are fit (with a sharp cutoff regulator at $\Lambda = 414\,\mathrm{MeV}$) to empirical nucleon-nucleon scattering phase shifts and properties of the deuteron [104]. It is worth mentioning that in the first-order Hartree-Fock approximation it is not necessary to include a regulator function since the nuclear interactions are probed only at small momenta $|\vec{p}_{1,2}| \le k_f \le 285\,\mathrm{MeV}$. The

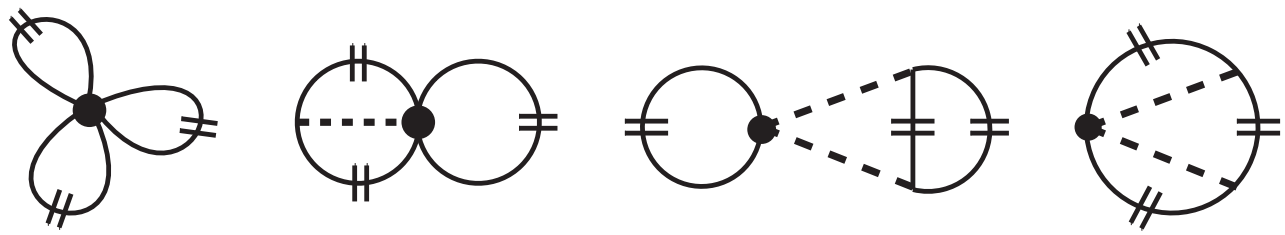

Figure 19: Three-body diagrams related to the contact ($c_E$), $1\pi$-exchange ($c_D$), and $2\pi$-exchange ($c_1, c_2, c_3$) components of the chiral three-nucleon interaction. The short double-line symbolizes the medium insertion $\Gamma(\vec{p}, \vec{q}\,)$ for inhomogeneous nuclear matter.

regulator function as well as its associated cutoff scale $\Lambda$ become relevant only at second order (and higher).

In the next step, the three-body contributions to the nuclear energy density functional $\mathcal{E}[\rho, \tau, \vec{J}\,]$ are included. The leading order chiral three-nucleon interaction consists of a contact piece (with low-energy constant $c_E$), a $1\pi$-exchange part (proportional to $c_D$), and a $2\pi$-exchange component (with low-energy constants $c_1$, $c_3$ and $c_4$). In order simplify the treatment of the three-body correlations in inhomogeneous nuclear systems, it has been assumed [89] that the relevant product of density-matrices can be represented in the factorized form $\Gamma(\vec{p}_1, \vec{q}_1\,)\,\Gamma(\vec{p}_2, \vec{q}_2\,)\,\Gamma(\vec{p}_3, -\vec{q}_1 - \vec{q}_2)$ in momentum space. This factorization ansatz respects the correct infinite nuclear matter limit, but it involves approximations compared to more sophisticated treatments explored in ref. [88]. In fact, the present approach is similar to the method "DME-I" considered in ref. [88].

The three-body contact-term proportional to $c_E$ (see Fig. 19) gives rise to a contribution to the energy per particle:

$$\bar{E}(\rho) = -\frac{c_E k_f^6}{12\pi^4 f_\pi^4 \Lambda}\,, \tag{86}$$

that is quadratic in the density $\rho = 2k_f^3/3\pi^2$. Obviously, all other strength functions $F_{\tau,d,so,J}(\rho)$ receive vanishing contributions due to the momentum-independence of the chiral contact interaction. The $1\pi$-exchange component of the chiral 3N-interaction involves the low-energy constant $c_D$. With three (inhomogeneous) medium insertions in the corresponding three-body diagram (shown in Fig. 19) one finds the following expressions for the strength functions:

$$\bar{E}(\rho) = \frac{g_A c_D m_\pi^6}{(2\pi f_\pi)^4 \Lambda}\Big\{\frac{u^6}{3} - \frac{3u^4}{4} + \frac{u^2}{8} + u^3 \arctan 2u - \frac{1+12u^2}{32}\ln(1+4u^2)\Big\}\,, \tag{87}$$

$$F_\tau(\rho) = \frac{2 g_A c_D m_\pi^4}{(4\pi f_\pi)^4 \Lambda}\Big\{(1+2u^2)\ln(1+4u^2) - 4u^2\Big\}\,, \tag{88}$$

$$F_d(\rho) = \frac{g_A c_D m_\pi}{(4 f_\pi)^4 \pi^2 \Lambda}\Big\{\frac{1}{2u}\ln(1+4u^2) - \frac{2u}{1+4u^2}\Big\}\,, \tag{89}$$

$$F_J(\rho) = \frac{3 g_A c_D m_\pi}{(4 f_\pi)^4 \pi^2 \Lambda}\Big\{2u - \frac{1}{u} + \frac{1}{4u^3}\ln(1+4u^2)\Big\}\,, \tag{90}$$

where $u = k_f/m_\pi$. We observe that there is no contribution to the spin-orbit strength $F_{so}(\rho)$, since neither the contact-vertex nor the $1\pi$-exchange component produces a spin-orbit interaction.

In the third diagram of Fig. 19, we show the three-body contribution arising from the $2\pi$-exchange Hartree term. With three (inhomogeneous) medium insertions, the corresponding energy density coupling strengths are written [89]:

$$\bar{E}(\rho) \;=\; \frac{g_A^2 m_\pi^6}{(2\pi f_\pi)^4}\Big\{(12c_1 - 10c_3)u^3 \arctan 2u - \frac{4}{3}c_3 u^6 + 6(c_3 - c_1)u^4$$

$$+(3c_1-2c_3)u^2+\left[\frac{1}{4}(2c_3-3c_1)+\frac{3u^2}{2}(3c_3-4c_1)\right]\ln(1+4u^2)\Big\}\,, \tag{91}$$

$$\begin{aligned} F_\tau(\rho) &= \frac{g_A^2 m_\pi^4}{(2\pi f_\pi)^4}\Big\{(5c_3-6c_1)u^2+\frac{(c_3-2c_1)u^2}{1+4u^2} \\ &\quad +\left[2c_1-\frac{3}{2}c_3+2(c_1-c_3)u^2\right]\ln(1+4u^2)\Big\}\,, \end{aligned} \tag{92}$$

$$\begin{aligned} F_d(\rho) &= \frac{g_A^2 m_\pi}{(8\pi)^2 f_\pi^4}\Big\{(10c_1-23c_3)\arctan 2u+16c_3u \\ &\quad +\frac{7c_3-5c_1}{u}\ln(1+4u^2)+\frac{6c_3u+16(2c_3-c_1)u^3}{3(1+4u^2)^2}\Big\}\,, \end{aligned} \tag{93}$$

$$F_{so}(\rho)=\frac{3g_A^2 m_\pi}{(8\pi)^2 f_\pi^4}\Big\{\frac{2}{u}(4c_1-3c_3)-4c_3u+\left[\frac{4}{u}(c_3-c_1)+\frac{3c_3-4c_1}{2u^3}\right]\ln(1+4u^2)\Big\}\,, \tag{94}$$

$$F_J(\rho)=\frac{3g_A^2 m_\pi}{(8\pi)^2 f_\pi^4}\Big\{\frac{3c_3-4c_1}{u}-2c_3u+\frac{4u(2c_1-c_3)}{1+4u^2}+\frac{4c_1-3c_3}{4u^3}\ln(1+4u^2)\Big\}\,, \tag{95}$$

which depend only on the isoscalar coupling constants $c_1$ and $c_3$. Note that the expression for the spin-orbit strength in eq. (94) provides the dominant part of the three-body contribution to $F_{so}(\rho)$, as suggested originally by Fujita and Miyazawa [41] in the context of $\Delta(1232)$-resonance excitation. In the present chiral effective field theory treatment without explicit $\Delta$ resonances, the two-step process $\pi N\to\Delta\to\pi N$ is written as an equivalent $\pi\pi NN$ contact vertex proportional to $c_3$.

Finally, we discuss the three-body $2\pi$-exchange Fock contribution, which is shown as the fourth diagram of Fig. 19. This term consists of a single closed nucleon ring that generates for isospin-symmetric nuclear matter non-vanishing contributions from both the isoscalar and isovector $\pi\pi NN$ contact vertices, the latter proportional to the low-energy constant $c_4$. In contrast to the three-body $2\pi$-exchange Hartree diagram, the Fock contribution involves integrals (over three Fermi spheres) that cannot be computed in closed analytical form. The resulting rather lengthy expressions for the various strength functions can be found in section 4.4. of ref. [89].

Let us now discuss the results for the nuclear energy density functional obtained in the first-order Hartree-Fock approximation. In Fig. 20 we show the contributions to the energy per particle $\bar{E}(\rho)$ from chiral two- and three-body forces for densities up to $\rho=0.2\,\mathrm{fm}^{-3}$. The dash-dotted line denotes the attractive two-body contributions, while the dashed line gives the repulsive three-body contributions. The results from the N$^3$LOW chiral nucleon-nucleon interaction are compared to those from the universal low-momentum NN potential $V_{\mathrm{low-k}}$ obtained by integrating over its diagonal (on-shell) partial-wave matrix elements. Indeed, the treatment of the two-body interaction via the chiral potential N$^3$LOW gives a fairly accurate reproduction of these results. The full line in Fig. 20 shows the sum of the two- and three-body contributions, which exhibits a first tendency for the saturation of nuclear matter. After including the kinetic energy $\bar{E}_{\mathrm{kin}}(\rho)=3k_f^2/10M_N-3k_f^4/56M_N^3$, however, the resulting saturation energy is still much too low. This particular feature of the Hartree-Fock approximation has been observed in similar studies [101, 68]. A much improved description of the nuclear matter equation of state is achieved by treating the two-body (and three-body) interaction at least to second order.

In Fig. 21 we reproduce the contributions to the strength function $F_\tau(\rho)$ associated with the surface gradient term in the energy density functional. We note that the two-body parts derived from $V_{\mathrm{low-k}}$ and the chiral N$^3$LOW potential are rather similar. The three-body part, which increases nearly linearly with the density, comes out relatively small. At nuclear matter saturation density $\rho_0=0.16\,\mathrm{fm}^{-3}$ it gives rise to a correction of about 20% compared to the two-body contribution. The bracketed term that

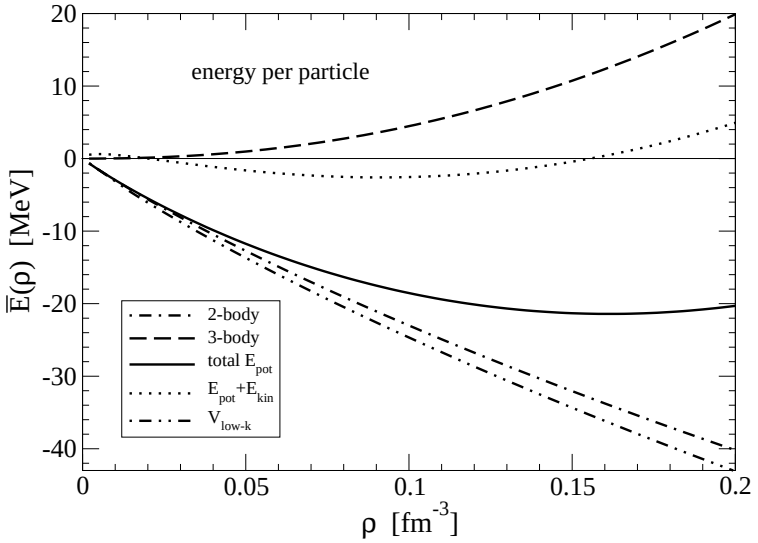


Figure 20: The energy per particle $\bar{E}(\rho)$ of isospin-symmetric nuclear matter derived from chiral nuclear interactions.

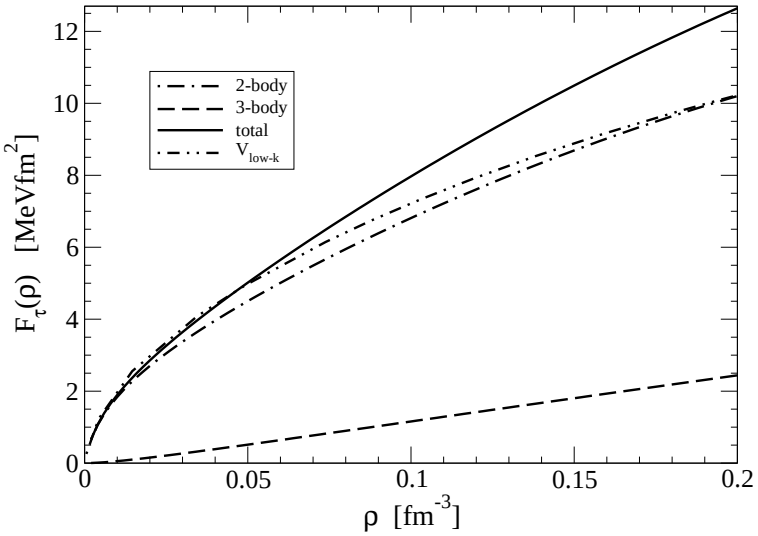


Figure 21: Contributions to the strength function $F_\tau(\rho)$ as a function of the nuclear density $\rho$.

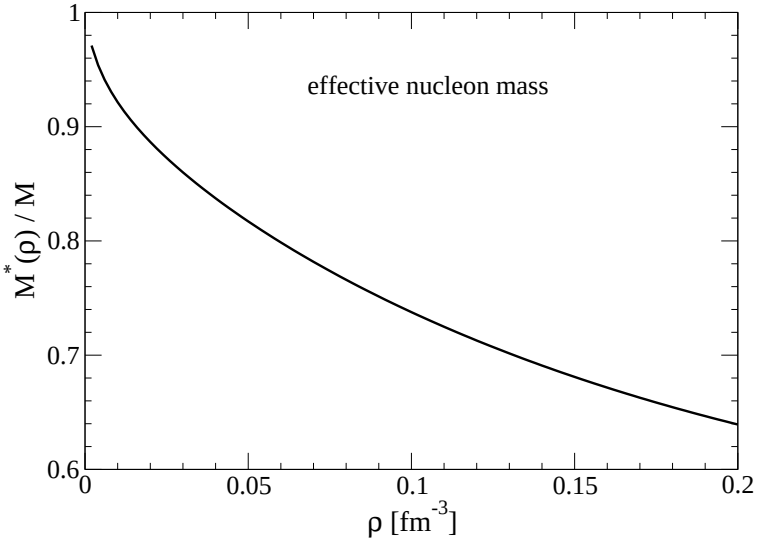


Figure 22: Ratio of the effective nucleon mass $M^*(\rho)$ to the free nucleon mass $M$ as function of $\rho$.

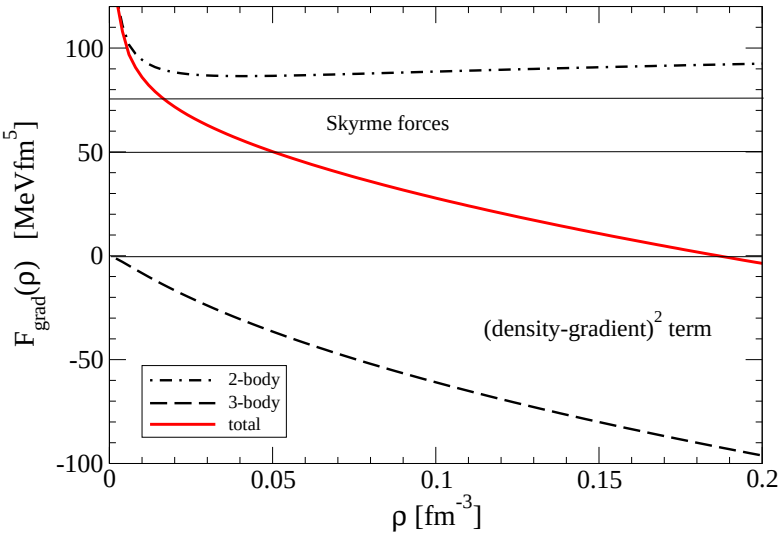


Figure 23: The strength function $F_\nabla(\rho)$ of the surface term $(\vec{\nabla}\rho)^2$ versus the nuclear density $\rho$.

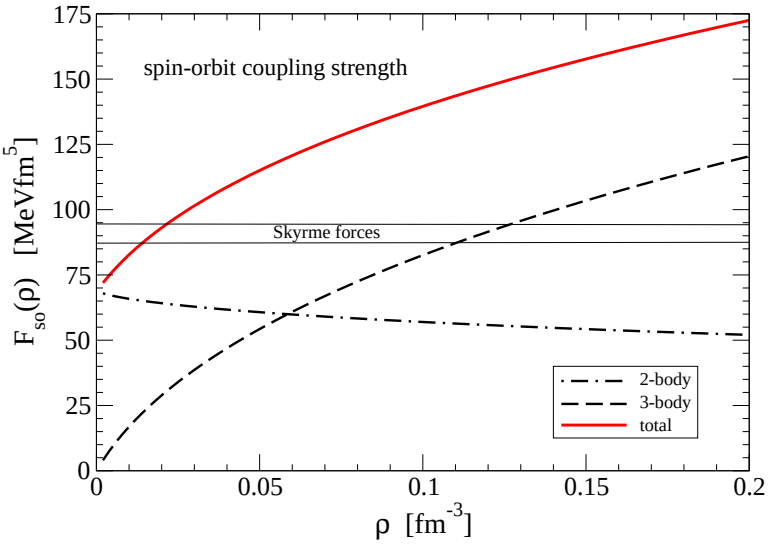


Figure 24: Spin-orbit strength function $F_{so}(\rho)$ as a function of the density $\rho$.

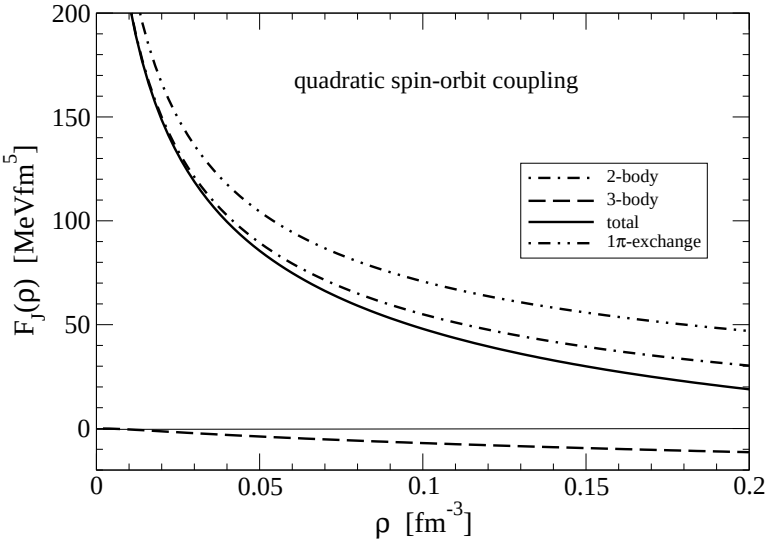


Figure 25: Strength function $F_J(\rho)$ of the squared spin-orbit density $\vec{J}^2$ versus $\rho$.

multiplies the kinetic energy density $\tau(\vec{r})$ in the expression for the nuclear energy density functional in eq. (72) can be interpreted as the reciprocal of a density-dependent effective nucleon mass:

$$M^*(\rho) = M_N \Big[ 1 - \frac{k_f^2}{2M_N^2} + 2M_N\, F_\tau(\rho) \Big]^{-1} . \tag{96}$$

In the improved density matrix expansion it is identical to the so-called "Landau" effective mass introduced in Fermi-liquid theory, and it is derived in the same way from the derivative of the single-particle potential $U(p, k_f)$ with respect to the momentum $p$ at the Fermi surface $p = k_f$. The relativistic increase in the mass is accounted for with the small correction term $-k_f^2/2M_N^2$. In Fig. 22 we show the ratio of effective nucleon mass to the free nucleon mass $M^*(\rho)/M_N$ as a function of the density $\rho$. In the Hartree-Fock approximation, the effective nucleon mass is reduced in comparison to the free-space mass, and the ratio reaches the value $M^*(\rho_0) \simeq 0.67 M_N$ at nuclear matter saturation density $\rho_0 = 0.16\,\mathrm{fm}^{-3}$. This is consistent with the range $0.7 < M^*(\rho_0)/M_N < 1$ determined from phenomenological Skyrme forces [93, 94]. On the other hand, second-order corrections from two-body forces significantly enhance the effective mass [106].

The strength function $F_\nabla(\rho)$ of the surface gradient term $(\vec{\nabla}\rho)^2$ is plotted in Fig. 23 as a function of the nuclear density. At very low densities this coupling strength exhibits a pronounced increase in the two-body contribution (dash-dotted line) that has its origin in $1\pi$-exchange. For larger densities, the two-body contributions are nearly independent of the density. The three-body contribution (dashed line) is sizable and negative. It reduces the two-body contribution such that the total value of $F_\nabla(\rho)$ (full line in Fig. 23) decreases with increasing density $\rho$. To compare with phenomenology we also show the band (of constant $F_\nabla(\rho)$-values) spanned by parameterized Skyrme forces [93, 94]. The Hartree-Fock result from realistic chiral two- and three-body forces is somewhat too small at densities close to $\rho_0/2 = 0.08\,\mathrm{fm}^{-3}$, where the surface energy in finite nuclei gains much of its weight. Iterated $1\pi$-exchange has been considered in ref. [107] from which it may be deduced that a treatment of the two-body interaction to second order in perturbation theory will increase the values of $F_\nabla(\rho)$.

Of special interest is the coupling strength $F_{so}(\rho)$ multiplying the spin-orbit term $\vec{\nabla}\rho \cdot \vec{J}$. Contributions from two- and three-body terms, as well as their total sum, are shown in Fig. 24. The coupling strength from two-body forces is dominated by the low-energy constant $3C_5/8$, as suggested also by the weak dependence of the dash-dotted line on the density $\rho$. Three-body forces induce a density-dependent spin-orbit interaction that considerably enhances the contribution from the N$^3$LOW two-body force. The most significant contribution arises in the Hartree term (94) proportional to the low-energy constant $c_3 = -4.78\,\mathrm{GeV}^{-1}$. With this particular value of $c_3$, the three-body spin-orbit strength is considerably larger than that proposed by Fujita and Miyazawa [41], where the $\Delta(1232)$-excitation mechanism would correspond to $c_3^{(\Delta)} = -g_A^2/2\Delta \simeq -2.9\,\mathrm{GeV}^{-1}$ ($\Delta = 293\,\mathrm{MeV}$ is the delta-nucleon mass splitting). At densities around half that of saturated nuclear matter, $\rho_0/2 = 0.08\,\mathrm{fm}^{-3}$, the total Hartree-Fock contribution exceeds the empirical spin-orbit coupling strength $F_{so}^{(\mathrm{emp})}(\rho) \simeq 90\,\mathrm{MeV\,fm}^5$ [93, 94] by nearly 50%. A compensating effect is therefore required, and it has been suggested in ref. [107] that the $1\pi$-exchange tensor force at second-order generates a spin-orbit coupling of the "wrong-sign". It is then reasonable to assume that the low-momentum two-nucleon tensor potential, when treated to second-order in perturbation theory, will reduce the strength of the spin-orbit coupling $F_{so}(\rho)$ to a value close to that suggested by phenomenology.

To conclude the description of the nuclear energy density functional in $N = Z$ even-even nuclei, we show in Fig. 25 the strength function $F_J(\rho)$ of the squared spin-orbit coupling. In contrast to all of the previous coupling strengths, $F_J(\rho)$ receives only a very small contribution from three-body forces. One observes that the two-body contribution is, however, strongly density-dependent, and at low densities it reaches quite large values. This strong density dependence originates primarily from the $1\pi$-exchange contribution, which for comparison we reproduce separately in Fig. 25 (dashed-double-dotted line).

At this point it should be emphasized that the $\vec{J}^2$-term in the energy density functional represents non-local Fock contributions from tensor forces, etc. It is therefore not surprising that there exists an outstanding $1\pi$-exchange contribution to the strength function $F_J(\rho)$.

## 6.3 *Isovector Part of the Nuclear Energy Density Functional*

The previous calculation of the nuclear energy density functional from chiral two- and three-nucleon forces can be extended in a straightforward manner to the isovector terms [90] relevant for nuclei with different proton and neutron densities. The additional isovector terms play an important role in the description of long isotopic chains of stable nuclei and for neutron-rich systems far from stability. By construction the density-matrix expansion of Gebremariam, Duguet and Bogner [85] applies separately to proton and neutron orbitals. It is therefore easily adapted to the situation of isospin-asymmetric nuclear systems with different proton and neutron local densities $\rho_{p,n}, \tau_{p,n}, \vec{J}_{p,n}$. After Fourier transforming to momentum space one obtains the medium insertion:

$$\begin{aligned}\Gamma_{\rm iv}(\vec{p},\vec{q}\,) &= \int d^3r\, e^{-i\vec{q}\cdot\vec{r}}\Big\{\frac{\mathbf{1}+\boldsymbol{\tau}_3}{2}\,\theta(k_p-|\vec{p}\,|)+\frac{\mathbf{1}-\boldsymbol{\tau}_3}{2}\,\theta(k_n-|\vec{p}\,|) \\ &\quad +\frac{\pi^2}{4k_f^4}\Big[k_f\,\delta'(k_f-|\vec{p}\,|)-2\delta(k_f-|\vec{p}\,|)\Big]\Big[\tau_p-\tau_n-\Big(k_f^2+\frac{\vec{\nabla}^2}{4}\Big) \\ &\quad \times(\rho_p-\rho_n)\Big]\boldsymbol{\tau}_3-\frac{3\pi^2}{4k_f^4}\,\delta(k_f-|\vec{p}\,|)\,(\vec{\sigma}\times\vec{p}\,)\cdot(\vec{J}_p-\vec{J}_n)\boldsymbol{\tau}_3+\ldots\Big\}\,, \end{aligned} \tag{97}$$

for the inhomogeneous isospin-asymmetric many-nucleon system. In the above expression, $\boldsymbol{\tau}_3$ denotes the third Pauli isospin matrix, and we have included only the relevant terms proportional to differences of proton and neutron densities: $\rho_p-\rho_n$, $\tau_p-\tau_n$, $\vec{J}_p-\vec{J}_n$. The two local Fermi momenta are related to the (particle) densities in the usual way: $\rho_p=k_p^3/3\pi^2$, $\rho_n=k_n^3/3\pi^2$, $\rho=\rho_p+\rho_n=2k_f^3/3\pi^2$. When working to quadratic order in deviations from isospin-symmetric nuclear systems, it is sufficient to employ an average Fermi momentum $k_f$ in the factors multiplying $\tau_p-\tau_n$ and $\vec{J}_p-\vec{J}_n$.

Up to second order in proton-neutron density differences and spatial gradients, the isovector part of the nuclear energy density functional reads:

$$\begin{aligned}&\mathcal{E}_{\rm iv}[\rho_p,\rho_n,\tau_p,\tau_n,\vec{J}_p,\vec{J}_n]=\frac{1}{\rho}(\rho_p-\rho_n)^2\,\tilde{A}(\rho)+\frac{1}{\rho}(\tau_p-\tau_n)(\rho_p-\rho_n)\,G_\tau(\rho) \\ &+(\vec{\nabla}\rho_p-\vec{\nabla}\rho_n)^2\,G_\nabla(\rho)+(\vec{\nabla}\rho_p-\vec{\nabla}\rho_n)\cdot(\vec{J}_p-\vec{J}_n)\,G_{so}(\rho)+(\vec{J}_p-\vec{J}_n)^2\,G_J(\rho)\,. \end{aligned} \tag{98}$$

Here, $\tilde{A}(\rho)$ is the interaction part of the isospin-asymmetry energy of homogeneous nuclear matter. The non-interacting (or kinetic energy) contribution $A_{\rm kin}(\rho)=k_f^2/6M_N$ to the isospin-asymmetry energy is included in the energy density functional through the kinetic energy density term, $\mathcal{E}_{\rm kin}=(\tau_p+\tau_n)/2M_N$. The strength function $G_\nabla(\rho)$ multiplying the isovector surface term $(\vec{\nabla}\rho_p-\vec{\nabla}\rho_n)^2$ can be decomposed as

$$G_\nabla(\rho)=\frac{1}{4\rho}\,G_\tau(\rho)+G_d(\rho)\,, \tag{99}$$

where $G_d(\rho)$ denotes all those contributions for which the $(\vec{\nabla}\rho_p-\vec{\nabla}\rho_n)^2$ factor originates from the momentum dependence of the interactions in an expansion up to order $\vec{q}^{\,2}$. Performing a Fourier transformation converts this factor $\vec{q}^{\,2}$ into $(\vec{\nabla}k_p-\vec{\nabla}k_n)^2\simeq(\vec{\nabla}\rho_p-\vec{\nabla}\rho_n)^2(\pi/k_f)^4$. The next-to-last term $(\vec{\nabla}\rho_p-\vec{\nabla}\rho_n)\cdot(\vec{J}_p-\vec{J}_n)\,G_{so}(\rho)$ in eq. (98) is the isovector spin-orbit interaction in nuclei. Depending on the sign and size of its strength function $G_{so}(\rho)$, the spin-orbit potentials for protons and neutrons receive different weightings from the gradients of the local proton and neutron densities.

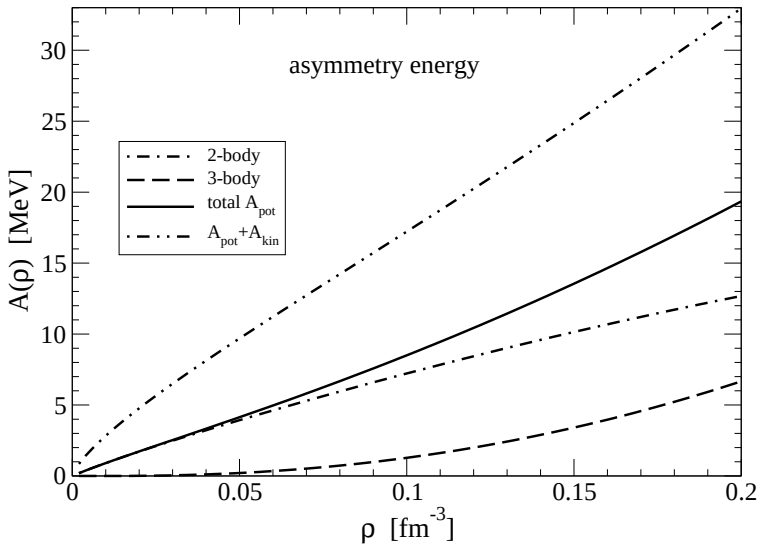


Figure 26: Contributions to the asymmetry energy $A(\rho)$ of nuclear matter.

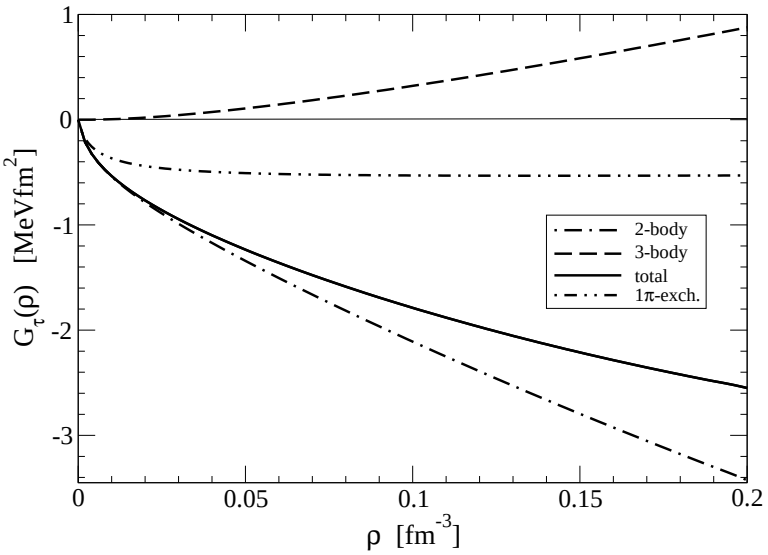


Figure 27: Contributions to the strength function $G_\tau(\rho)$ versus the nuclear density $\rho$.

The two- and three-body contributions to the isovector strength functions $\tilde{A}(\rho), G_\tau(\rho), G_d(\rho), G_{so}(\rho)$ and $G_J(\rho)$ follow the same pattern as outlined in the previous section for the isoscalar strength functions. The corresponding analytical expressions can be found in ref. [90]. An interesting observation is that the Fujita-Mayazawa mechanism for induced spin-orbit couplings from three-body forces is not operative in the isovector channel, since the $2\pi$-exchange three-body Hartree diagram leads to a vanishing contribution to $G_{so}(\rho)$.

The results for the isosvector strength functions are shown in Figs. 26–30. The following features can be observed. The Hartree-Fock approximation seems to work better for isovector quantities. The asymmetry energy at saturation density comes out as $A(\rho_0) = 26.5\,\mathrm{MeV}$, which agrees within 20% with the empirical value $(35 \pm 2)\,\mathrm{MeV}$. In fact, a second-order calculation [106] with two-nucleon forces increased the asymmetry energy by approximately 20% and reached the empirical value. The strength functions $G_\tau(\rho)$ and $G_\nabla(\rho)$, related to the splitting of the proton and neutron effective masses and the isosvector surface term $(\vec{\nabla}\rho_p - \vec{\nabla}\rho_n)^2$, are typically one order of magnitude smaller than their isoscalar analogs $F_\tau(\rho)$ and $F_\nabla(\rho)$. Due to the absence of a large three-body term, the isovector spin-orbit coupling strength $G_{so}(\rho)$ is now dominated by the short-distance contribution (namely, the low-energy constant $C_5/8$) and thus has only a very weak density dependence. The quadratic spin-orbit

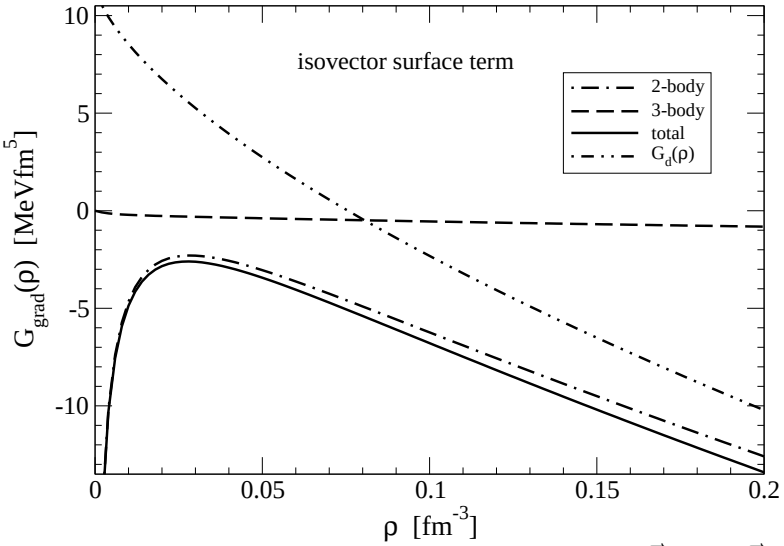


Figure 28: Strength function $G_\nabla(\rho)$ of the isovector surface term $(\vec{\nabla}\rho_p - \vec{\nabla}\rho_n)^2$ versus the nuclear density $\rho$.

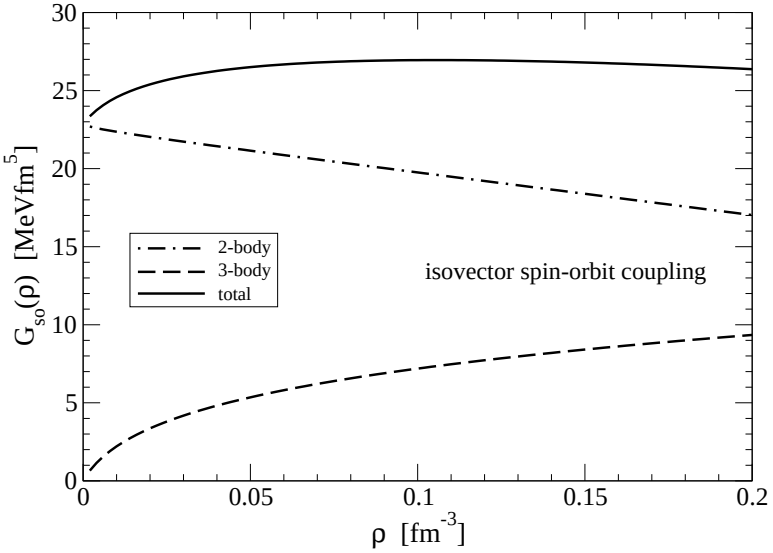


Figure 29: Strength function $G_{so}(\rho)$ of the isovector spin-orbit coupling term $(\vec{\nabla}\rho_p - \vec{\nabla}\rho_n) \cdot (\vec{J}_p - \vec{J}_n)$ versus the nuclear density $\rho$.

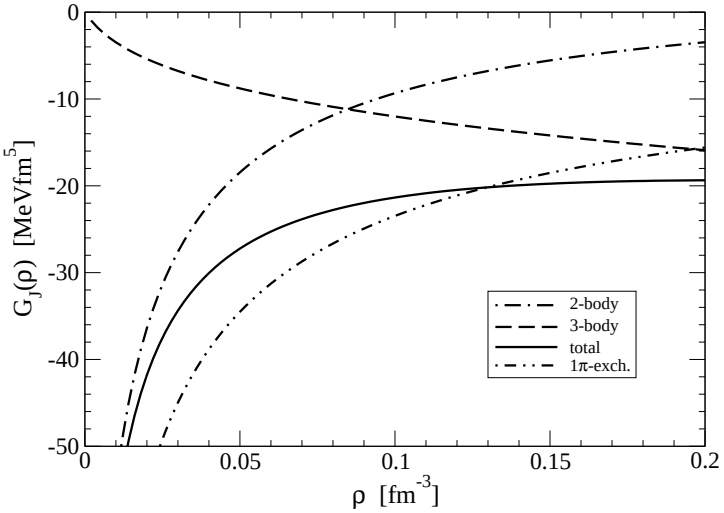


Figure 30: Strength function $G_J(\rho)$ multiplying the squared isovector spin-orbit density $(\vec{J}_p - \vec{J}_n)^2$ versus the nuclear density $\rho$.

coupling strength $G_J(\rho)$ is again dominated by $1\pi$-exchange contribution which induces a strong density dependence. It should be noted that within Skyrme phenomenology the isovector part of the energy density functional is presently not well determined. For example, no definite choice could be made in ref. [108] between different density dependences ($\sim \rho_p + \gamma\rho_n, \gamma = 0, 1, 2$) for the neutron spin-orbit potential in Pb isotopes.

The physics of nuclear structure at large neutron excesses will be explored in the near future at rare isotope facilities. The predictions obtained from chiral two- and three-body interactions with their definite isospin-dependence can serve as a guideline for the theoretical exploration of this field.

# 7 Chiral Effective Interactions and Fermi Liquid Theory

Landau's theory of normal Fermi liquids [109] has long served as a standard basis for understanding strongly-interacting Fermi systems at low temperatures. Although more than fifty years old, Landau's original insights foreshadowed key ideas in the development of effective field theories [110] and the renormalization group [111, 112, 113]. In Fermi liquid theory, the relevant degrees of freedom associated with low-energy, long-wavelength excitations of a many-body Fermi system are quasiparticles interacting in the vicinity of the Fermi surface through a residual force. Although the quasiparticle interaction is not necessary weak, small perturbations of the system excite relatively few quasiparticles, which then forms the basis for an expansion of the theory in terms of the quasiparticle density.

The microscopic foundation for Fermi liquid theory is based on an analysis of the one- and two-particle Green's functions [114]. In the vicinity of the Fermi surface, the one-body Green's function can be decomposed into quasiparticle and background contributions, and the effects of the background contribution are absorbed into the effective coupling between quasiparticles. In the original applications of Fermi liquid theory to finite nuclei [115, 116], the quasiparticle couplings were adjusted to empirical data, resulting in a phenomenological theory capable of linking seemingly disconnected phenomena. The perturbative approach to nuclear Fermi liquid theory based on microscopic models of the strong nuclear force was initiated by Brown and collaborators [117] and has in recent years been updated to take advantage of the improved convergence properties of chiral and low-momentum nuclear two- and three-body forces [118, 119, 106, 120, 121].

In the present section we review the Fermi liquid description of nuclear and neutron matter in the context of chiral effective field theory. A microscopic approach framed in many-body perturbation theory is shown to provide a successful description of many nuclear matter observables when the leading-order medium corrections from two- and three-body forces are included. The extrapolation to pure neutron matter is considered, and applications relevant for neutron star structure and evolution are discussed. We focus on the convergence of the perturbative expansion with chiral nuclear forces and the role of chiral three-nucleon forces. For a more general review of the Fermi liquid approach to nuclear many-body systems, we refer the reader to ref. [122].

## 7.1 *Symmetric Nuclear Matter*

Numerous properties of isospin-symmetric nuclear matter in the vicinity of the saturation density $\rho_0$ are well constrained by empirical data and serve as a benchmark for microscopic approaches to nuclear structure. Within the framework of Fermi liquid theory, specific nuclear observables are directly related to the central components of the quasiparticle interaction, which has the general form

$$\mathcal{F}_{\rm cent}(\vec{p}_1, \vec{p}_2) = \frac{1}{N_0} \sum_{L=0}^{\infty} \left[ F_L + F'_L \, \vec{\tau}_1 \cdot \vec{\tau}_2 + (G_L + G'_L \, \vec{\tau}_1 \cdot \vec{\tau}_2) \, \vec{\sigma}_1 \cdot \vec{\sigma}_2 \right] P_L(\cos\theta), \tag{100}$$

where $N_0 = 2M^* k_f/\pi^2$ is the density of states at the Fermi surface, and we have set $|\vec{p}_1| = |\vec{p}_2| = k_f$, which allows one to write the quasiparticle interaction in terms of $\cos\theta = \hat{p}_1 \cdot \hat{p}_2$. The noncentral parts of

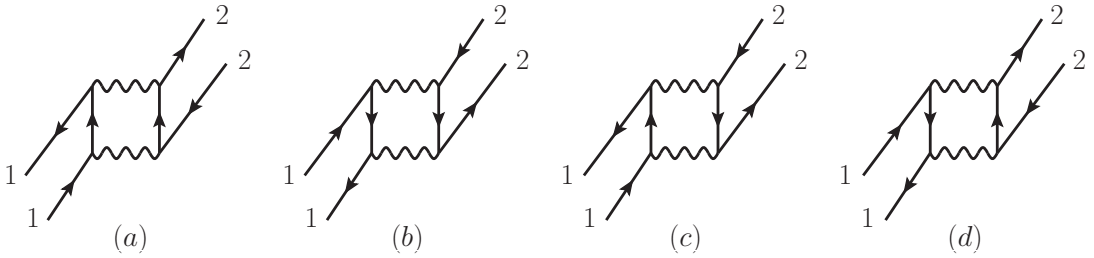


Figure 31: Diagrams contributing to the second-order quasiparticle interaction (all interactions represented by wavy lines are antisymmetrized): (a) particle-particle diagram, (b) hole-hole diagram, and (c)+(d) particle-hole diagrams.

the quasiparticle interaction, which are particularly relevant for neutron matter, will be discussed in the following section. The relationship between individual Fermi liquid parameters and nuclear observables are well known [116]:

$$\begin{aligned}
\text{Quasiparticle effective mass}: \quad \frac{M^*}{M_N} &= 1 + F_1/3, \\
\text{Compression modulus}: \quad \mathcal{K} &= \frac{3k_F^2}{M^*}\,(1+F_0)\,, \\
\text{Isospin asymmetry energy}: \quad \beta &= \frac{k_F^2}{6M^*}(1+F_0'), \\
\text{Orbital } g\text{-factor}: \quad g_l &= \frac{1+\tau_3}{2} + \frac{F_1' - F_1}{6(1+F_1/3)}\tau_3, \\
\text{Spin-isospin response}: \quad g'_{NN} &= \frac{4M_N^2}{g_{\pi N}^2 N_0} G_0'.
\end{aligned} \tag{101}$$

Within the framework of many-body perturbation theory, the quasiparticle interaction is derived by functionally differentiating the total energy density twice with respect to the particle occupation densities $\delta n_{\vec{p},s,t}$:

$$\delta\mathcal{E} = \sum_{\vec{p}st} \epsilon_{\vec{p}}\,\delta n_{\vec{p}st} + \frac{1}{2}\sum_{\substack{\vec{p}_1 s_1 t_1 \\ \vec{p}_2 s_2 t_2}} \mathcal{F}(\vec{p}_1 s_1 t_1; \vec{p}_2 s_2 t_2)\,\delta n_{\vec{p}_1 s_1 t_1}\,\delta n_{\vec{p}_2 s_2 t_2} + \cdots, \tag{102}$$

where $s_i$ and $t_i$ label the spin and isospin quantum numbers. The first- and second-order contributions are shown diagrammatically in Fig. 31. As shown in the first row of Table 1, the quasiparticle interaction computed at leading order with chiral two-body forces shares many features with previous calculations employing $G$-matrix effective interactions. In particular, the quasiparticle effective mass $M^*/M_N = 0.70$ is significantly less than unity, the nuclear symmetry energy $\beta = 21\,\text{MeV}$ is too small compared to the empirical value $\beta_{emp} \simeq 30 - 35\,\text{MeV}$, and the compression modulus $\mathcal{K} = -44\,\text{MeV}$ is negative and implies the instability of nuclear matter to density fluctuations. This last feature was quite common in previous calculations of the Fermi liquid parameters with $G$-matrix effective interactions [123, 124, 125] and was remedied with the inclusion of virtual collective excitations, represented diagrammatically as the sum of particle-hole bubble diagrams and encoded in the Babu-Brown induced interaction [126], which provided sufficient screening in the scalar-isoscalar channel to render nuclear matter stable.

Recent chiral effective field theory calculations have systematically studied the second-order contributions to the quasiparticle interaction, given in rows 3-5 of Table 1. The particle-particle term (represented diagrammatically Fig. 31(a)) is found to enhance the attraction in the spin- and isospin-independent interaction, while the particle-hole terms (Fig. 31(c) and (d)) are found to be strongly

| Chiral 2N + 3N interactions at $k_F = 1.33$ fm$^{-1}$ | | | | | | | | |
|---|---|---|---|---|---|---|---|---|
| | $f_0$ [fm$^2$] | $g_0$ [fm$^2$] | $f_0'$ [fm$^2$] | $g_0'$ [fm$^2$] | $f_1$ [fm$^2$] | $g_1$ [fm$^2$] | $f_1'$ [fm$^2$] | $g_1'$ [fm$^2$] |
| $V_{2N}^{(1)}$ | $-1.274$ | 0.298 | 0.200 | 0.955 | $-1.018$ | 0.529 | 0.230 | 0.090 |
| $V_{2N}^{(2-pp)}$ | $-1.461$ | 0.023 | 0.686 | 0.255 | 0.041 | $-0.059$ | 0.334 | 0.254 |
| $V_{2N}^{(2-hh)}$ | $-0.271$ | 0.018 | 0.120 | 0.041 | 0.276 | 0.041 | $-0.144$ | $-0.009$ |
| $V_{2N}^{(2-ph)}$ | 1.642 | $-0.057$ | 0.429 | 0.162 | 0.889 | $-0.143$ | 0.130 | 0.142 |
| $V_{3N}^{(1)}$ | 1.218 | 0.009 | 0.009 | $-0.295$ | $-0.073$ | $-0.232$ | $-0.232$ | $-0.179$ |

Table 1: Fermi liquid parameters ($L = 0, 1$) computed at nuclear matter saturation density from the Idaho N$^3$LO chiral nucleon-nucleon potential as well as from the leading N$^2$LO chiral three-nucleon force.

repulsive. Together these two contributions largely cancel in the calculation of the $F_0$ Landau parameter, and since the second-order particle-hole diagram accounts for much of the full Babu-Brown induced interaction, the stabilization mechanism against density fluctuations for chiral nuclear interactions must be qualitatively different than in the case of the $G$-matrix effective interactions. As seen in Table 1 both the $f_1$ and $f_0'$ Landau parameters receive coherent contributions from all second-order diagrams. This results in a quasiparticle effective mass at the Fermi surface that is nearly equal to the free-space nucleon mass. Taken alone, this would substantially decrease the isospin asymmetry energy. However, the second-order contributions also play a dominant role in enhancing the isospin dependence of the quasiparticle interaction. At nuclear matter saturation density, the resulting isospin asymmetry energy is $\beta = 34\,\mathrm{MeV}$, which is in very good agreement with the empirical value. These results obtained from the Idaho chiral two-nucleon force are qualitatively the same those from evolved low-momentum NN interactions [106].

In the chiral effective field theory description of nuclear interactions, three-body forces enter at N$^2$LO in the chiral power counting. The first-order contributions from the leading-order three-nucleon force are shown diagrammatically in Fig. 12 and have been computed analytically for the first time in ref. [120]. The surprising feature revealed in these calculations is the substantial repulsion present in the spin- and isospin-independent quasiparticle interaction resulting from two-pion exchange dynamics and to a lesser extent the chiral three-nucleon contact interaction. As shown in the left panel of Fig. 32, the Landau parameter $f_0$ grows strongly with the density and provides more than sufficient repulsion to stabilize nuclear matter at the empirical saturation density, resulting in a compression modulus of $\mathcal{K} =$ MeV. This qualitative behavior is foreseen already in calculations of the nuclear matter equation of state with chiral and low-momentum interactions, which require three-nucleon forces in order to achieve saturation at the empirical density [99]. However, the magnitude of $f_0$ relative to the other Landau parameters, as seen in Fig. 32 and compiled at nuclear matter density in the last row of Table 1, is unexpectedly large. The momentum dependence of the quasiparticle interaction in this channel is especially weak, producing only a very small decrease in the quasiparticle effective mass. The scalar-isovector and vector-isoscalar interactions are identical and nearly zero when averaged over all angles. Three-nucleon forces therefore play a minor role in determining the isospin asymmetry energy of nuclear matter, which was already well described with two-nucleon forces alone.

In the right panel of Fig. 32 we show the density dependence of the full quasiparticle interaction for an evolved low-momentum nucleon-nucleon potential combined with a three-nucleon force whose low-energy constants are refit at the low-momentum cutoff scale [99]. Qualitatively similar results hold for the unevolved Idaho nucleon-nucleon interaction and associated three-nucleon force, but the variation in cutoff scale and low-energy constants provides an important means for studying the theoretical uncertainties present in the perturbative calculation. From Fig. 32 one sees that the density dependence

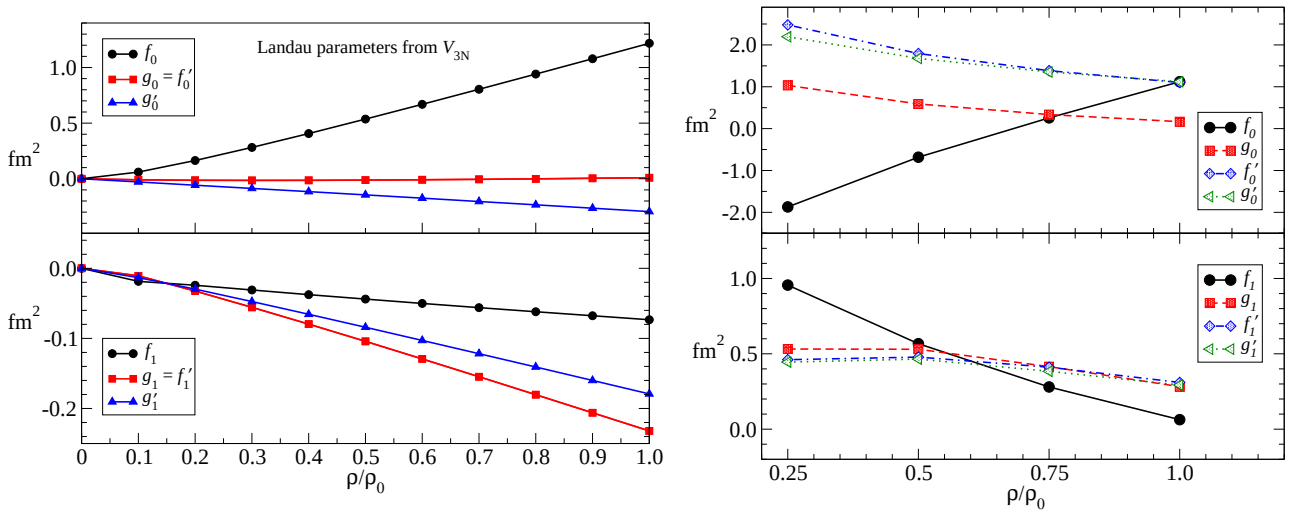


Figure 32: Left panel: density-dependent $L = 0, 1$ Fermi liquid parameters obtained from the leading-order chiral three-nucleon force with low-energy constants given in ref. [32]. Right panel: density-dependent $L = 0, 1$ Fermi liquid parameters computed from low-momentum chiral two-nucleon and three-nucleon interactions at the resolution scale $\Lambda = 2.1\,\mathrm{fm}^{-1}$.

of the spin- and isospin-independent quasiparticle interaction is particularly strong. This suggests that obtaining a quantitatively correct description of the effective mass and compressibility of nuclear matter at the saturation density is nontrivial. In contrast, the remaining components of the quasiparticle interaction have a weak and strikingly similar density dependence. Although most properties of symmetric nuclear matter are well reproduced as discussed above, the anomalous orbital $g$-factor $\delta g_l \simeq 0.07 \pm 0.02$ is considerably weaker than the value $\delta g_{l,\mathrm{exp}} \simeq 0.23 \pm 0.03$ extracted from an experimental analysis of the isovector giant dipole sum rule [127]:

$$\int_0^{\omega_{\max}} d\omega\, \sigma(E1) = \frac{2\pi\alpha}{M_N}\frac{NZ}{A}(1 + 2\delta g_l)\,, \tag{103}$$

where $\alpha = 1/137$. Overall, however, the perturbative calculation including the first-order (free-space) contribution from two-body forces together with the leading Pauli-blocking and core polarization effects from two- and three-body forces provides a successful description of isospin-symmetric nuclear matter in the vicinity of the empirical saturation density.

## 7.2 *Neutron Matter*

In contrast to the case of isospin-symmetric nuclear matter, the quasiparticle interaction in pure neutron matter is largely unconstrained empirically but is highly relevant for neutrino processes in neutron stars [128, 129, 130, 131] as well as the response of neutron star matter to strong magnetic fields [132, 133, 134, 135]. Previous calculations with microscopic and phenomenological nuclear potentials have given qualitatively different predictions for the magnetic susceptibility of neutron matter, with some phenomenological potentials even giving rise to a ferromagnetic phase transition at several times nuclear matter saturation density [135, 136, 137]. Both the magnetic susceptibility of neutron matter as well as neutrino absorption, emission, and elastic scattering rates depend on noncentral components of the quasiparticle interaction [138, 139] as discussed in refs. [133, 130, 131]. Recently, these questions have been revisited within the framework of chiral effective field theory including three-nucleon forces [121].

In the long-wavelength limit, the quasiparticle interaction in pure neutron matter has the general

| | Chiral 2NF + 3NF ($k_f = 1.7\,\mathrm{fm}^{-1}$) | | | | | | | | |
|---|---|---|---|---|---|---|---|---|---|
| $L$ | 0 | | | 1 | | | 2 | | |
| | $V_{2N}^{(1)}$ | $V_{2N}^{(2)}$ | $V_{3N}^{(1)}$ | $V_{2N}^{(1)}$ | $V_{2N}^{(2)}$ | $V_{3N}^{(1)}$ | $V_{2N}^{(1)}$ | $V_{2N}^{(2)}$ | $V_{3N}^{(1)}$ |
| $f$ [fm$^2$] | $-0.700$ | 0.069 | 1.319 | $-1.025$ | 1.197 | $-0.037$ | $-0.230$ | $-0.500$ | $-0.293$ |
| $g$ [fm$^2$] | 1.053 | 0.293 | $-0.283$ | 0.613 | 0.159 | $-0.364$ | 0.337 | $-0.089$ | 0.043 |
| $h$ [fm$^2$] | 0.270 | $-0.212$ | 0.075 | 0.060 | 0.106 | 0.164 | $-0.040$ | $-0.143$ | $-0.087$ |
| $k$ [fm$^2$] | 0 | $-0.156$ | 0 | 0 | 0.085 | 0 | 0 | 0.063 | 0 |
| $l$ [fm$^2$] | 0 | 0.135 | $-0.168$ | 0 | $-0.031$ | $-0.134$ | 0 | $-0.279$ | 0.083 |

Table 2: Fermi liquid parameters for the quasiparticle interaction in neutron matter at a density corresponding to a Fermi momentum of $k_f = 1.7\,\mathrm{fm}^{-1}$. The low-energy constants of the N$^2$LO chiral three-nucleon force are chosen to be $c_1 = -0.81\,\mathrm{GeV}^{-1}$ and $c_3 = -3.2\,\mathrm{GeV}^{-1}$.

form [139]:

$$\begin{aligned}\mathcal{F}(\vec{p}_1,\vec{p}_2\,) &= f(\vec{p}_1,\vec{p}_2\,) + g(\vec{p}_1,\vec{p}_2\,)\vec{\sigma}_1\cdot\vec{\sigma}_2 + h(\vec{p}_1,\vec{p}_2\,)S_{12}(\hat{q}) + k(\vec{p}_1,\vec{p}_2\,)S_{12}(\hat{P}) \\ &\quad + l(\vec{p}_1,\vec{p}_2\,)(\vec{\sigma}_1\times\vec{\sigma}_2)\cdot(\hat{q}\times\hat{P}),\end{aligned} \tag{104}$$

where $\vec{q} = \vec{p}_1 - \vec{p}_2$ denotes the momentum transfer in the exchange channel, $\vec{P} = \vec{p}_1 + \vec{p}_2$ is the center-of-mass momentum of the quasiparticle pair, and $S_{12}(\hat{v})$ defines the tensor operator $S_{12}(\hat{v}) = 3\vec{\sigma}_1\cdot\hat{v}\,\vec{\sigma}_2\cdot\hat{v} - \vec{\sigma}_1\cdot\vec{\sigma}_2$. The quasiparticle interaction in eq. (104) is invariant under parity, time-reversal, and transformations that interchange particle labels. The presence of the medium allows for the possibility of terms that break Galilean invariance and that depend explicitly on the center of mass momentum $\vec{P}$; namely, $S_{12}(\hat{P})$ and $A_{12}(\hat{q},\hat{P}) = (\vec{\sigma}_1\times\vec{\sigma}_2)\cdot(\hat{q}\times\hat{P})$. In ref. [121] a practical method has been developed for extracting the various scalar functions from a spin-space decomposition of the quasiparticle interaction. Additionally, three-nucleon force contributions to the noncentral quasiparticle interaction were computed for the first time.

The central quasiparticle interaction in neutron matter is qualitatively similar to that described in the previous section for isospin-symmetric nuclear matter (with $\vec{\tau}_1\cdot\vec{\tau}_2 \to 1$). The individual contributions from two- and three-nucleon forces to the $L = 0, 1, 2$ Landau parameters at various orders in perturbation theory for $k_f = 1.7\,\mathrm{fm}^{-1}$ are shown in Table 2. The first-order contribution from two-nucleon forces is simply a kinematically constrained version of the free-space interaction and therefore must be independent of the total quasiparticle momentum $\vec{P}$. Second-order contributions give rise to all possible noncentral interactions, which from Table 2 are seen to be significantly smaller than the central components. The exchange tensor interaction present in the free-space nucleon-nucleon interaction is largely reduced by Pauli-blocking effects in the nuclear medium. The center-of-mass tensor interaction arises solely from Pauli-blocking and core polarization effects at second-order in perturbation theory with two-body forces, while the novel spin-nonconserving cross-vector interaction $A_{12}(\hat{q},\hat{P})$ is generated both from two- and three-body forces, whose momentum-averaged contributions are of comparable strength.

At leading order the compressibility $\mathcal{K}$ of neutron matter at $\rho_0$ is unphysically small in comparison to auxiliary-field diffusion Monte Carlo calculations with realistic two- and three-nucleon forces which find that at $\rho = 0.16\,\mathrm{fm}^{-3}$, $\mathcal{K} \simeq 520\,\mathrm{MeV}$ [136]. Second-order contributions from chiral two-body forces do little to change this picture, but as in the case of symmetric nuclear matter the leading-order chiral three-nucleon force provides substantial additional repulsion, yielding a compression modulus $\mathcal{K} = 550\,\mathrm{MeV}$. The $f_1$ Landau parameter governing the quasiparticle effective mass at the Fermi surface again receives a nearly negligible contribution from three-body forces, but strong polarization effects at second order increases the effective mass from $M^*/M_N = 0.82$ to $M^*/M_N = 1.04$. As seen in Fig.

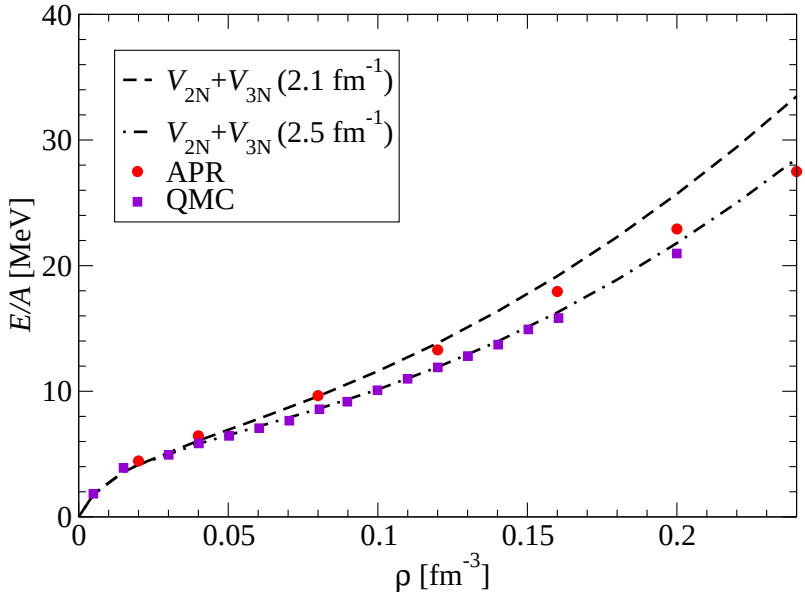


Figure 33: Energy per particle of neutron matter from both chiral and low-momentum two- and three-body interactions. The cutoff scale associated with the low-momentum interaction is $\Lambda = 2.1\,\mathrm{fm}^{-1}$. The curve labeled 'APR' is taken from the variational calculations of Akmal *et al.* [54], and the curve labeled 'QMC' is taken from the quantum Monte Carlo calculations in refs. [140, 49].

34 the Landau parameters $f_L$ associated with the spin-independent quasiparticle interaction depend sensitively on the neutron density.

Neglecting effects from noncentral interactions, the magnetic susceptibility is determined by the Landau parameter $G_0$:

$$\chi = \mu_n^2 \frac{N_0}{1+G_0}, \tag{105}$$

where $\mu_n = -1.913$ is the free-space neutron magnetic moment in units of the nuclear magneton, and $G_0 = N_0 g_0$. Noncentral components in the quasiparticle interaction result in effective charges (magnetic moments) that are not scalars under rotations of the quasiparticle momentum. The spin susceptibility then involves separately the longitudinal and transverse components of the magnetic moment [132, 133]. The Landau parameter $g_0$ decreases with the nuclear density as shown in Fig. 34, but there is no evidence for a spin-instability in the vicinity of nuclear matter saturation density.

As a consistency check on the perturbative calculation of the quasiparticle interaction in neutron matter, we reproduce in Fig. 33 the neutron matter equation of state at zero temperature computed to the same order in many-body perturbation theory. The results agree well with variational and Monte Carlo calculations of neutron matter employing realistic and phenomenological nuclear forces [54, 140, 49]. The recent neutron matter calculation [69] including the N$^3$LO chiral three- and four-neutron forces gives results that are very similar to those shown in Fig. 33. The dependence on the resolution scale arises mostly from the different choice of the low-energy constant $c_3$ in the two calculations. Recently, it has been shown that refitting $c_3$ to peripheral partial waves with the running of the cutoff scale yields a much reduced regulator dependence of the neutron matter equation of state [70].

The dynamics of supernovae explosions are particularly sensitive to neutrino processes occurring in the neutrinosphere, a warm and low-density ($n \simeq \rho_0/10$) gas of neutron-rich matter. At such small densities, three-nucleon correlations are expected to be negligible, and an accurate understanding of

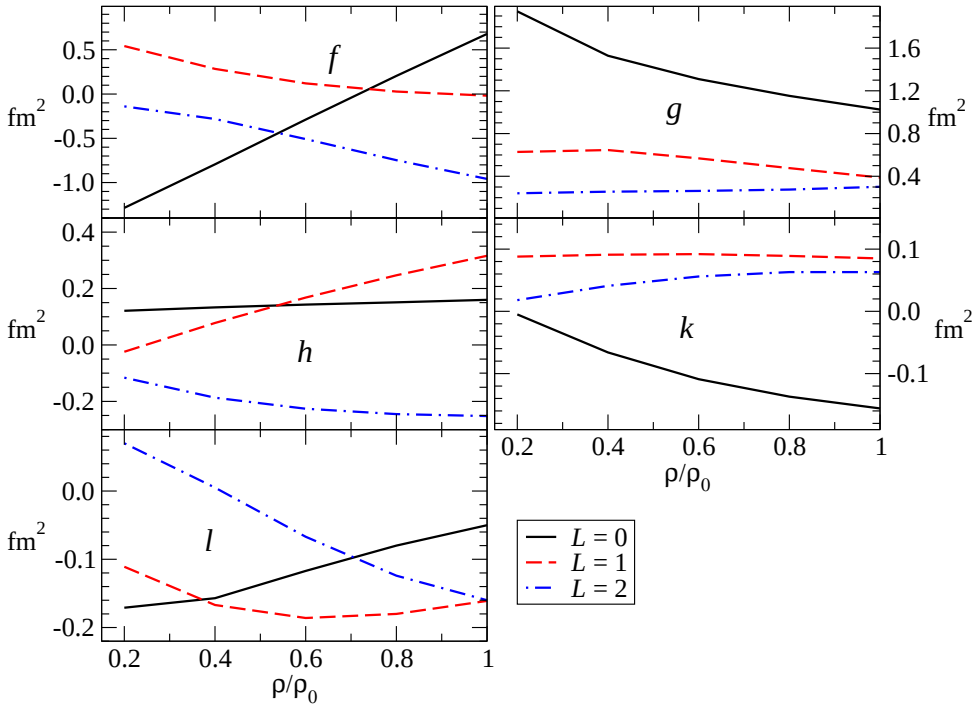


Figure 34: (Color online) Density-dependent Fermi liquid parameters inlcuding first- and second-order contributions from the chiral N$^3$LO nucleon-nucleon potential of ref. [31] as well as the N$^2$LO chiral three-nucleon force to leading order.

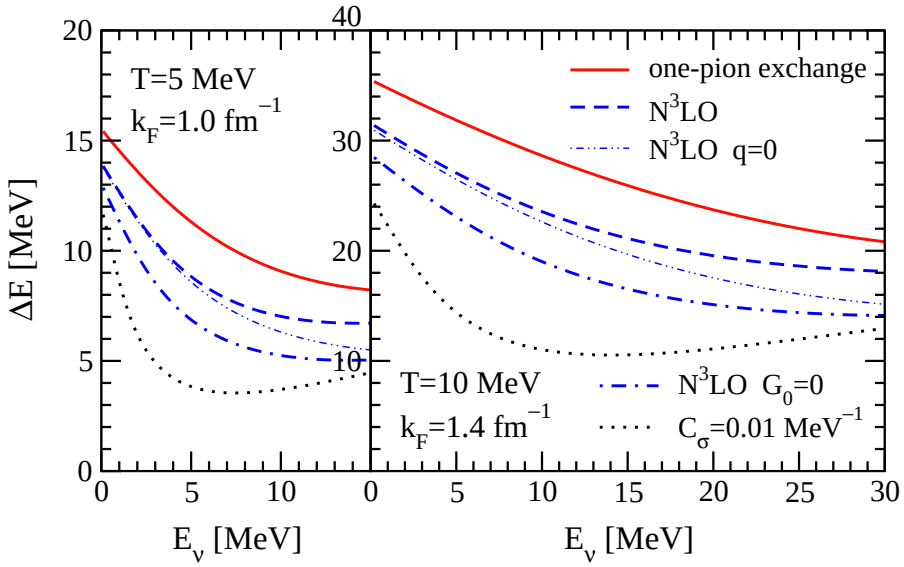


Figure 35: The rms energy transfer in neutrino scattering from neutron matter as a function of the temperature, density, and neutrino energy. Results are computed with chiral two-body forces at different orders in the chiral power counting. Figure reproduced from ref. [131].

neutrino scattering, production, and annihilation rates is accessible from two-nucleon forces alone. These processes determine the supernova neutrino spectrum and may be important for heating effects that re-energize the shock wave. The typical scale for neutrino energies $\epsilon_\nu \simeq 30\,\mathrm{MeV}$ and momenta $p_\nu \simeq 0.15\,\mathrm{fm}^{-1}$ justifies a treatment within linear response theory. Supernova simulations generally include neutrino-pair bremsstrahlung and absorption rates computed in the one-pion exchange approximation. For degenerate conditions, where the temperature is small relative to the neutron Fermi energy, Landau's Fermi liquid theory is applicable has been used in recent work [131] to compute spin-spin response function of neutron matter employing chiral two-body interactions at $\mathrm{N^3LO}$.

Within Fermi liquid theory, the density-density and spin-spin response functions are computed by solving the transport equation for quasiparticles. The relaxation rate that is used to approximate the collision integral in the Landau transport equation involves contributions from central and noncentral components of the quasiparticle interaction, the latter being essential for describing two-nucleon response. Contributions from chiral nuclear interactions beyond the leading-order one-pion exchange potential substantially reduce the relaxation rate, which consequently reduces the mean-square energy loss in neutrino scattering, as shown in Fig. 35.

# 8 Nuclear Chiral Thermodynamics

## 8.1 *Nuclear Phase Diagram and Liquid-Gas Transition*

The thermodynamic properties of nuclear and neutron matter play an important role in applications to heavy-ion collisions and astrophysics. The plateau observed in the caloric curve of the nuclear fragments in nucleus-nucleus collisions can be viewed as the trace of a first-order liquid-gas phase transition [141, 142, 143]. In the context of nuclear astrophysics, the recent observation of a two-solar-mass neutron star [144] strongly constrains the equation of state of hadronic matter and rules out various exotic models which tend to produce softer equations of state.

Previous chapters have introduced and developed the framework of chiral effective field theory and its application to the nuclear many-body problem at zero temperature. In the present section we review progress that has been achieved in extending this framework to finite temperatures. The previous ordering scheme for the nuclear energy density in terms of the number of medium insertions is now generalized and applied to the free energy density as a function of density $\rho$ and temperature $T$. Introducing the free energy per nucleon, $\bar{F}(\rho,T)$, the free energy density can be written as the sum of convolution integrals:

$$\begin{aligned}\rho\,\bar{F}(\rho,T) &= 4\int_0^\infty dp\,p\,\mathcal{K}_1(p)\,n(p) + \int_0^\infty dp_1 \int_0^\infty dp_2\,\mathcal{K}_2(p_1,p_2)\,n(p_1)\,n(p_2) \\ &\quad + \int_0^\infty dp_1 \int_0^\infty dp_2 \int_0^\infty dp_3\,\mathcal{K}_3(p_1,p_2,p_3)\,n(p_1)\,n(p_2)\,n(p_3) + \rho\,\bar{\mathcal{A}}(\rho,T)\ , \end{aligned} \tag{106}$$

where

$$n(p) = \frac{p}{2\pi^2}\Big[1+\exp\frac{p^2/2M_N-\tilde{\mu}}{T}\Big]^{-1} \tag{107}$$

is the density of nucleon states in momentum space. It is the product of the temperature- dependent Fermi-Dirac distribution and a kinematical prefactor $p/2\pi^2$ that has been included in $n(p)$ for convenience. Complete expressions of the kernels $\mathcal{K}_j$ can be found in [145]. The term $\bar{\mathcal{A}}(\rho,T)$ is called the anomalous contribution. It is associated with a Fock term involving second order $1\pi$-exchange [146] and arises from the smoothing of the Fermi surface at nonzero temperature. In the range of temperatures

considered here the effect of the anomalous term is small. The one-body effective "chemical potential" $\tilde{\mu}$ in the distribution $n(p)$ is related to the density by

$$\rho = 4 \int_0^\infty dp\, p\, n(p)\,. \tag{108}$$

The kernel $\mathcal{K}_1$ is the non-interacting nucleon gas contribution, while the kernels $\mathcal{K}_2$ and $\mathcal{K}_3$ encode the effects of the interactions among two and three nucleons. The pressure is then computed from the standard thermodynamic relation

$$P(\rho, T) = \rho^2 \, \frac{\partial \bar{F}(\rho, T)}{\partial \rho}\,. \tag{109}$$

In addition to isospin-symmetric nuclear matter, the extension to asymmetric nuclear matter and neutron matter has also been explored. The only changes required involve isospin factors and the introduction of separate proton and neutron thermal occupation probabilities $d_p(p_j)$ and $d_n(p_j)$. Note that for pure neutron matter the Pauli principle forbids a (momentum independent) three-body contact interaction. The behavior at very low density is governed by the large neutron-neutron scattering length, $a_{nn} \simeq 19$ fm [48], and as discussed in Section 5.2 an all-order resummation is required for a realistic description at low densities ($\rho_n < 0.02\,\mathrm{fm}^{-3}$).

In this section we first concentrate on the equation of state of isospin-symmetric nuclear matter for different temperatures, featuring the liquid-gas phase transition. The calculations are then extended to isospin-asymmetric matter, focusing on the change of thermodynamic properties with varying proton-neutron asymmetry. The topics of interest are the asymmetry free energy, its dependence on density and temperature and the validity of the (empirically observed) parabolic approximation for the free energy as a function of the asymmetry parameter, $\delta = (\rho_n - \rho_p)/(\rho_n + \rho_p)$.

The free energy per particle $\bar{F}(\rho, T)$ is calculated using eq. (106) as a function of density $\rho$ for a sequence of temperatures up to 25 MeV, with the input for the interaction kernels $\mathcal{K}_n$ specified in ref. [145]. The result is shown in Fig. 36. The dotted lines indicate the non-physical behavior of the equation of state in the first-order liquid-gas transition region. This unphysical part is then replaced by the physical one (solid lines) obtained from the Maxwell construction. At zero temperature the free energy is equal to the internal energy of the system, which has the well-known saturation point located at $\bar{E}_0 = -16.0$ MeV and $\rho_0 = 0.16$ fm$^{-3}$, corresponding to a Fermi momentum of $k_{f0} = 1.33\,\mathrm{fm}^{-1} = 262$ MeV. At finite temperatures the free energy develops a singular behavior for $\rho \to 0$, a feature that is present in numerous other many-body calculations [54, 147].

In Fig. 37 we show isotherms of the pressure $P(\rho, T)$ as a function of the temperature and density. The picture that emerges is reminiscent of a Van der Waals gas with its generic first-order liquid-gas phase transition. As outlined in Section 4.3, chiral nucleon-nucleon dynamics generates intermediate-range attractive interactions (e.g., from $2\pi$-exchange with intermediate $\Delta$-excitations) that exhibit a characteristic $e^{-2\,m_\pi r}/r^6$ behavior at distances on the order of $1 - 2\,\mathrm{fm}$ (see ref. [40]). Such mechanisms provide nearly half of the attraction required to bind nuclear matter at zero temperature. The liquid-gas phase transition then results from a sensitive balance between intermediate range attraction and short-range repulsion, the latter encoded in contact terms representing dynamics unresolved at the scales relevant for typical nuclear Fermi momenta $k_f$ considered here.

The critical temperature for the liquid-gas phase transition is observed at $T_c \simeq 15.1$ MeV. For temperatures less than the critical temperature $T_c$, the usual Maxwell construction is applied, where the pressure is kept constant in the liquid-gas coexistence region. Empirical estimates of the critical temperature are deduced from fission and multi-fragmentation measurements, which indicate a value of $T_c \simeq 15 - 20\,\mathrm{MeV}$ [148]. Similar values for the critical temperature are obtained from calculations [149] employing phenomenological Skyrme interactions.

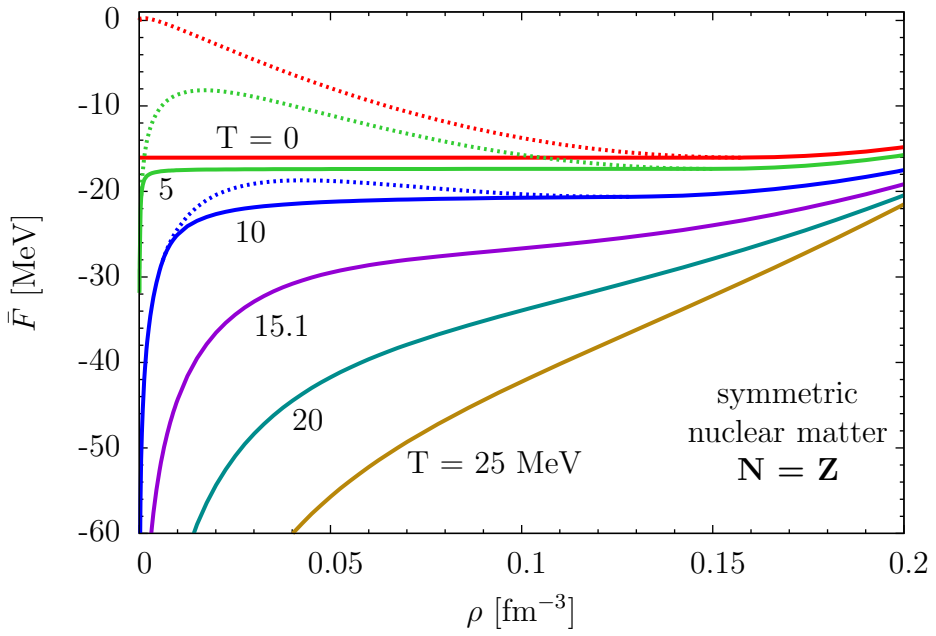


Figure 36: Free energy per particle of isospin-symmetric nuclear matter as a function of the temperature and baryon density $\rho$. The dotted line denotes the non-physical part of the free energy in the liquid-gas coexistence region. The physical free energy (solid line) is obtained using the Maxwell construction.

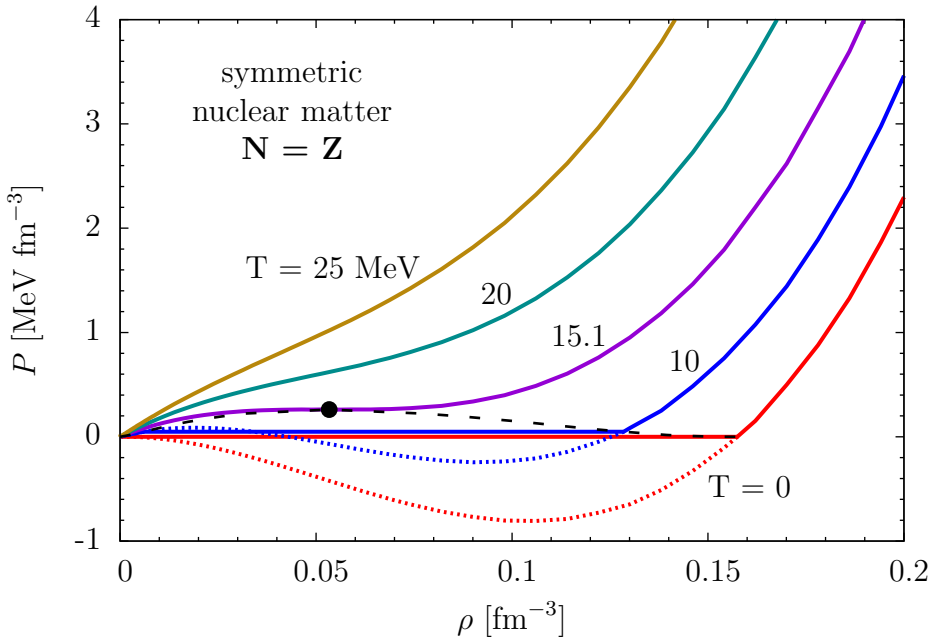


Figure 37: Pressure isotherms as a function of density and temperature for isospin-symmetric nuclear matter displaying a first-order liquid-gas phase transition. The dotted lines at low temperature indicate the non-physical behavior of the isotherms in the transition region, and the physical pressure is calculated from the Maxwell construction. The dashed line delineates the boundary of the coexistence region, and the dot denotes the critical point at $T_c \simeq 15.1$ MeV and $\rho_c \simeq \rho_0/3$.

In Fig. 38 we show the dependence of the pressure on the nucleon chemical potential (including the free nucleon mass),

$$\mu = M_N + \left(1 + \rho \frac{\partial}{\partial \rho}\right) \bar{F}(\rho, T)\,. \tag{110}$$

The non-physical part of the pressure is shown as the dotted curves in Fig. 37 and manifested in the double-valued behavior of $P$ at temperatures below the critical temperature. In the coexistence region, the physical pressure and chemical potential are constant and given according to the Maxwell construction. The temperature at which the pressure becomes single-valued is the critical temperature $T_c$.

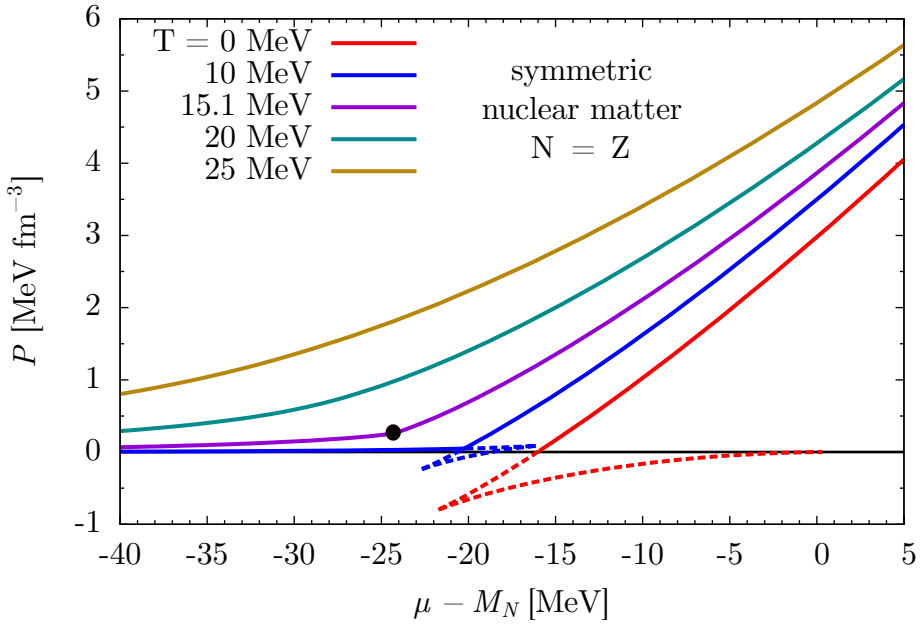


Figure 38: Dependence of the pressure isotherms on the nucleon chemical potential $\mu$ for symmetric nuclear matter. The non-physical behavior of the equation of state in the liquid-gas coexistence region for temperatures below $T_c$ is denoted with the dotted lines. The physical pressure and chemical potential in the coexistence region are constant and determined from the Maxwell construction. The critical point is denoted with the large dot.

The $T-\rho$ phase diagram, shown in Fig. 39, collects the relevant information regarding the liquid-gas phase transition. The first-order transition region ends at the critical point ($T_c = 15.1\,\mathrm{MeV}$) and is denoted with the dot. The associated critical values of the pressure, baryon chemical potential, and density are found to be $P_c \simeq 0.261$ MeV fm$^{-3}$, $\mu_c \simeq 914.7$ MeV, and $\rho_c \simeq 0.053\,\mathrm{fm}^{-3}$. The $T-\rho$ phase diagram indicates that the liquid-gas coexistence region extends over a wide range of densities up until the Fermi liquid phase is realized at $\rho_0 = 0.16\,\mathrm{fm}^{-3}$, the equilibrium density of nuclear matter.

At zero temperature the third law of thermodynamics provides important constraints on features of the $T-\rho$ diagram. In particular, at $T = 0$ the boundary of the phase coexistence region has an infinite slope in the $T-\rho$ diagram. Additionally, the chemical potential at zero temperature is given by the total energy per particle at the saturation point, that is, $\mu = M_N + \bar{E}_0 \simeq 923$ MeV.

## 8.2 *Isospin-Asymmetric Nuclear Matter*

It is now of interest to investigate how the liquid and gas phases characteristic of isospin-symmetric ($N = Z$) nuclear matter evolve with changing proton fraction, $x_p = Z/A$. The properties of isospin-

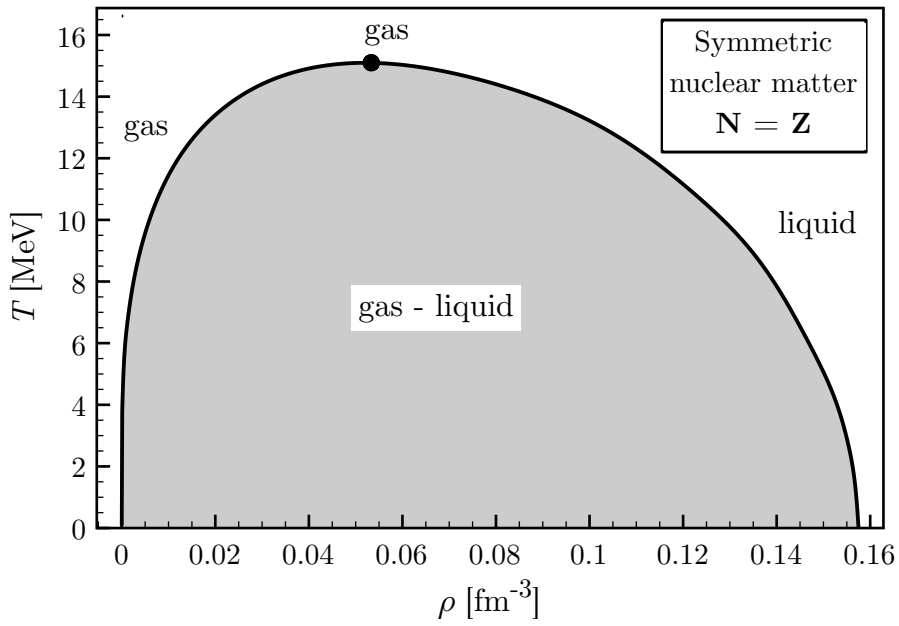


Figure 39: The phase diagram of isospin-symmetric nuclear matter. The critical point is indicated by the dot on the boundary of the phase coexistence region.

asymmetric matter with $0.5 > x_p > 0$ are governed by the detailed isospin dependence of the chiral NN interaction. It is almost entirely controlled by the isospin dependence of one- and two-pion exchange processes once the relevant nucleon-nucleon contact terms are fit to the empirical isospin asymmetry energy $A(\rho_0, T = 0) \simeq 34\,\mathrm{MeV}$.

Consider the evolution of the saturation point, defined as the minimum of the energy per nucleon at $T = 0$, as the proton fraction decreases. The result is shown in Fig. 40. Starting from its value for symmetric nuclear matter, $\bar{E}_0 \simeq -16$ MeV at $\rho_0 \simeq 0.157\,\mathrm{fm}^{-3}$, the binding energy per particle continuously reduces in magnitude with decreasing $x_p$ until it vanishes for a value of the proton fraction $x_p \simeq 0.12$, beyond which the neutron-rich matter is unbound at zero temperature.

In Fig. 41 we show the phase diagram as a function of the proton fraction $x_p$. The dashed line shows the trajectory of the critical point and its disappearance for proton fractions below $x_p \simeq 0.05$. At this value of the proton fraction, the coexistence region reduces to a single point, indicating the absence of a liquid-gas phase transition. Neutron-rich matter with $x_p \leq 0.05$ therefore exists only in a gaseous phase. We note as well that the critical point disappears at a small but nonzero value of the pressure.

From Fig. 41 we see that for proton fractions above $x_p \simeq 0.1$, the liquid-gas coexistence region starts at $\rho = 0$. At $T = 0$ and from $x_p = 0.1$ to 0.5, the boundary between the coexistence and Fermi liquid regimes covers a density range between about $0.5\,\rho_0$ and nuclear matter saturation density density $\rho_0$. The behavior of the coexistence region changes qualitatively for a proton fraction $x_p = 0.12$, which is the point at which the zero-temperature binding energy vanishes. From Fig. 40 we observe that for $x_p \leq 0.12$ the absolute minimum of the energy per particle is located at $\rho = 0$ but there may still exist a local minimum in $\bar{E}(\rho, x_p)$ at a finite value of the density. This indicates that neutron-rich nuclear matter with values of $x_p \leq 0.12$ is in the gaseous phase at very low density and $T = 0$. As the density increases, the neutron-rich matter then enters the coexistence region. For values of the proton fraction $0.05 \leq x_p \leq 0.12$, nuclear matter will not be self-bound but may nevertheless still have a liquid-gas phase transition.

The treatment of nuclear matter chiral thermodynamics presented thus far is oversimplified at low densities where nuclear clustering occurs (mainly driven by the Coulomb repulsion of the protons). Previous work [150] that combines the appearance of deuteron, triton and helium clusters with relativistic

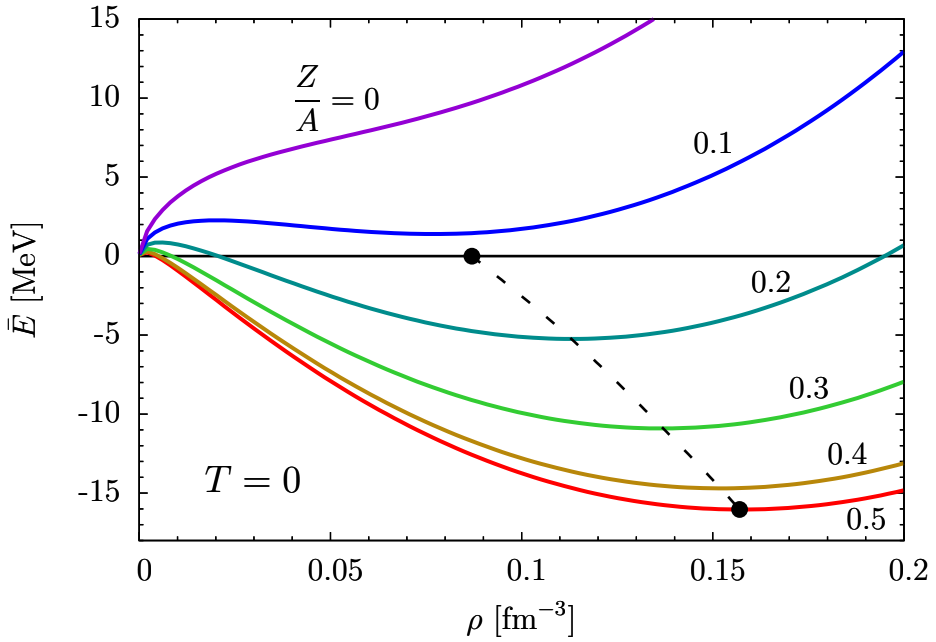


Figure 40: Dependence of the energy per nucleon (and saturation point) of nuclear matter on the proton fraction $x_p$ at $T = 0$. The dashed line denotes the evolution of the saturation point with varying proton fraction. For proton fractions below $x_p = 0.12$, the energy remains positive at all densities.

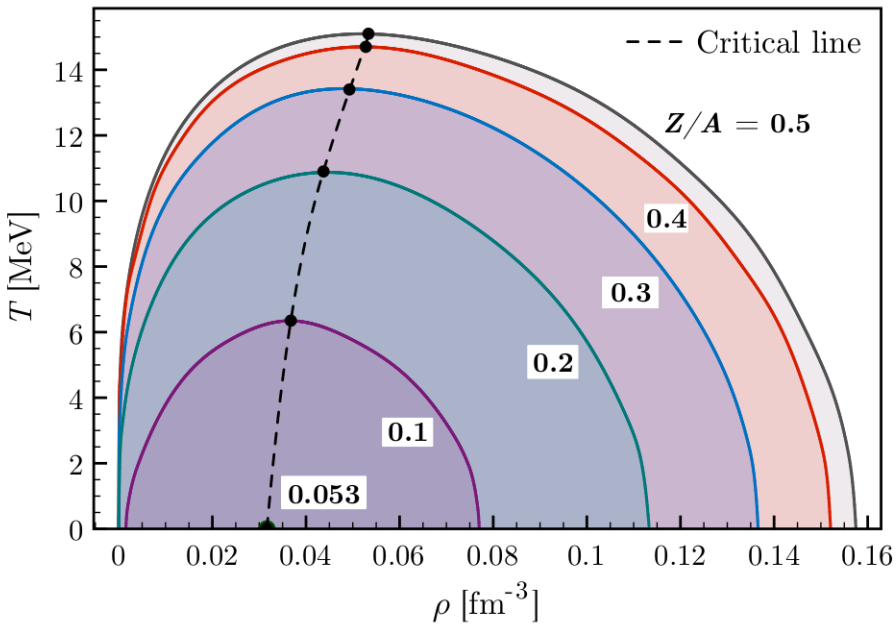


Figure 41: Dependence of the nuclear matter phase diagram on the proton fraction $x_p$. The evolution of the critical point is given by the dashed line.

mean-field theory suggests, however, that only modest changes in the $T-\mu$ phase diagram arise. When clustering effects are included, the position of the critical point changes by less than 1% in $\mu_c$ and less than 10% in $T_c$.

The free energy per particle can be expanded in powers of the nuclear asymmetry parameter $\delta = (\rho_n - \rho_p)/\rho = 1 - 2x_p$ around the free energy at $\delta = 0$:

$$\bar{F}(\rho_p, \rho_n, T) = \bar{F}(\rho, T) + A(\rho, T)\,\delta^2 + \mathcal{O}(\delta^4)\,, \tag{111}$$

which defines the asymmetry free energy per particle $A(\rho, T)$. If isospin-symmetry breaking effects are ignored, the expansion of the free energy per particle includes only even powers of $\delta$. In this approximation, nuclear matter is invariant under the interchange of neutrons and protons.

The validity of the parabolic approximation has been shown in ref. [145], where the free energy difference relative to isospin-symmetric nuclear matter as a function of $\delta^2$ for different nucleon densities $\rho = \rho_n + \rho_p$ has been analyzed. At $T = 0$ the quadratic dependence on $\delta$ holds very well even up to large values of the isospin asymmetry parameter. For higher temperature (e.g., $T = 20\,\mathrm{MeV}$) one observes a slight bending, especially at low density.

At nuclear matter saturation density $\rho_0$, the contact terms of the isospin-dependent part of the nucleon-nucleon interaction have been fit to the isospin asymmetry energy $A(\rho_0, T = 0) \simeq 34.0\,\mathrm{MeV}$. Previous determinations from fits of nuclear masses [43, 151] as well as relativistic mean-field models constrained by the properties of specific nuclei [152] or by giant dipole resonances [153] give values of $A(\rho_0)$ in the range $33 - 37\,\mathrm{MeV}$. The asymmetry energy at a lower density, $\rho = 0.1\ \mathrm{fm}^{-3}$, has also been estimated in the latter paper and yields a value for the isospin asymmetry energy between 21 and 23 MeV. This range is slightly below the value $A(\rho = 0.1\,\mathrm{fm}^{-3}, T = 0) \simeq 23.9$ MeV computed within the present chiral effective field theory framework.

In the vicinity of the nuclear matter saturation density $\rho_0$, the asymmetry energy at zero temperature can be expanded in powers of $\rho - \rho_0$:

$$A(\rho) = A(\rho_0) + L\,\frac{\rho - \rho_0}{3\,\rho_0} + \frac{K_{as}}{2}\left(\frac{\rho - \rho_0}{3\,\rho_0}\right)^2 + \ldots \tag{112}$$

The coefficients of the linear and quadratic terms (in $\rho - \rho_0$) are found in the present case to be $L \simeq 90$ MeV and $K_{as} \simeq 153$ MeV. In particular, this value of $L$ is consistent with empirical constraints from isospin diffusion, which give $L = 88 \pm 25$ MeV [154].

For small values of the isospin asymmetry $\delta$, the saturation density is reduced to $\rho_0(1 - 3L\,\delta^2/K)$. The nuclear compression modulus $K(\delta)$ is then often expressed in terms of an expansion in powers of $\delta$:

$$K(\delta) = K + K_\tau \delta^2 + \mathcal{O}(\delta^4)\,, \qquad K_\tau = K_{as} - 6\,L\,, \tag{113}$$

where $K$ is the compression modulus of isosopin-symmetric nuclear matter, and $K_\tau$ is referred to as the isobaric compressibility. The value calculated in the present framework is $K_\tau = -388$ MeV. Recent measurements of giant monopole resonances in even-mass-number isotopes yields the result $K_\tau = -550 \pm 100$ MeV [155].

## 8.3 *Comparisons to other Approaches*

In the present section we discuss recent calculations of the thermodynamic properties of nuclear matter within the self-consistent Green's function method or mean-field theory [156, 157, 158, 159, 160]. As noted in ref. [156], many previous studies of nuclear matter at nonzero temperature carried out in the mean-field approximation treat the temperature dependence in a simplistic way, namely, the zero-temperature step-function momentum distribution is just replaced by the corresponding Fermi-Dirac

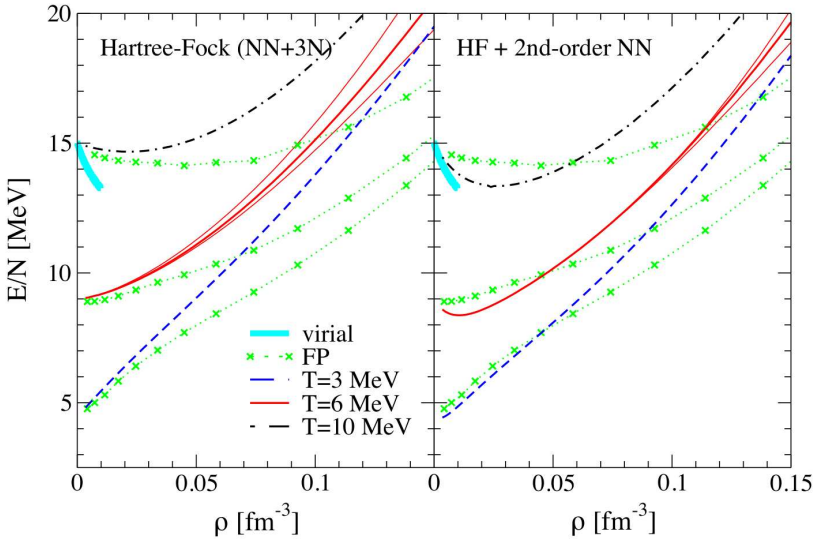


Figure 42: Energy per particle of neutron matter calculated at temperatures $T = 3, 6$ and 10 MeV as function of density, using low momentum NN and 3N interactions. Left: Hartree-Fock results. Right: results including 2nd order NN interactions. Also shown for comparison are curves from a many-body calculation (FP) [162] and a model-independent virial expansion (virial) [147] at low density.

distribution. Such an approach neglects the temperature dependence of the phenomenological interactions that account for nuclear correlations. In microscopic many-body methods, on the other hand, Pauli-blocking effects generated by the nuclear medium are weakened as the temperature increases. Hence, nuclear matter properties and correlations depend on the temperature in a non-trivial way.

In the SCGF formalism, the set of equations relating the in-medium $T$-matrix, the nucleon self-energy, and the single-particle Green's function are solved self-consistently. The equation of state of isospin-symmetric nuclear matter has been calculated in this approach [158] starting from the high-precision CD-Bonn and Nijmegen nucleon-nucleon potentials. The contributions from three-nucleon forces are included through an effective (medium-dependent) two-body interaction. Three-body correlations are found to strongly affect the pressure $P(\rho, T, \delta)$ and result in a liquid-gas coexistence region that is much reduced in size. The critical temperatures associated with the CD-Bonn nucleon-nucleon potential and the Nijmegen potential are $T_c = 12.5\,\mathrm{MeV}$ and $T_c = 11.5\,\mathrm{MeV}$, respectively. The critical density is found to be $\rho_c \simeq 0.09 - 0.11\,\mathrm{fm}^{-3}$, while the critical pressure has the value $0.15\,\mathrm{MeVfm}^{-3}$. The results obtained within a chiral effective field theory treatment and described in previous sections are therefore significantly different than the results based on the self-consistent Green's function approach with one-boson exchange nuclear interactions.

The properties of nuclear matter have also been calculated [160] within the framework of relativistic mean field theory incorporating density-dependent meson-nucleon couplings that account for effects of the medium. Such a method has been successful in previous calculations of finite nuclei and infinite nuclear matter. The critical temperature $T_c = 13.2$ MeV is found for symmetric nuclear matter, and for proton fractions below $x_p \simeq 0.07$ the liquid-gas coexistence region vanishes. The picture that emerges in these calculations is closer to the one reported in the present review. The main difference between the two is that mean field theory gives a slightly smaller phase transition region.

To close this section we mention the work of ref. [161] in which the energy per particle of neutron matter has been calculated at several temperatures $T \leq 10$ MeV as a function of density, using a low-momentum neutron-neutron interaction that is close in spirit to the chiral interaction discussed in this review. Two- and three-body interactions are taken into account. Representative results from these

calculations are displayed in Fig. 42. The left panel shows first order (Hartree-Fock) results, including a comparison with a model-independent virial expansion at low density. The right panel demonstrates significant improvements when the NN interaction is treated in second order.

# 9 Thermodynamics of the Chiral Condensate

The chiral condensate $\langle\bar{q}q\rangle$ is defined as the expectation value of the scalar quark density and plays a fundamental role in QCD as an order parameter for the spontaneous breaking of chiral symmetry that occurs at low energy scales. The dependence of $\langle\bar{q}q\rangle$ on the temperature and baryon density is key to locating the chiral restoration transition boundary in the phase diagram of QCD. The condensate is expected to vanish at high temperatures and/or densities, signaling the crossover from the Nambu-Goldstone phase, in which chiral symmetry is spontaneously broken, to the Wigner-Weyl realization of chiral symmetry in QCD.

It is therefore of principal interest to perform a systematic calculation of the thermodynamics of the chiral condensate [163]. For such a calculation it is necessary to understand the dependence of the free energy density on the light quark mass (or equivalently, the pion mass). In-medium chiral effective field theory provides the appropriate framework for such a study, given that the theory provides explicit access to the pion mass dependence through one- and two-pion exchange dynamics and the resulting two- and three-body correlations in the nuclear medium.

The starting point is the free energy density, $\mathcal{F}(\rho,T)=\rho\bar{F}(\rho,T)$, of spin-saturated isospin-symmetric nuclear matter, given by the series of convolution integrals in eq. (106). This series is written in terms of one-body, two-body and three-body kernels, $\mathcal{K}_1, \mathcal{K}_2$ and $\mathcal{K}_3$, respectively.

The one-body kernel $\mathcal{K}_1$ in eq. (106) represents the contribution of the non-interacting nucleon gas to the free energy density and it reads [146]:

$$\mathcal{K}_1(p)=M_N+\tilde{\mu}-\frac{p^2}{3M_N}-\frac{p^4}{8M_N^3}\,. \tag{114}$$

The first term in $\mathcal{K}_1$ gives the leading contribution (density times nucleon rest mass) to the free energy density. The remaining terms account for (relativistically improved) kinetic energy corrections.

The two- and three-body kernels, $\mathcal{K}_2$ and $\mathcal{K}_3$, specifying all one- and two-pion exchange processes up to three loop order for the free energy density, are given in their explicit form in refs. [146, 39, 145]. Let us recall that after fixing a few contact terms the free energy density computed from these interaction kernels provides a realistic nuclear equation of state up to densities $\rho\leq 2\,\rho_0$. What matters in the present context is the dependence of the kernels $\mathcal{K}_2$ and $\mathcal{K}_3$ on the light quark mass, $m_q$, or equivalently, on the pion mass, $m_\pi$, that is introduced by pion propagators and by pion loops.

The Feynman-Hellmann theorem is used to establish an exact relation between the temperature- and density-dependent quark condensate $\langle\bar{q}q\rangle(\rho,T)$ and the derivative of the free energy density of nuclear matter with respect to the light quark mass $m_q$. From the Gell-Mann-Oakes-Renner relation $m_\pi^2 f_\pi^2=-m_q\langle 0|\bar{q}q|0\rangle$, the ratio of the in-medium to vacuum quark condensate is given by

$$\frac{\langle\bar{q}q\rangle(\rho,T)}{\langle 0|\bar{q}q|0\rangle}=1-\frac{\rho}{f_\pi^2}\frac{\partial\bar{F}(\rho,T)}{\partial m_\pi^2}\,, \tag{115}$$

where the derivative of the free energy density with respect to $m_\pi^2$ is taken at fixed $T$ and $\rho$. Both the vacuum quark condensate $\langle 0|\bar{q}q|0\rangle$ and the pion decay constant $f_\pi$ are taken in the chiral limit. Similarly, $m_\pi^2$ represents the leading linear term in the expansion of the squared pion mass in terms of the quark mass.

The quark mass dependence in the one-body kernel $\mathcal{K}_1$ is implicit through its dependence on the nucleon mass $M_N$. The condition $\partial\rho/\partial M_N = 0$ leads to the dependence of the effective one-body chemical potential $\tilde{\mu}$ on the nucleon mass $M_N$:

$$\frac{\partial\tilde{\mu}}{\partial M_N} = \frac{3\rho}{2M_N\Omega_0''}\,, \qquad \Omega_0'' = -4M_N\int_0^\infty dp\,\frac{n(p)}{p}\,. \tag{116}$$

The nucleon sigma term $\sigma_N = \langle N|m_q\bar{q}q|N\rangle = m_\pi^2\,\partial M_N/\partial m_\pi^2$ relates the variation of the nucleon mass to that of the pion mass. Combining the above two relationships then leads to the expression for the derivative of the one-body kernel with respect to the pion mass:

$$\frac{\partial\mathcal{K}_1}{\partial m_\pi^2} = \frac{\sigma_N}{m_\pi^2}\Big\{1 + \frac{3\rho}{2M_N\Omega_0''} + \frac{p^2}{3M_N^2} + \frac{3p^4}{8M_N^4}\Big\}\,. \tag{117}$$

In the zero temperature limit, the terms in eq. (117) provide the linear decrease of the chiral condensate with the nucleon density. The corrections from the kinetic energy account for the small difference between the scalar and vector densities. The nucleon sigma term is determined empirically at the physical pion mass to be $\sigma_N = (45 \pm 8)\,\mathrm{MeV}$ [26]. Recently, smaller values of the nucleon sigma term have been suggested based on lattice QCD calculations of the quark mass dependence of baryon masses and accurate chiral extrapolations [165]. The value of $\sigma_N$ determined in this way is consistent with the empirical value to within the experimental uncertainty. However, a considerably larger nucleon sigma term, $\sigma_N \simeq 60\,\mathrm{MeV}$, has recently been discussed in ref. [166]. In the present discussion based on ref. [163], the central value $\sigma_N = 45\,\mathrm{MeV}$ has been employed.

There are some three-loop contributions that are of special relevance for the in-medium quark condensate. The corresponding two-pion exchange mechanisms arise from the chiral symmetry breaking $\pi\pi NN$ contact-vertex proportional to $c_1 m_\pi^2$. Note that this parameter is equivalent to the leading contribution (linear in the quark mass) to the nucleon sigma term $\sigma_N = -4c_1 m_\pi^2 + \mathcal{O}(m_\pi^3)$. Concerning the free energy density $\rho\bar{F}(\rho,T)$ or the equation of state of nuclear matter the $c_1 m_\pi^2$ contributions are almost negligible. However, when taking the derivative with respect to $m_\pi^2$ as required for the calculation of the in-medium condensate, these contributions turn out to be of similar importance as other interaction terms. The pertinent two- and three-body kernels $\mathcal{K}_{2,3}^{(c_1)}$ can be found in ref. [163].

It is meaningful to incorporate also effects from thermal pions. The pressure (or free energy density) of thermal pions gives rise, through its $m_\pi^2$-derivative, to a further reduction of the $T$-dependent in-medium condensate. In the two-loop approximation of chiral perturbation theory one finds the following shift of the chiral condensate ratio due to the presence of a pionic heat bath [167, 168, 169]:

$$\frac{\delta\langle\bar{q}q\rangle(T)}{\langle 0|\bar{q}q|0\rangle} \;=\; -\frac{3m_\pi^2}{(2\pi f_\pi)^2}H_3\Big(\frac{m_\pi}{T}\Big)\Big\{1 + \frac{m_\pi^2}{8\pi^2 f_\pi^2}\Big[H_3\Big(\frac{m_\pi}{T}\Big) - H_1\Big(\frac{m_\pi}{T}\Big) + \frac{2-3\bar{\ell}_3}{8}\Big]\Big\}\,, \tag{118}$$

where the functions $H_{1,3}(m_\pi/T)$ are defined by integrals over the Bose distribution of thermal pions:

$$H_1(y) = \int_y^\infty dx\,\frac{1}{\sqrt{x^2-y^2}(e^x-1)}\,, \qquad H_3(y) = y^{-2}\int_y^\infty dx\,\frac{\sqrt{x^2-y^2}}{e^x-1}\,. \tag{119}$$

It is worth emphasizing that in-medium chiral perturbation theory with this dynamical input yields a realistic nuclear matter equation of state [39, 145], including a proper description of the liquid-gas phase transition with critical temperature $T_c \simeq 15\,\mathrm{MeV}$. The three-loop calculation of the free energy density is expected to be reliable up to about twice nuclear matter saturation density and for temperatures below about $T \sim 100$ MeV, where the hot and dense hadronic matter remains in the spontaneously broken chiral symmetry regime.

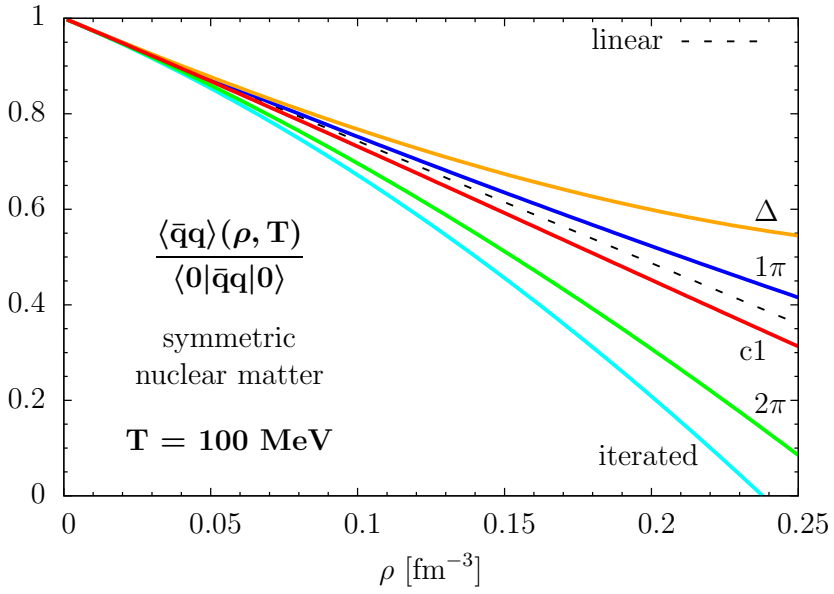


Figure 43: Density dependence of the chiral condensate at temperature $T = 100$ MeV. Starting from the linear density dependence (dashed curve) associated with the free nucleon Fermi gas, the following interaction contributions are successively added: one-pion exchange Fock contribution, iterated one-pion exchange, irreducible two-pion exchange, two-pion exchange with intermediate $\Delta$ excitations, two-pion exchange contribution proportional to the low-energy constant $c_1$. For the sake of clarity in presenting the pattern of medium modifications, the contribution from thermal pions is omitted here

In Fig. 43 we show a typical example ($T = 100$ MeV) of the effects of interaction contributions to the density dependence of $\langle\bar{q}q\rangle(\rho, T)$ arising from the pion mass derivative of the chiral two- and three-body kernels $\mathcal{K}_2$ and $\mathcal{K}_3$. Of particular importance is the pion-mass dependence of the terms involving virtual $\Delta(1232)$ excitations, which delay the tendency towards chiral symmetry restoration as the density increases. Summing together all one- and two-pion exchange processes contributing to $\partial\mathcal{K}_2/\partial m_\pi^2$ and $\partial\mathcal{K}_3/\partial m_\pi^2$, the chiral condensate at $T = 100$ MeV is not far from the linear density dependence characteristic of a free Fermi gas. However, this behavior is the result of a subtle balance between attractive and repulsive correlations and their detailed pion-mass dependences. Iterated one-pion exchange and irreducible two-pion exchange alone would have resulted in the system becoming unstable not far above normal nuclear matter saturation density as can be seen in Fig. 43. In the chiral limit ($m_\pi \to 0$) this instability would have appeared even at much lower densities. This emphasizes once again the importance of including $\Delta(1232)$-excitations, and it also highlights the significance of explicit chiral symmetry breaking in governing nuclear scales.

In Fig. 44 we show the variation of the chiral condensate with both the baryon density $\rho$ and the temperature $T$. All nuclear correlation effects are included as well as the small additional shift from thermal pions, which is visible only at the highest temperature considered here ($T = 100$ MeV). The actual crossover transition can be extracted from lattice QCD simulations and has the value $T \sim 170$ MeV [170].

At zero temperature, the decrease in the chiral condensate beyond nuclear matter saturation density is hindered as a result of three-body correlations encoded in $\mathcal{K}_3$ which grow faster than $\mathcal{K}_2$ as the density increases. As the temperature rises, the influence of $\mathcal{K}_3$ relative to $\mathcal{K}_2$ is reduced, so that at $T = 100$ MeV only a small net effect remains in comparison to the free Fermi gas.

At $T = 0$, the solid line in Fig. 44 does not yet account for the coexistence region of the nuclear liquid and gas phases [145]. Any first-order phase transition is expected to be visible also in other order parameters, and the dashed line in Fig. 44 based on the usual Maxwell construction indicates this effect.

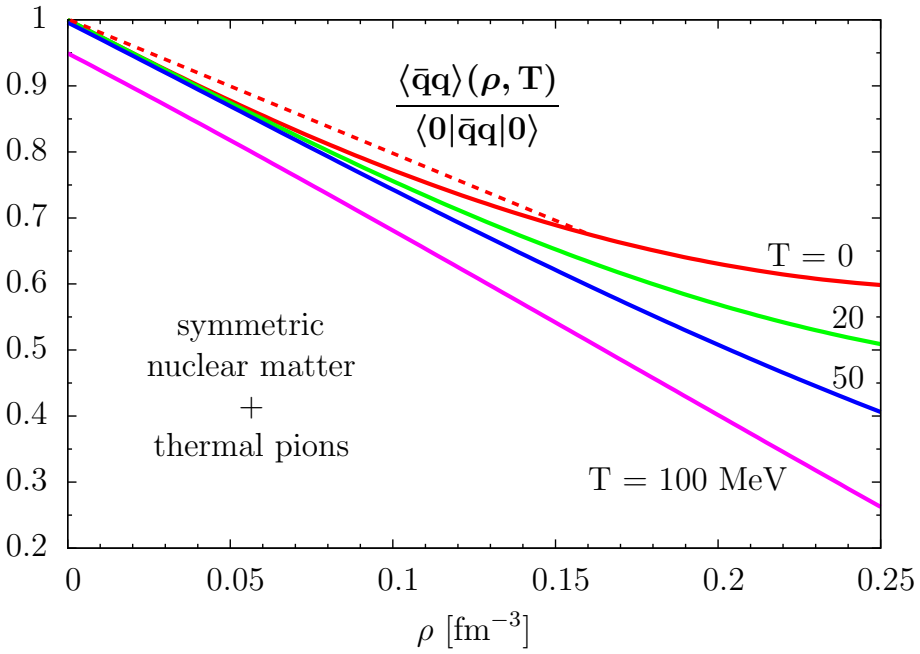


Figure 44: Ratio of the in-medium chiral condensate to its vacuum value as a function of the baryon density $\rho$ and temperature in isospin-symmetric nuclear matter. Effects of thermal pions are included, and the dashed line at $T \simeq 0$ results from the Maxwell construction in the nuclear liquid-gas coexistence region.

This feature becomes much more pronounced when the chiral condensate is plotted as a function of the baryon chemical potential at low temperatures:

$$\mu = M_N + \left(1 + \rho\frac{\partial}{\partial\rho}\right)\bar{F}(\rho, T)\,. \tag{120}$$

The discontinuity associated with the first-order liquid-gas transition at $T$ smaller $T_c \simeq 15\,\mathrm{MeV}$ is clearly visible in Fig. 45. Another effect generated by the first-order liquid-gas phase transition is that the frequently advocated "low-density theorem" requires modification:

$$\frac{\langle\bar{q}q\rangle(\rho)}{\langle 0|\bar{q}q|0\rangle} = 1 - \frac{\widetilde{\sigma}_N}{m_\pi^2 f_\pi^2}\rho\,. \tag{121}$$

In this equation the effective nucleon sigma term $\widetilde{\sigma}_N \simeq 36\,\mathrm{MeV}$ represents the quark mass dependence of the sum $M_N + \bar{E}_0$, where $\bar{E}_0 \simeq -16\,\mathrm{MeV}$ is the binding energy per particle of nuclear matter at the saturation density. The standard version of eq. (121) contains the nucleon sigma term $\sigma_N$ in vacuum and assumes that at sufficiently low densities nuclear matter can be treated as a non-interacting Fermi gas.

The results discussed here set important nuclear physics constraints for the QCD equation of state at baryon densities and temperatures that are of interest in relativistic heavy-ion collisions. In particular, there is no indication for chiral symmetry restoration at temperatures $T \leq 100\,\mathrm{MeV}$ and baryon densities at least up to about twice nuclear matter saturation density. The effects of intermediate $\Delta(1232)$-isobar excitations (i.e. the strong spin-isospin polarizability of the nucleon) together with Pauli blocking in the nuclear medium play a crucial role in stabilizing the scalar quark condensate at and beyond nuclear matter saturation density.

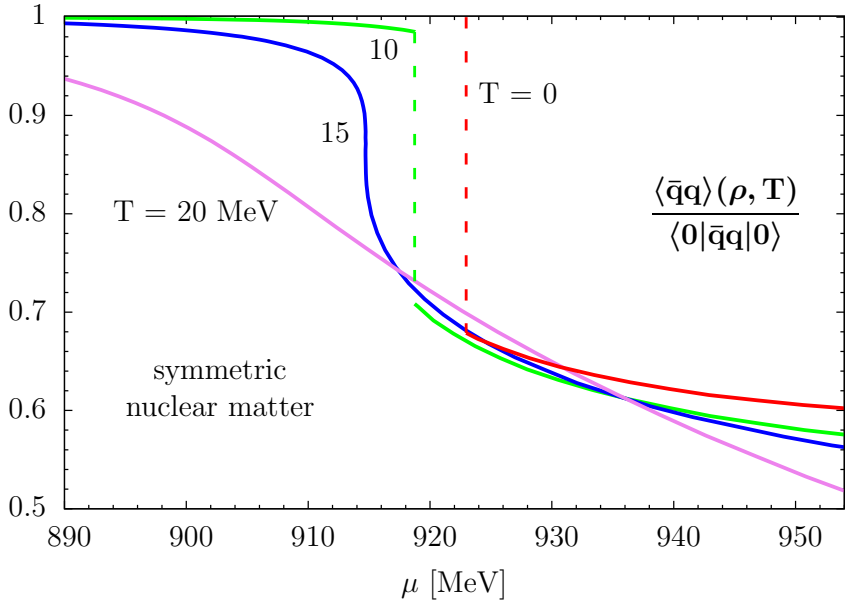


Figure 45: Ratio of chiral condensate relative to its vacuum value as function of baryon chemical potential in isospin-symmetric nuclear matter at low temperatures within the liquid-gas phase coexistence region.

# 10 Concluding Remarks and Outlook

Chiral Effective Field Theory, as a low-energy realization of QCD in its sector with light ($u$ and $d$) quarks, is not only a successful framework for the description of pion-pion and pion-nucleon interactions. With its systematic counting scheme in powers of "small" $Q/\Lambda_\chi$ (where $Q$ stands generically for momentum, energy or the pion mass, and $\Lambda_\chi \sim 1$ GeV is the spontaneous chiral symmetry breaking scale), chiral EFT has also become the basis for the modern theory of nuclear forces. The present review goes still one step further and reports on recent developments concerning the application of chiral EFT to nuclear many-body problems, both at zero and finite temperatures.

The additional "small" scale introduced by the many-body system is the Fermi momentum. Its typical magnitude in nuclear physics, $k_f \sim 2m_\pi$, implies that the chiral dynamics of pions in a low-energy, low-temperature nuclear environment should also be controlled by an expansion in powers of $k_f/\Lambda_\chi$. Indeed, the typical average distance between two nucleons in equilibrium nuclear matter, $d \simeq 1.8$ fm, is again comparable to a "pionic" scale, just slightly larger than the Compton wavelength of the pion. Furthermore, another characteristic parameter of nuclear matter, its compression modulus, happens to be of a magnitude comparable to twice the pion mass. The only quantity that falls out of this pionic scales scenario is the binding energy per nucleon. Its value $B/A \simeq 16$ MeV is abnormally small and indicates a quantitative fine-tuning: the well-known subtle balance between intermediate-range attraction and strong short-range repulsion in the nucleon-nucleon interaction.

Details of the short-range NN interaction remain unresolved at momentum scales $p \leq k_f$. Chiral EFT assigns a limited number of NN contact terms to the physics at short distance ($r < 1$ fm), with prefactors (a set of low-energy constants) to be determined by experiment. While the strengths of these contact terms generally require non-perturbative resummation techniques to be performed at low densities, the intermediate and long range forces governed by one- and two-pion exchange processes in the medium are supposed to be accessible to perturbative methods. This is the essence of in-medium chiral perturbation theory. In this perturbative hierarchy, three-nucleon forces enter naturally at a well-defined order of the low-momentum expansion.

Such a conceptual framework turns out to be remarkably successful. Much of the well established phenomenology associated with the nuclear many-body problem can now be given more systematic foundation that relies substantially on the well-established spontaneous chiral symmetry breaking pattern of low-energy QCD. The nuclear mean field experienced by nucleons as quasiparticles, including its extension to the optical potential for scattering, the density functional approach to finite systems, Landau-Migdal Fermi liquid theory, thermodynamics and the phase diagram of nuclear matter featuring the liquid-gas phase transition - all these important aspects of nuclear theory are covered in this report. As a bonus of this framework that permits investigating the energy density and related quantities systematically as a function of the pion mass, reliable statements about the behavior of the quark condensate at temperatures up to about 100 MeV and densities reaching twice the density of normal nuclear matter can be made, indicating stability of this chiral order parameter considerably beyond previous expectations that were based merely on the Fermi gas limit.

Of course, many further reaching questions still need to be addressed. So far, the calculations of the energy density (and of the free energy density at finite temperature) have been carried out up to three-loop order. This includes important three-body forces but does not (yet) cover issues of convergence beyond this order, e.g. concerning the role of four-nucleon correlations. At this point Monte Carlo studies of the kind performed in ref. [172] may prove useful in the near future. As a further important topic, the quest for a sufficiently stiff equation-of-state satisfying the constraints imposed by the existence of a two-solar-mass neutron star [144] is under investigation.

# References


[1] H. Yukawa, *Proceedings of the Physico-Mathematical Society of Japan* 17, 48 (1935)

[2] M. Taketani, S. Nakamura, and M. Sasaki, *Prog. Theor. Phys.* 6 (1951) 581

[3] M. Taketani, *Prog. Theor. Phys. Suppl.* 3 (1956) 1

[4] M. Taketani, S. Machida and S. Ohnuma, *Prog. Theor. Phys.* 7 (1952) 146

[5] M. Konuma, H. Miyazawa and S. Otsuki, *Phys. Rev.* 107 (1957) 320 ; *Prog. Theor. Phys.* 19 (1958) 17

[6] Y. Fujimoto and H. Miyazawa, *Prog. Theor. Phys.* 5 (1950) 1052

[7] G. E. Brown and W. Weise, *Phys. Reports* 22 (1975) 279 ;
T. E. O. Ericson and W. Weise, *Pions and Nuclei*, Oxford Univ. Press, 1988

[8] S. Weinberg, *Phys. Rev. Lett.* 17 (1966) 616 ; *Phys. Rev. Lett.* 18 (1967) 188

[9] J. Gasser and H. Leutwyler, *Ann. Phys. (N.Y.)* 158 (1984) 142

[10] E. Epelbaum, *Prog. Part. Nucl. Phys.* 57 (2006) 654

[11] E. Epelbaum, H.-W. Hammer and Ulf.-G. Meissner, *Rev. Mod. Phys.* 81 (2009) 1773

[12] R. Machleidt and D. R. Entem, *Phys. Reports* 503 (2011) 1

[13] J. Goldstone, *Nuovo Cim.* 19 (1961) 155

[14] Y. Nambu and G. Jona-Lasinio, *Phys. Rev.* 122 (1961) 345 ; *Phys. Rev.* 124 (1961) 246

[15] S. L. Adler and R. F. Dashen, *Current Algebras*, Benjamin, New York (1968) ; B. W. Lee, *Chiral Dynamics*, Gordon and Breach, New York (1972).

[16] U. Vogl and W. Weise, *Prog. Part. Nucl. Phys.* 27 (1991) 195

[17] T. Hatsuda and T. Kunihiro, *Phys. Reports* 247 (1994) 221

[18] S. Klimt, M. Lutz, U. Vogl and W. Weise, *Nucl. Phys.* A 516 (1990) 429

[19] G. 't Hooft, *Phys. Rev.* D 345 (1976) 3432

[20] M. Gell-Mann, R. Oakes and B. Renner, *Phys. Rev.* 175 (1968) 2195

[21] S. Weinberg, *Physica* A 96 (1979) 327
[22] H. Leutwyler, *Ann. Phys. (NY)* 235 (1994) 165
[23] A. W. Thomas and W. Weise, *The Structure of the Nucleon*, Wiley-VCH, Berlin (2001)
[24] G. Ecker and M. Mojzis, *Phys. Lett.* B 365 (1996) 312
[25] V. Bernard, N. Kaiser and U.-G. Meissner, *Int. J. Mod. Phys.* E 4 (1995) 193
[26] J. Gasser, H. Leutwyler and M.E. Sainio, *Phys. Lett.* B 253 (1991) 252, 260
[27] T. R. Hemmert, B. R. Holstein and J. Kambor, *Phys. Lett.* B 395 (1997) 89
[28] N. Kaiser, R. Brockmann and W. Weise, *Nucl. Phys.* A 625 (1997) 758
[29] P. Büttiker and U.-G. Meissner, *Nucl. Phys.* A 668 (2000) 97
[30] M. C. M. Rentmeester, R. G. E. Timmermans and J. J. de Swart, *Phys. Rev.* C 67 (2003) 044001
[31] D. R. Entem and R. Machleidt, *Phys. Rev.* C 68 (2003) 041001(R)
[32] D. Gazit, S. Quaglioni and P. Navrátil, *Phys. Rev. Lett.* 103 (2009) 102502
[33] S. Ishikawa and M. R. Robilotta, *Phys. Rev.* C 76 (2007) 102502
[34] V. Bernard et al., *Phys. Rev.* C 77 (2008) 064004
[35] V. Bernard et al., *Phys. Rev.* C 84 (2011) 054001
[36] E. Epelbaum, *Phys. Lett.* B 639 (2006) 456
[37] J. Behringer *et al.*, *Review of Particle Physics*, *Phys. Rev.* D 86 (2012) 010001
[38] J. Ahrens *et al.*, *Phys. Rev. Lett.* 87 (2001) 022003
[39] S. Fritsch, N. Kaiser and W. Weise, *Nucl. Phys.* A 750 (2005) 259
[40] N. Kaiser, S. Gerstendörfer and W. Weise, *Nucl. Phys.* A 637 (1998) 395
[41] J. Fujita and H. Miyazawa, *Prog. Theor. Phys.* **17** (1957) 366
[42] N. Kaiser, S. Fritsch and W. Weise, *Nucl. Phys.* A 697 (2002) 255
[43] J. P. Blaizot, *Phys. Reports* 64 (1980) 171
[44] D. H. Youngblood, H. L. Clark and Y.-W. Lui, *Phys. Rev. Lett.* 82 (1999) 691
[45] M. V. Stoitsov, P. Ring and M. M. Sharma, *Phys. Rev.* C 50 (1994) 1445
[46] B. Friedman and V.R. Pandharipande, *Nucl. Phys.* A 361 (1981) 502
[47] W. Zwerger (ed.), *BCS-BEC Crossover und Unitary Fermi Gas*, *Lecture Notes in Physics* 836 (2012)
[48] Q. Chen et al., *Phys. Rev.* C 77 (2006) 054002
[49] S. Gandolfi et al., *Phys. Rev.* C 79 (2009) 054005
[50] A. Gezerlis and J. Carlson, *Phys. Rev.* C 81 (2011) 025803
[51] N. Kaiser, *Nucl. Phys.* A 860 (2011) 41
[52] H. W. Hammer and R. J. Furnstahl, *Nucl. Phys.* A 678 (2000) 277
[53] J.V. Steele, nucl-th/00100066
[54] A. Akmal, V. R. Pandharipande and D. G. Ravenhall, *Phys. Rev.* C 58 (1998) 1804
[55] A. Schwenk and C. J. Pethick, *Phys. Rev. Lett.* 95 (2005) 160401
[56] P. Navrátil, V. G. Gueorguiev, J. P. Vary, W. E. Ormand and A. Nogga, *Phys. Rev. Lett.* 99 (2007) 042501
[57] G. Hagen, T. Papenbrock, D. J. Dean, A. Schwenk, A. Nogga, M. Wloch and P. Piecuch *Phys. Rev.* C 76 (2007) 034302
[58] J. W. Holt, N. Kaiser and W. Weise, *Phys. Rev.* C 79 (2009) 054331

[59] J. W. Holt, N. Kaiser and W. Weise, *Phys. Rev.* C 81 (2010) 024002

[60] K. Hebeler and A. Schwenk, *Phys. Rev.* C 82 (2010) 014314

[61] T. Otsuka, T. Suzuki, J. D. Holt, A. Schwenk and Y. Akaishi, *Phys. Rev. Lett.* 105 (2010) 032501

[62] J. Menéndez, D. Gazit and A. Schwenk, *Phys. Rev. Lett.* 107 (2011) 062501

[63] P. Maris, J. P. Vary, P. Navratil, W. E. Ormand, H. Nam and D. J. Dean, *Phys. Rev. Lett.* 106 (2011) 202502

[64] J. D. Holt, J. Menéndez and A. Schwenk, *Eur. Phys. J.* A 49 (2013) 39.

[65] J. D. Holt, T. Otsuka, A. Schwenk and T. Suzuki, *J. Phys.* G 39 (2012) 085111

[66] A. T. Gallant et al., Phys. Rev. Lett. 109 (2012) 032506

[67] R. Roth, S. Binder, K. Vobig, A. Calci, J. Langhammer and P. Navratil, *Phys. Rev. Lett.* 109 (2012) 052501

[68] K. Hebeler, S. K. Bogner, R. J. Furnstahl, A. Nogga and A. Schwenk, *Phys. Rev.* C 83 (2011) 031301

[69] I. Tews, T. Krueger, K. Hebeler and A. Schwenk, *Phys. Rev. Lett.* 110 032504 (2013) 032504

[70] L. Coraggio, J. W. Holt, N. Itaco, R. Machleidt and F. Sammarruca, *Phys. Rev.* C 87 (2013) 014322

[71] N. Kaiser, *Eur. Phys. J.* A 48 (2012) 58

[72] J. P. Jeukenne, A. Lejeune and C. Mahaux, *Phys. Rep.* 25 (1976) 83

[73] P. Grange, J. P. Cugnon and A. Lejeune, *Nucl. Phys.* A 473 (1987) 365

[74] W. Haider, A. M. Kobos and J. R. Rook, *Nucl. Phys.* A 480 (1988) 1

[75] L. G. Arnold, B. C. Clark, R. L. Mercer and P. Schwandt, *Phys. Rev.* C 23 (1981) 1949

[76] B. ter Haar and R. Malfliet, *Phys. Rep.* 149 (1987) 207

[77] W. H. Dickhoff and C. Barbieri, *Prog. Part. Nucl. Phys.* 52 (2004) 377

[78] S. J. Waldecker, C. Barbieri and W. H. Dickhoff, *Phys. Rev.* C 84 (2011) 034616

[79] N. Kaiser, S. Fritsch and W. Weise, *Nucl. Phys.* A 700 (2002) 343

[80] J. W. Holt, N. Kaiser, G. A. Miller and W. Weise, arXiv:1304.3175

[81] A. J. Koning and J. P. Delaroche, *Nucl. Phys.* A 713 (2003) 231

[82] J. M. Luttinger, *Phys. Rev.* 121 (1961) 942

[83] J. W. Negele and K. Yazaki, *Phys. Rev. Lett.* 47 (1981) 71

[84] S. Fantoni, B. L. Friman and V. R. Pandharipande, *Phys. Lett.* B 104 (1981) 89

[85] B. Gebremariam, T. Duguet and S. K. Bogner, *Phys. Rev.* C 82 (2010) 014305

[86] B. Gebremariam, S. K. Bogner and T. Duguet, *Nucl. Phys.* A 851 (2011) 17

[87] M. Stoitsov et al., *Phys. Rev.* C 82 (2010) 054307

[88] S. K. Bogner, R.J. Furnstahl and L. Platter, *Eur. Phys. J.* A 39 (2009) 219

[89] J. W. Holt, N. Kaiser and W. Weise, *Eur. Phys. J.* A 47 (2011) 128

[90] N. Kaiser, *Eur. Phys. J.* A 48 (2012) 36

[91] M. Bender, P. H. Heenen and P. G. Reinhard, *Rev. Mod. Phys.* 75 (2003) 121

[92] J. R. Stone and P. G. Reinhard, *Prog. Part. Nucl. Phys.* 58 (2007) 587

[93] E. Chabanat et al., *Nucl. Phys.* A 627 (1997) 710; A 635 (1998) 231

[94] N. Chamel, S. Goriely and J. M. Pearson, *Nucl. Phys.* A 812 (2008) 72

[95] B. D. Serot and J. D. Walecka, *Int. J. Mod. Phys.* E 6 (1997) 515

[96] T. Niksic, D. Vretenar and P. Ring, *Prog. Part. Nucl. Phys.* 66 (2011) 519

[97] T. Lesinski, T. Duguet, K. Bennaceur and J. Meyer, *Eur. Phys. J.* A 40 (2009) 121

[98] J. E. Drut, R. J. Furnstahl and L. Platter, *Prog. Part. Nucl. Phys.* 64 (2010) 120

[99] S. K. Bogner, R. J. Furnstahl and A. Schwenk, *Prog. Part. Nucl. Phys.* 65 (2010) 94

[100] S. K. Bogner, T. T. S. Kuo and A. Schwenk, *Phys. Rep.* 386 (2003) 1

[101] S. K. Bogner, R. J. Furnstahl, A. Nogga and A. Schwenk, *Nucl. Phys.* A 763 (2005) 59

[102] R. Roth et al., *Phys. Rev.* C 73 (2006) 044312

[103] J. W. Negele and D. Vautherin, *Phys. Rev.* C 5 (1972) 1472

[104] L. Coraggio et al., *Phys. Rev.* C 75 (2007) 024311

[105] E. Epelbaum, W. Glöckle and Ulf-G. Meissner, *Nucl. Phys.* A 747 (2005) 362

[106] J. W. Holt, N. Kaiser and W. Weise, *Nucl. Phys.* A 870-871 (2011) 1

[107] N. Kaiser and W. Weise, *Nucl. Phys. J.* A 836 (2010) 256

[108] P. G. Reinhard and H. Flocard, *Nucl. Phys.* A 584 (1995) 467

[109] L. D. Landau, *Sov. Phys. JETP* 3 (1957) 920; 5 (1957) 101; 8 (1959) 70

[110] J. Polchinski, in: *Proc. 1992 Theor. Adv. Studies Institute in Elementary Particle Physics*, Eds. J. Harvey and J. Polchinski (World Scientific, Singapore, 1993), hep-th/9210046

[111] R. Shankar, *Rev. Mod. Phys.* 66 (1994) 129

[112] G. Y. Chitov and D. Sénéchal, *Phys. Rev.* B 52 (1995) 129

[113] N. Dupuis and G. Y. Chitov, *Phys. Rev.* B 54 3040 (1996) 3040 .

[114] A. A. Abrikosov and I. M. Khalatnikov, *Rep. Prog. Phys* 22 (1959) 329

[115] A. B. Migdal and A. I. Larkin, *Sov. Phys. JETP* 18 (1964) 717

[116] A. B. Migdal, *Theory of Finite Fermi Systems and Applications to Atomic Nuclei* (Interscience, New York, 1967)

[117] G. E. Brown, *Rev. Mod. Phys.* 43 (1971) 1

[118] A. Schwenk, G. E. Brown and B. Friman, *Nucl. Phys.* A 703 (2002) 745

[119] A. Schwenk, B. Friman and G. E. Brown, *Nucl. Phys.* A713 (2003) 191

[120] J. W. Holt, N. Kaiser and W. Weise, *Nucl. Phys.* A 876 (2012) 61

[121] J. W. Holt, N. Kaiser and W. Weise, *Phys. Rev.* C 87 (2013) 014338

[122] B. Friman, K. Hebeler and A. Schwenk, *Lecture Notes in Physics* 852 (2012) 245

[123] O. Sjöberg, *Ann. Phys.* 78 (1973) 39

[124] O. Sjöberg, *Nucl. Phys.* A 209 (1973) 363

[125] S. O. Bäckman, G. E. Brown and J. A. Niskanen, *Phys. Rep.* 124 (1985) 1

[126] S. Babu and G. E. Brown, *Ann. Phys.* 78 (1973) 1

[127] G. E. Brown and M. Rho, *Nucl. Phys.* A338 (1980) 269

[128] N. Iwamoto and C. J. Pethick, *Phys. Rev.* D 25 (1982) 313

[129] J. Navarro, E. S. Hernández and D. Vautherin, *Phys. Rev.* C 60 (1999) 045801

[130] G. I. Lykasov, C. J. Pethick and A. Schwenk, *Phys. Rev.* C 78 (2008) 045803

[131] S. Bacca, K. Hally, C.J. Pethick and A. Schwenk, *Phys. Rev.* C 80 (2009) 032802

[132] P. Haensel and A. J. Jerzak, *Phys. Lett.* B 112 (1982) 285

[133] E. Olsson, P. Haensel and C. J. Pethick, *Phys. Rev.* C 70 (2004) 025804

[134] C. J. Pethick and A. Schwenk, *Phys.Rev.* C 80 (2009) 055805

[135] M. A. Pérez-García, J. Navarro and A. Polls, *Phys. Rev.* C 80 (2009) 025802

[136] S. Fantoni, A. Sarsa and K. E. Schmidt, *Phys. Rev. Lett.* 87 (2001) 181101

[137] A. Rios, A. Polls and I. Vidaña, *Phys. Rev.* C 71 (2005) 055802

[138] P. Haensel and J. Dabrowski, *Nucl. Phys.* A 254 (1975) 211

[139] A. Schwenk and B. Friman, *Phys. Rev. Lett.* 92 (2004) 082501

[140] P. Armani, A. Y. Illarionov, D. Lonardoni, F. Pederiva, S. Gandolfi, K. Schmidt and S. Fantoni, *J. Phys. Conf. Ser.* 336 (2011) 012014

[141] D. H. E. Gross, *Rep. Prog. Phys.* 53 (1990) 605

[142] J. Pochodzalla et al., *Phys. Rev. Lett.* 75 (1995) 1040

[143] J. B. Natowitz, et al., *Phys. Rev.* C 65 (2002) 034618

[144] P. B. Demorest et al., *Nature* 467 (2010) 1081

[145] S. Fiorilla, N. Kaiser and W. Weise, *Nucl. Phys.* A 880 (2012) 65

[146] S. Fritsch, N. Kaiser and W. Weise, *Phys. Lett.* B545 (2002) 73

[147] C. J. Horowitz and A. Schwenk, *Phys. Lett.* B 638 (2006) 153

[148] V. A. Karnaukhov et al., *Phys. At. Nucl.* 71 (2008) 2067

[149] G. Sauer, H. Chandra and U. Mosel, *Nucl. Phys.* A 264 (1976) 221

[150] S. Typel, G. Röpke, T. Klähn, D. Blaschke and H. H. Wolter, *Phys. Rev.* C 81 (2010) 015803

[151] P. A. Seeger and W. M. Howard, *Nucl. Phys.* A 238 (1975) 491

[152] D. Vretener, T. Niksic and P. Ring, *Phys. Rev.* C 68 (2003) 024310

[153] L.-G. Cao and Z.-Y. Ma, *Chin. Phys. Lett.* 25 (2008) 1625

[154] B.-A. Li, L.-W. Chen and C. M. Ko, *Phys. Rep.* 464 (2008) 113

[155] T. Li et al., *Phys. Rev. Lett.* 99 (2007) 162503

[156] A. Rios, A. Polls, A. Ramos and H. Müther. *Phys. Rev.* C 78 (2008) 044314

[157] I. Vidana, C. Providencia, A. Polls and A. Rios, *Phys. Rev.* C 80 (2009) 045806

[158] V. Soma, P. Bozek, *Phys. Rev.* C 80 (2009) 025803

[159] A. Rios, *Nucl. Phys.* A 845 (2010)

[160] C. Wu, Z. Ren, *Phys. Rev.* C 83 (2011) 044605

[161] L. Tolos, B. Friman and A. Schwenk, *Nucl. Phys.* A 806 (2008) 105

[162] B. Friedman and V. R. Pandharipande, *Nucl. Phys.* A 361 (1981) 502

[163] S. Fiorilla, N. Kaiser and W. Weise, *Phys. Lett.* B 714 (2012) 251

[164] W. Kohn and J. M. Luttinger, *Phys. Rev.* 118 (1960) 41; J. M. Luttinger and J. C. Ward, *Phys. Rev.* 118 (1960) 1417

[165] S. Dürr et al., *Phys. Rev.* D 85 (2012) 014509; A. Semke and M. F. M. Lutz, *Phys. Rev.* D 85 (2012) 034001

[166] J. M. Alarcon, J. Martin Camalich and J. A. Oller, *Phys. Rev.* C 83 (2012) 051503

[167] P. Gerber and H. Leutwyler, *Nucl. Phys.* B 321 (1989) 387

[168] D. Toublan, *Phys. Rev.* D 56 (1997) 5629

[169] N. Kaiser, *Phys. Rev.* C 59 (1999) 2945

[170] A. Bazavov et al., *Phys. Rev.* D 80 (2009) 014504; S. Borsanyi et al., *JHEP* 09 (2010) 073

[171] J.B. Natowitz et al., *Phys. Rev. Lett.* 89 (2002) 212701

[172] A. Gezerlis *et al.*, arXiv:1303.6243 [nucl-th]